Response of Idealized Structural Systems to Simulated M9 Cascadia Subduction Zone Earthquakes Considering Local Soil Conditions

Gloria E. de Zamacona Cervantes

A thesis

submitted in partial fulfillment of the

requirements for the degree of

Master of Science

University of Washington

2019

Reading Committee:

Jeffrey W. Berman, Co-Chair

Marc O. Eberhard, Co-Chair

Alex Grant

Program Authorized to Offer Degree:

Civil and Environmental Engineering

University of Washington

Abstract

Response of Idealized Structural Systems to Simulated M9 Cascadia Subduction Zone Earthquakes Considering Local Soil Conditions

Gloria E. de Zamacona Cervantes

Chair of the Supervisory Committee:
Jeffrey W. Berman and Marc O. Eberhard
Civil and Environmental Engineering

A research team from the United States Geological Survey and the University of Washington developed thirty full-rupture scenarios of magnitude-9 (M9) Cascadia Subduction Zone earthquakes. The simulated M9 motions account for the varying geology in western Washington and include the effects of basin amplification for periods above 1s. The hazard level considered by the current Washington State bridge design provisions is based on the 2014 National Seismic Hazard Maps, which do not take into consideration the amplification of long-period ground motions by the deep sedimentary basins that underlie much of the Puget Sound region. As a result, the bridge design spectral accelerations for cities located on sedimentary basins are lower for long periods than the spectral accelerations for simulated M9 motions.

The response of three types of nonlinear, single-degree-of-freedom oscillators to an M9 event indicate that an event of this magnitude could inflict significant damage to short-period

structures located near the Pacific Coast and to long-period structures located on the deep sedimentary basins that underlie much of the Puget Sound region. Furthermore, older structures designed to lower standards are likely to suffer damage for all periods.

TABLE OF CONTENTS

LIST OF FIGURES

LIST OF TABLES

ACKNOWLEDGEMENTS

This thesis, which is the final product of the research that I have worked on over the past two years as a graduate student, would have not been possible without the support, help, and guidance of some wonderful people. I want to begin by thanking my advisors, Marc Eberhard and Jeff Berman, for making me a part of this wonderful project and for always helping me, pushing me, and guiding me. I must admit that I felt rather lost when I first joined this research project, but I never felt like I wasn't a part of the team. Both Marc and Jeff believed in my abilities and gave me the courage to push through and make it to this point.

An equally important person in this journey has been Nasser Marafi. I would have not been able to achieve most of what is being presented here if it wasn't for him. He was my go-to person for anything and everything, and I cannot thank him enough for all that he has done. He taught me how to be a better researcher, engineer, and how to write code. His willingness to help me even when he was halfway around the world is something that I appreciate a lot and I feel very lucky to have worked with him.

I also want to thank Alex Grant, Arthur Frankel, and Erin Wirth for creating the baseline and soil-adjusted ground motions that made my work possible. Their expertise on geotechnical engineering and seismology taught me something new every time we met. Thank you to every member of the extended M9 team for being passionate about the research that's being done. Seeing everyone's dedication to his or her own research project gave me the motivation to keep working on mine.

I want to thank the amazing friends that I made while being a graduate student at the University of Washington. Anne and Sarah are two of the smartest, strongest, and most driven people that I have ever met. They each inspire me to push myself past my limit, always give it my all, and to make sure that I do my part in representing women in STEM. They also appreciate Timothée Chalamet just as much as I do, so I have no doubt that our friendship will be everlasting. Andrew and I worked together my first quarter at UW and ever since he has been a close friend of mine. He has given me countless research and life advice and seeing him never fails to put a smile on my face. Alec and Max have been witnesses of the rollercoaster of emotions that come with research, and I want to thank them for always letting me rant and for saying (or in some cases not saying) exactly what I need to hear.

The most important people to acknowledge are my parents. I would have not been able to move 2,000 miles across the country if I didn't have their unconditional support. Thank you both so much for supporting me and always believing in me. Everything from heartfelt words of encouragement to the unsolicited 'work on your thesis' text has allowed me to achieve something that I only ever thought was kinda-sorta possible. I want you to know that none of your sacrifices have gone unnoticed or have been in vain. To my sisters, I hope I have been a good example of what hard work can achieve. Thank you for always being there for me and for always being down to go on a night drive. ¡Los amo!

Last, but certainly not least, I want to thank my boyfriend, Chris. Thank you for believing in me unconditionally and for reminding me that I can do this. Your support throughout these past two years has meant the world to me and I thank you for you always managing to make my stress, doubts, and fears go away.

Chapter 1. BACKGROUND AND MOTIVATION

1.1 Introduction to Cascadia Subduction Zone

The 25,000 mi [40,000 km] horseshoe-shaped path along the Pacific Ocean is known as the Ring of Fire, or Circum-Pacific belt (Figure 1.1). This region is characterized by its high volcanic and seismic activity, which results from the denser oceanic plates subducting under the less dense continental plates they border (Encyclopædia Britannica, Inc. 2019). Approximately 81% of the world's largest earthquakes occur in such locations, and for the continent of North America, this means that the Pacific Northwest is a highly seismic region (USGS 2019d).

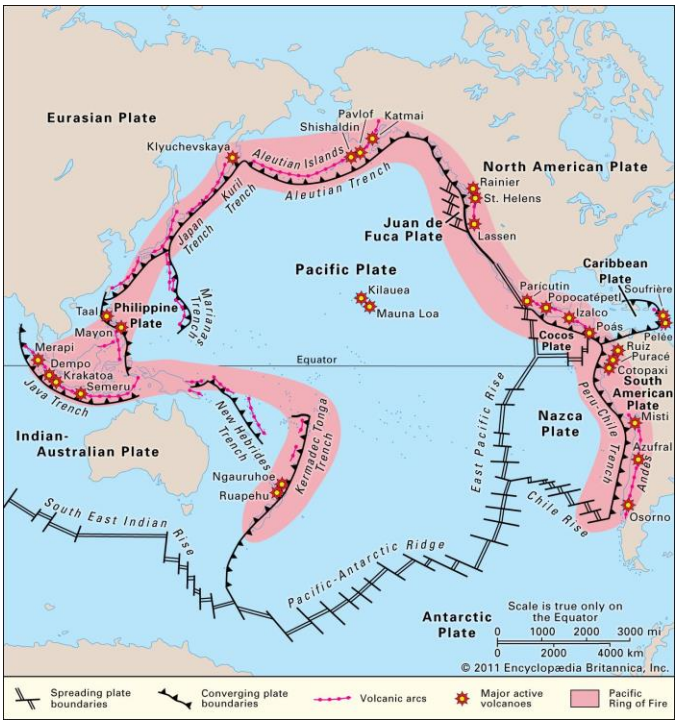

Figure 1.1. The Ring of Fire (Figure from Encyclopædia Britannica, Inc. 2019)

The Cascadia Subduction Zone, CSZ, is the plate tectonic boundary where the Juan de Fuca and North American Plates converge (Figure 1.2). This is a 621-mile [1,000-km] long fault that stretches from southern British Columbia, Canada, to northern California, USA (PNSN 2019). The interface between the two plates has the potential to produce magnitude 9 or greater megathrust earthquakes in the form of either deep intraslab earthquakes, or shallow interslab earthquakes. The last known megathrust earthquake in the northwest occurred in 1700 A.D, 319 years ago, and the geological evidence indicates that the return period for earthquakes of this magnitude is anywhere from 400 to 600 years (PNSN 2019).

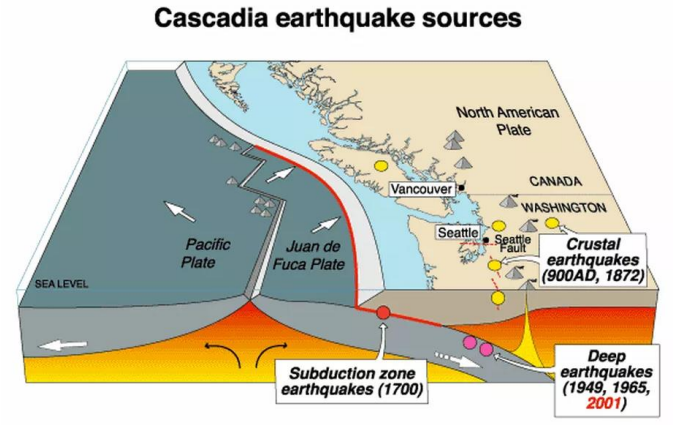

Figure 1.2. Pacific Northwest earthquake sources (Figure from USGS 2019)

The lack of recorded seismic data of large CSZ earthquakes makes it difficult to predict the characteristics of the ground motions that would result from the full rupture of the CSZ. Records of large-magnitude motions from similar subduction regions, such as in Japan and Chile, indicate that the ground motions are expected to have long durations, and that deep sedimentary basins will amplify the shaking (Marafi et al. 2017). The National Seismic Hazard Maps, NSHM, used

for current building and bridge design seismic provisions in the United States do not take into account the effects of long durations or the ground motion amplifications due to deep basins (Petersen et al. 2014).

The following sections contain information regarding the development of the Cascadia Subduction Zone 3D model, the research that has been performed on deep sedimentary structures using simulated M9 motions, and the research that has been performed on long-duration ground motions on bridge pier models. These sections also identify the need for studying: (1) the impact of geographic location on the simulated ground-motion spectral acceleration, (2) the impact of a variety of soil classes on the spectral acceleration from simulated ground motions, and (3) the vulnerability of bridges (idealized as single-degree-of-freedom systems) in western Washington State.

1.2 CASCADIA SUBDUCTION ZONE MODEL

A large set of broadband (0-10 Hz) synthetic seismograms for magnitude-9, M9, CSZ earthquakes considering thirty full-rupture scenarios were developed as part of a collaboration between the United States Geological Survey, USGS, and the University of Washington (Frankel et al. 2018, Wirth et al. 2018). The project utilized the three-dimensional velocity model developed by Stephenson et al. (2017) for the region west of the Cascade Mountains, and the range of scenarios originated from three-dimensional physics-based simulations that varied in hypocenter location, slip distribution, and down-dip rupture edge.

Two methodologies were used to create low- and high-frequency ground motion components, with the final M9 broadbands produced by combining the low- and high-frequency components (Frankel et al. 2018). Low frequencies (0-1 Hz) were computed with the use of a 3D finite-difference model. This model is 4^{th} order in space, 2^{nd} order in time, and has grid spacing

that varies with depth (Liu and Archuleta 2002; Frankel et al. 2018). The top 3.1 mi [5 km] uses 328 ft. [100 m] grid spacing, and for depths between 3.1-37.3 mi. [5-60 km] the horizontal spacing changes to 984 ft. [300 m]. The velocity model has a minimum S-wave or shear-wave velocity, V_S, of 1968 ft./s [600 m/s], similar to the velocity of surficial glacial sediments, which corresponds to the type of soil found in much of the Puget Sound region (Frankel et al. 2018). This velocity model incorporates several deep sedimentary basins from the Pacific Northwest, including the basins surrounding the Puget Lowlands, and the Portland and Tualatin basins (Frankel et al. 2018; Stephenson et al. 2017), and it was used to model the background slip and M8 sub-events (Marafi et al. 2019; Frankel et al. 2018). Figure 1.3 shows a schematic of the background slip and M8 sub-event for the low frequency model.

High frequency (1-10 Hz) components of ground motions were computed with a stochastic synthetic procedure for P and S waves (Frankel et al. 2018; Wirth et al. 2018). This model does not include the basin amplification or de-amplification effects, as it does not account for the basin characteristics for frequencies above 1 Hz (Marafi et al. 2019b). Matched filters at 1.0 Hz were applied to the S-wave stochastic and finite-difference synthetics. The final broadband seismograms were assembled by adding together the stochastic S-waves and low-frequency simulations, and then joining the stochastic P-waves.

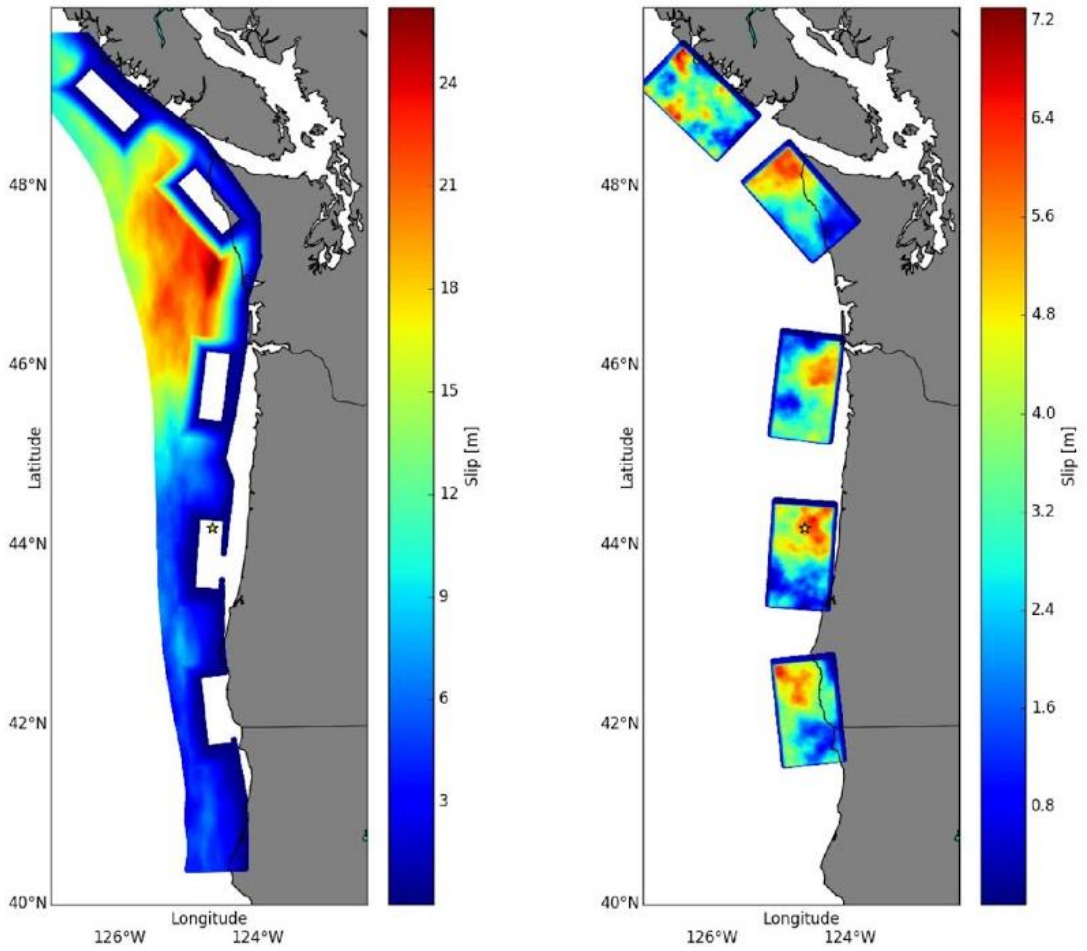

(a) Background slip (b) M8 sub-events

Figure 1.3. CSZ Finite-difference Models for (a) background slip and (b) M8 sub-event from Frankel et al. (2018)

1.3 Effects of Basins on RC Wall Buildings

Marafi et al. (2019b) studied the effects of the simulated M9 ground motions on the performance of mid- and high-rise reinforced concrete core-wall residential buildings in Seattle. This study utilized ground motions for a site with an average shear-wave velocity in the upper 30 meters, V_{S30}, equal to 1640 ft./s [500 m/s], and it found that the median spectral accelerations from the M9 ground motions exceeded the MCE_R (2000-year return period risk-adjusted Maximum Considered Earthquake) for periods between 1.5 to 4.0 seconds. For building design

practices consistent with ASCE 7-16, the median maximum inter-story drift for the M9 motions exceeded the drift inter-story ratio for MCE_R spectra motions that do not consider the effects of basins. The M9 motions' drift ratios, however, were 0.67 times the median of the maximum drifts for MCE_R spectra motions that do consider the effects of basins. Furthermore, the study found that there is an 11% average collapse probability for code-enhanced, ASCE 7-16 building archetypes.

1.4 BRIDGE MODELING

Changramohan et al. (2016) conducted nonlinear analysis of a ductile reinforced concrete bridge pier in order to analyze the effect of long-duration ground motions on collapse capacity. The study utilized a zero-length plastic hinge that followed the Modified Ibarra-Medina-Krawinkler peak-oriented hysteretic model (OpenSees, McKenna 2016). The authors found that ground-motion duration had the greatest effect on modern, ductile structures. This finding was explained by the tendency of non-ductile structures to collapse soon after yielding, which reduced the influence of ground-motion duration on collapse capacity. In addition, the study found that the median collapse capacity estimated by the long-duration ground motion set was 17% lower than that of the short-duration set.

1.5 RESEARCH GOALS

Previous research regarding structural behavior during a M9 earthquake has been conducted for midrise and tall buildings located in Seattle and with simulated ground motions corresponding to a site with shear-wave velocity, V_{S30}, near 1640 ft./s [500 m/s] (Marafi et al. 2019b). That study did not consider other locations in the Pacific Northwest or other site conditions. Furthermore, the past research did not account for the structural behavior of bridges.

To evaluate the vulnerability of bridge inventories, it is necessary to consider a wide variety of locations and site condition, and thus, research is needed in three key areas:

1. The effects of location in terms of inside/outside basin have been taken into consideration for two cities (Seattle and La Grande) near the Puget Sound Region (Marafi et al. 2019a and 2019b). However, many Washington coastal cities are expected to experience large spectral accelerations due to their greater proximity to the fault, and many cities in the interior of the state (but outside a sedimentary basin) might not experience spectral accelerations higher than the current design accelerations. The combined effects of location and basin amplification will be studied in this research.
2. Many bridges are supported by soils with average shear-wave velocity in the first 30 meters lower than 1968 ft./s [600 m/s], which represent site classes D – F. Propagation of the existing ground motions through a soil column with a lower surface shear-wave velocity would produce the simulated ground motions for softer soils, and utilizing the ground motions corresponding to softer soils would highlight the impact of different soil classes on simulated M9 spectral acceleration. The wider range of soil conditions would be more representative of the soils found in the state of Washington. Research will be performed to study the effects of local soil conditions on simulated M9 spectral accelerations.
3. The effects of long-duration ground motions on the collapse capacity of bridge piers have been studied (Changramohan et al. 2016), but without taking into account the effects of location (including basin amplification), different soil conditions, or M9

ground motions. Research on the effect of M9 simulated ground motions on single-degree-of-freedom systems with nonlinear bridge properties will be performed.

1.6 SCOPE OF WORK

This thesis studies the response of idealized structural systems to simulated M9 Cascadia Subduction Zone earthquakes, considering the effects of local soil conditions and geographic location. Its aim is to be used as a preliminary study to understand the effects that a magnitude-9 earthquake would have on Washington State bridges. The thesis chapters reflect the process followed in order to understand the current national and Washington State bridge design codes, conduct a parametric study, analyze the results from the parametric study, and draw conclusions.

- Chapter 2 discusses the evolution of the National Seismic Hazard Maps and highlights the difference in design spectral accelerations between the previous and current Washington bridge design codes (AASHTO-17 and WSDOT-18, respectively).
- Simulated M9 ground motions are introduced in Chapter 3, and a first comparison is made between the current bridge design spectral accelerations and the spectral accelerations obtained from the baseline M9 simulations. Furthermore, the chapter explores the effects of location and basin amplification of long-duration ground motions, without considering the effects of site conditions.
- In Chapter 4, the baseline simulated M9 ground motions are adjusted to represent the effects of softer soils (V_{S30} less than 1968 ft./s [600 m/s]), and the amplification ratio between each new soil class and the baseline is computed.
- The development of three idealized structural systems with properties that reflect current bridge design is reported in Chapter 5. These systems differ in their type of

nonlinear behavior, and they serve as the basis for the parametric study conducted in Chapter 6. The parametric study consists of observing the response of each structural system due to location, period, ground motion direction, realization, soil class, and profile.

- Lastly, Chapter 7 presents the conclusions reached and highlights areas of future work.

Chapter 2. EVOLUTION OF NATIONAL SEISMIC HAZARD MAPS

The current national design provisions for bridges (AASHTO-17) rely on the ground-motion maps that the USGS published in 2002 (Khaleghi 2017) and site coefficients that originally appeared in 1994 (FEMA 222A and 223A). In the latest revisions to their Bridge Design Manuals, the states of Washington, Oregon, and California adopted the 2014 USGS maps and new site coefficients (Khaleghi 2017). The current bridge design code that the State of Washington uses is referred to as WSDOT-18.

In late 2018, the USGS developed a model that takes into account the amplification of long-period ground motions in deep sedimentary basins (Petersen et al. 2018). In the future, this model would likely affect the way that future bridges are designed in the Puget Sound region, much of which is located above a sedimentary basin. However, the 2018 USGS hazard model is still in draft form, and it is unknown when WSDOT might adopt this model, so the 2018 USGS model will not be considered in this thesis.

This chapter discusses the variations among the 1000-year return period (7% probability of exceedance in 75 years) design spectral acceleration values for bridges located in soil Site Class C for two versions of the United States Geological Survey, USGS, National Seismic Hazard Maps: USGS 2002 and USGS 2014. These parameters were selected because they correspond to the design maps and return period utilized in old (and national) as well as current Washington bridge design codes (AASHTO-17 and WSDOT-18, respectively). Furthermore, soil Site Class C was selected in order to facilitate comparison with the baseline simulated M9 ground motions (Chapter 3), which were generated having a V_{S30} of 1968 ft./s [600 m/s]. Information regarding

the map version, the return period, and the site coefficient source for the two bridge design codes analyzed are compared in Table 2.1.

The variations among the Site Class C design spectral accelerations for the two bridge codes are presented in terms of contour maps for the State of Washington and bar graphs for ten representative cities. Information on how the bridge design spectral acceleration values compare to building design spectral acceleration values can be found in Appendix A.

Table 2.1. Bridge Design Codes Information

Bridge Code	**AASHTO-17**	**WSDOT-18**
Return Period (Years)	975	1000
USGS Map Version	2002	2014
Site Coefficient Source	NEHRP 1994	NEHRP 2015

2.1 METHODOLOGY

Table 2.2 shows the site class definitions used by both of the bridge design codes. These classifications are the same for all design codes, as they come from the NEHRP Recommended Provisions for Seismic Regulations for New Buildings, and they have remained unchanged since 1994 (FEMA 222A and 223A; FEMA P-1050-1). The site coefficients (for Peak Ground Acceleration, Short-Period Spectral Acceleration, and Long-Period Spectral Acceleration) for these site classes vary depending on the USGS map version used. The 2002 USGS map uses Site Class B as its reference layer (rock, V_{S30} = 2500 – 5000 ft./s [760 – 1524 m/s]), and the site coefficients are given by NEHRP 1994 (FEMA 222A and 223A; Appendix B, Tables B.1 – B. 3). For this reason, the site class coefficients listed in Tables B.1 – B.3 are equal to 1.0 for Site Class B, regardless of the mapped peak ground acceleration.

For the 2014 map, the reference site class changed to the boundary layer between site classes B and C, known as the B/C boundary or "B Unmeasured" layer (rock/dense soil, V_{S30} = 2500 ft./s [760 m/s]). The site coefficients for this map version are given by NEHRP 2015 (FEMA P1050-1; Appendix B, Tables B.4 – B.6). The Site Class C design accelerations for each design code were obtained by applying the corresponding site coefficients to the reference site values. Additional information regarding site coefficients is available in Section 2.4.

Table 2.2. Site Class Definitions

Site Class	**Soil Profile Name**	**Average Properties in top 100 ft.**		
		Soil shear-wave velocity, V_{s30} (ft./s)	Standard penetration resistance, N (blows/ft.)	Soil undrained shear strength, S_u (psf)
A	Hard rock	$V_{s30} > 5000$	-	-
B	Rock	$2500 < V_{s30} \leq 5000$	-	-
C	Very dense soil and soft rock	$1200 < V_{s30} \leq 2500$	$N > 50$	$S_u \geq 2000$
D	Stiff soil profile	$600 < V_{s30} \leq 1200$	$15 \leq N \leq 50$	$1000 \leq S_u \leq 2000$
E	Soft soil profile	$V_{s30} < 600$	$N < 15$	$S_u < 1000$
F	Soils requiring a site response analysis	-	-	-

Ten representative cities were selected to characterize the regional variation of expected ground motions in western Washington State. Figure 2.1 shows the locations of these cities, and Table 2.3 lists their latitude, longitude, and depth to soil layer with a shear-wave velocity of 2,500 m/s (denoted as $Z_{2.5}$). The measurement of $Z_{2.5}$ can be used as a one-dimensional proxy for the depth of the sedimentary basin at any location, because basins have deep sediment layers with lower shear-wave velocities than outside the basins, which results in greater values of $Z_{2.5}$ than non-basin areas. The selected cities lay within the boundaries of the Cascadia Subduction Zone model (Chapter 1) and are utilized in the remaining chapters.

The representative cities can be organized into four categories based on their location and value of $Z_{2.5}$. The four categories are:

(1) Coastal Cities without Basin. Cities that are located near the Pacific Coast were categorized as "Coastal Cities." This category includes the cities of Forks and Ocean Shores. Note that both cities have a value of $Z_{2.5}$ less than 1.0 km, which indicates that they are not located on a sedimentary basin.

(2) Inland Cities without Basin. No-basin inland cities are cities located on the interior of the state and with a value of $Z_{2.5}$ less than 2.0 km. This category includes the cities of Olympia, Vancouver, and Graham. Note that $Z_{2.5}$ for Olympia is equal to 1.96 km, and the value for Vancouver is 1.76 km, which places these cities near the arbitrary 2.0-km boundary between non-basins and shallow basins.

(3) Inland Cities on Shallow Sedimentary Basins. Shallow sedimentary basin cities are those that have a $Z_{2.5}$ value between 2.0 and 3.0 km. This category is made up of the cities of Port Angeles, Port Townsend, and Tacoma.

(4) Inland Cities on Deep Sedimentary Basins. Deep sedimentary basin cities are cities that have a $Z_{2.5}$ value greater than 3.0 km. The cities of Seattle and Everett make up this fourth category.

Table 2.3. Key Characteristics of Representative Cities

Region	City Name	Latitude	Longitude	$Z_{2.5}$ (km)	Category
Olympic Peninsula	Forks	47.9504	-124.3855	0.76	Coastal w/o Basin
	Ocean Shores	46.9737	-124.1563	0.98	Coastal w/o Basin
	Port Angeles	48.1181	-123.4307	2.29	Inland Shallow Basin
Puget Sound Region	Olympia	47.0379	-122.9007	1.96	Inland w/o Basin
	Port Townsend	48.1170	-122.7604	2.84	Inland Shallow Basin
Southern Region	Vancouver	45.6272	-122.6727	1.76	Inland w/o Basin
Puget Sound Region	Tacoma	47.2529	-122.4443	2.86	Inland Shallow Basin
	Seattle	47.6062	-122.3321	6.70	Inland Deep Basin
	Graham	47.0529	-122.2943	0.20	Inland w/o Basin
	Everett	47.9790	-122.2021	3.42	Inland Deep Basin

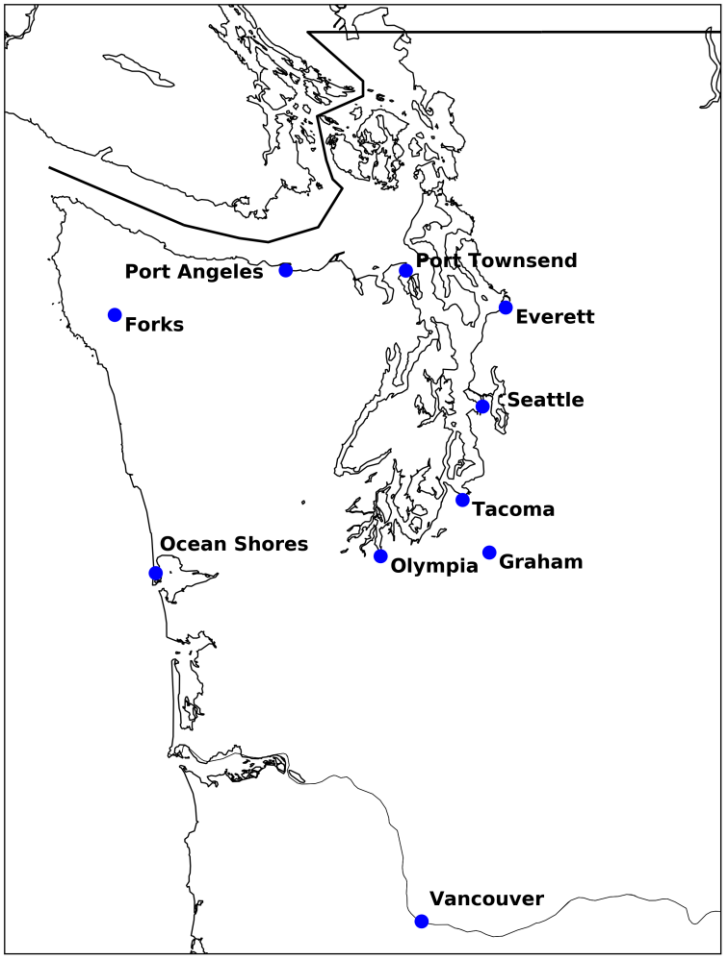

Figure 2.1. Location of Representative Cities

The values of design spectral acceleration for Site Class C (used to create contour maps and bar graphs) were obtained with the use of one of two methods, depending on the design code.

- The design spectral values for the AASHTO-17 Specifications were computed by performing two-dimensional spatial interpolation of the 2002 USGS hazard curve text files for PGA, 0.20 second (5 Hz), and 1.00 second (1 Hz) spectral accelerations (https://earthquake.usgs.gov/hazards/hazmaps/conterminous/2002/data.php), based on the specified latitude, longitude, and return period of 975 years. Straight-line interpolation based on reference site acceleration was used to obtain the necessary site coefficients and modify the reference accelerations.

- The design spectral values for WSDOT-18 Specifications were computed from spectral acceleration data for ground motions with a seven percent probability of exceedance in seventy-five years (provided by Arthur Frankel from USGS). Two-dimensional spatial interpolation based on specified latitude and longitude for each acceleration type was performed in order to obtain the necessary spectral acceleration values. The spectral acceleration values were modified according to the corresponding site coefficients obtained via straight-line interpolation (based on reference site acceleration).

2.2 DESIGN SPECTRAL ACCELERATIONS

The Site Class C design spectral acceleration contour maps for the State of Washington are compared side-by-side in Figure 2.2 for both bridge design codes. For each design code, contour maps are shown for peak ground acceleration, PGA, short-period design spectral acceleration at a period of 0.2 seconds (5 Hz), S_{DS}, and long-period design spectral accelerations at a period of 1.0 second (1 Hz), S_{D1}. All the maps in Figures 2.2 show that, as expected, the design accelerations consistently decrease moving from west to east for all the three design accelerations.

The ten cities studied (Figure 2.1) were arranged from West to East to capture the variation in their design spectral acceleration values (Figure 2.3). For all ten cities, and for both design codes, the values of the design short-period acceleration, S_{DS}, are higher than either the PGA or the spectral acceleration at 1.0s, S_{D1}. Figures 2.2 and 2.3 show that the Olympic Peninsula region has the highest values of design spectral acceleration for both design codes. For example, for AASHTO-17, the cities located on the Olympic Peninsula (Forks, Ocean Shores, and Port Angeles) have design values between 0.3 – 0.50 g for PGA, 0.8 – 1.2 g for S_{DS}, and 0.45 – 0.70 g

for S_{D1} (Figures 2.2 & 2.3). The WSDOT-18 design acceleration values for those same cities ranged from 0.6 – 0.75 g for PGA, 1.2 – 1.4 g for S_{DS}, and 0.50 – 0.70 g for S_{D1} (Figures 2.2 & 2.3).

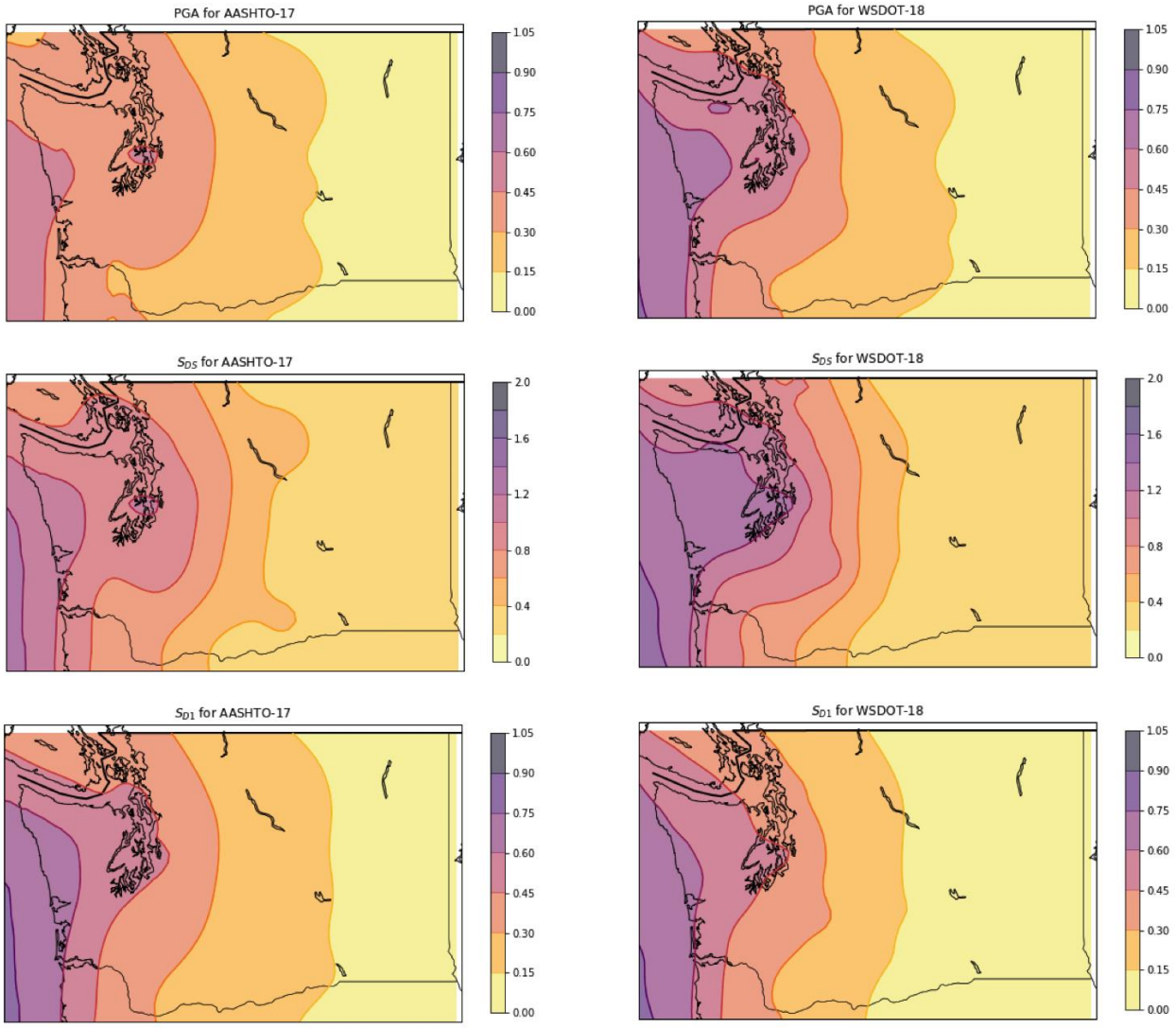

Figure 2.2. Washington State Design S_a Contour Maps for AASHTO-17 & WSDOT-18 (Site Class C)

Figure 2.3 shows that WSDOT-18 design code results in the highest PGA and S_{DS} values, and the AASHTO-17 code resulted in higher S_{D1} values for nine of the ten cities (except for Port Angeles). This indicates that using the 2002 map produces lower values than the 2014 map for short periods, but higher values for long periods. The figure also illustrates how none of the

codes take into account basin amplification effects because the S_{D1} values are lower than the S_{DS} values, which would not be the case if either code included basin effects as it is known that basins amplify spectral accelerations at periods greater than 1 second (Chapter 1) and would therefore result in larger S_{D1} values.

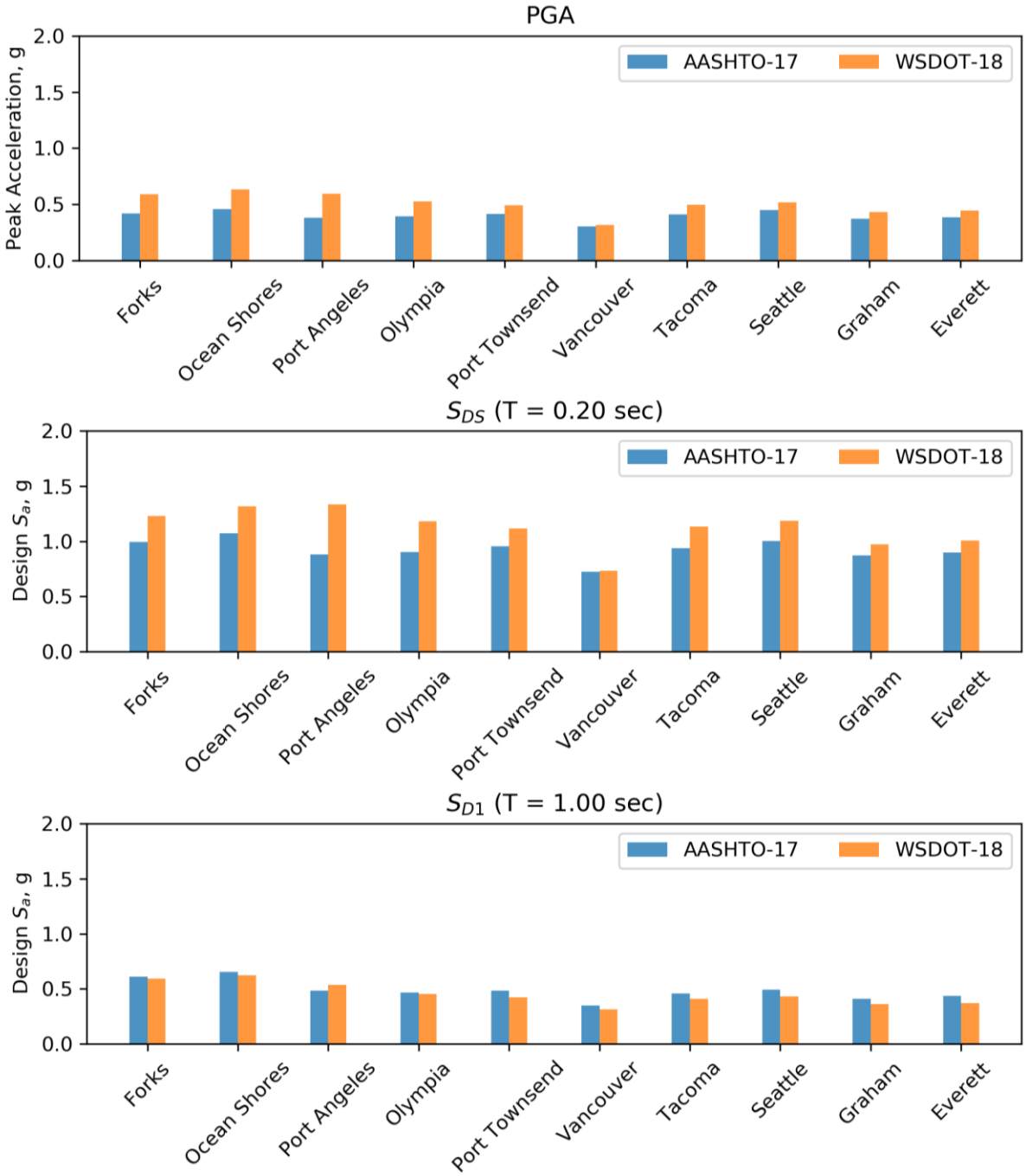

Figure 2.3. Washington Cities Design S_a Values According to Design Code (Site Class C)

2.3 COMPARING AASHTO-17 AND WSDOT-18 DESIGN VALUES

Figure 2.4 shows contour maps of the percentage change in PGA, S_{DS}, and S_{D1} caused by modifying the USGS map version (from 2002 to 2014) but maintaining the return period the same. The contour maps show that changing the map version increased the PGA and S_{DS} for the Olympic Peninsula and Western Washington coast, but decreased them for the mid-portion of the eastern border of Washington State. The percentage change in S_{D1} is negative throughout the whole state with the most negative values concentrating along the mid-portion of the eastern border.

Figure 2.5 shows that the difference in percent change values between PGA and S_{DS} is greatest amongst the western-most cities (Forks, Ocean Shores, and Port Angeles) with an absolute value difference range of 5% to 16%, and smallest amongst the cities closest to the Puget Sound (Olympia, Port Townsend, Tacoma, and Seattle), which have an absolute value difference range of 1% to 2%.

Figure 2.4 shows that changing the USGS map version increased S_{DS} percent change in the West coast between +15% and +45%, and decreased the percent change in the East border between +7.5% and -22.5%. Figures 2.4 and 2.5 also show that the largest increase in S_{DS} is concentrated in the region located directly between the Olympic Peninsula and the Puget Sound Region. This can be seen visually by the darkening of the red contour shades (Figure 2.4), and graphically by the spike in S_{DS} percent change values along Port Angeles and Olympia (Figure 2.5).

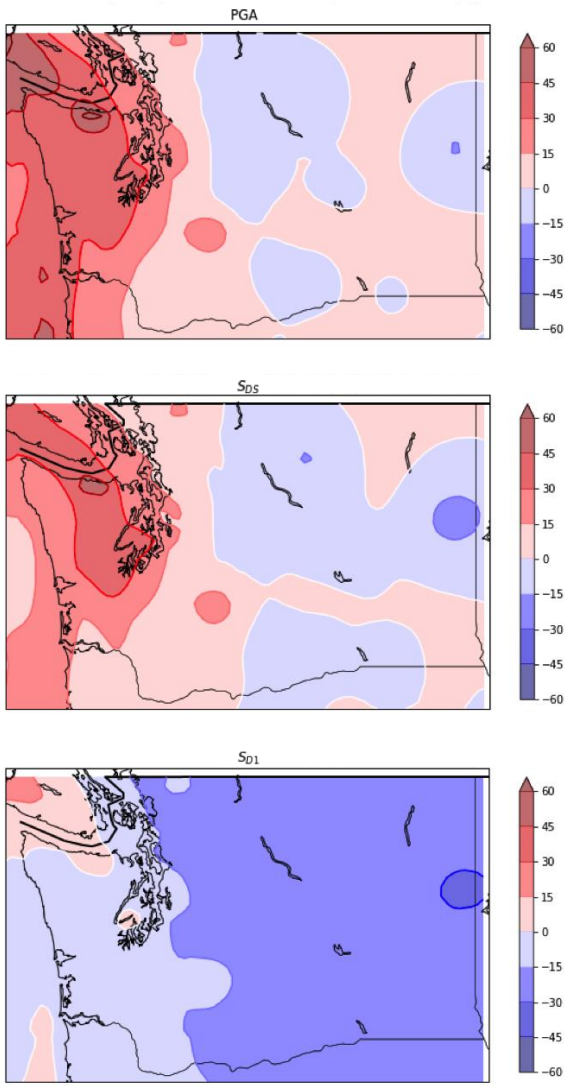

Figure 2.4. Washington State Design S_a Percent Change Contours Caused by Changing USGS Map Version (WSDOT-18/AASHTO-17, ~1000-year Return Period, Site Class C)

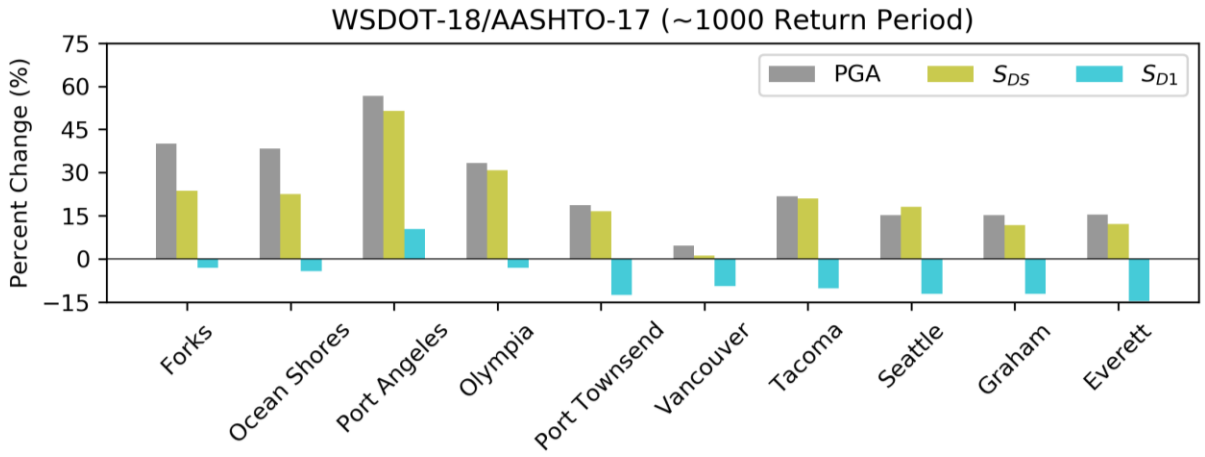

Figure 2.5. Washington Cities Design S_a Percent Change Values Caused by Changing USGS Map Version (WSDOT-18/AASHTO-17, ~1000-year Return Period, Site Class C)

2.4 Changes in Site Coefficients

The values from the contour maps developed in Sections 2.2 and 2.3 were created for Site Class C. Because the two USGS map versions referred to different reference site classes, the reference accelerations obtained for the AASHTO-17 and WSDOT-18 specifications had to be adjusted accordingly for Site Class C. Appendix B (Tables B.1 – B.6) shows the site coefficients for the 2002 and 2014 USGS maps. In order to obtain the appropriate spectral acceleration values for other site classes, corresponding site coefficients must be applied.

For Site Class C, the design spectral acceleration values are either greater than or equal to the reference spectral acceleration values obtained from the 2002 USGS map. This resulted from the fact that the 2002 map utilizes Site Class B as the reference site class, which means that for any given reference acceleration (PGA, S_S, or S_1), the coefficients (F_{pga}, F_a, and F_v) have a value of 1.0. For Site Class C, the PGA and S_{DS} were greater than or equal to the reference accelerations because the straight-line interpolation was performed with F_{pga} and F_a coefficients that ranged from 1.0 – 1.2. The straight-line interpolation used to obtain the S_{D1} values utilized

F_v coefficients that ranged between 1.3 and 1.7, which resulted in design spectral accelerations larger than the reference accelerations.

The design spectral acceleration values obtained from the 2014 USGS map were all greater than the reference spectral accelerations because the F_{pga} and F_a coefficients range between 1.2 – 1.3, and the F_v range between 1.4 – 1.5. In these tables (Tables B.4 – B.6) because the reference layer is the B/C boundary, the site coefficients for B Unmeasured are 1.0, those for Site Class B or A are less than 1.0, and those for classes greater than B/C are greater than 1.0. In addition to changing the reference site class, one more column for PGA, S_s, and S_1 was added to the pre-existing tables.

Tables 2.4, 2.5, and 2.6 show the ratio of site coefficients for each site class and acceleration level obtained when the 2014 site coefficients were divided by the 2002 coefficients, in order to capture the effect of modifying the site coefficients along with the USGS map version. These tables show that for Site Class C the values of F_{pga} and F_a increases between 0% and 10 % and 8% and 20%, respectively, while the values of F_v changes between -12% and 15%. Therefore, the percent changes reported in Section 2.3 are not just a result of utilizing the updated map version, but also of utilizing different site coefficients.

Table 2.4 Ratio Values of F_{pga} as Function of Site Class and Mapped Peak Ground Acceleration (2014/2002)

Site Class	Mapped Peak Ground Acceleration					
	PGA ≤ 0.10	PGA = 0.20	PGA = 0.30	PGA = 0.40	PGA = 0.50	PGA ≥ 0.60
A	1.00	1.00	1.00	1.00	1.00	1.00
B Measured	0.90	0.90	0.90	0.90	0.90	0.90
B Unmeasured	1.00	1.00	1.00	1.00	1.00	1.00
C	1.08	1.00	1.09	1.20	1.20	1.20
D	1.00	1.00	1.08	1.09	1.10	1.10
E	0.96	1.12	1.33	1.55	1.33	1.22
F						

Table 2.5 Ratio Values of F_a as Function of Site Class and Mapped Short Period Spectral Acceleration Coefficient (2014/2002)

Site Class	Mapped Spectral Response Acceleration Coefficient at Short Periods					
	$S_s \leq 0.25$	$S_s = 0.50$	$S_s = 0.75$	$S_s = 1.00$	$S_s = 1.25$	$S_s \geq 1.50$
A	1.00	1.00	1.00	1.00	1.00	1.00
B Measured	0.90	0.90	0.90	0.90	0.90	0.90
B Unmeasured	1.00	1.00	1.00	1.00	1.00	1.00
C	1.08	1.08	1.09	1.20	1.20	1.20
D	1.00	1.00	1.00	1.00	1.00	1.00
E	0.96	1.00	1.08			
F						

Table 2.6 Ratio Values of F_v as Function of Site Class and Mapped Long Period Spectral Acceleration Coefficient (2014/2002)

Site Class	Mapped Spectral Response Acceleration Coefficient at 1-Second Periods					
	$S_1 \leq 0.10$	$S_1 = 0.2$	$S_1 = 0.3$	$S_1 = 0.4$	$S_1 = 0.50$	$S_1 \geq 0.60$
A	1.00	1.00	1.00	1.00	1.00	1.00
B Measured	0.80	0.80	0.80	0.80	0.80	0.80
B Unmeasured	1.00	1.00	1.00	1.00	1.00	1.00
C	0.88	0.94	1.00	1.07	1.15	1.07
D	1.00	1.10	1.11	1.19	1.20	1.13
E	1.20	1.03	1.00	1.00	0.92	0.83
F						

Chapter 3. SPECTRAL ACCELERATIONS FOR BASELINE SIMULATED M9 GROUND MOTIONS

This chapter discusses the spectral accelerations obtained from the baseline simulated M9 ground motions and compares these values with the design spectral accelerations from the AASHTO-17 and WSDOT-18 bridge design codes, discussed in Chapter 2. The simulated M9 motions used here are referred to as the baseline motions, because they were generated for a site with a soil profile having a V_{S30} of 1968 ft./s [600 m/s] (i.e. within Site Class C). The effects of different site conditions on the simulated M9 ground motions are discussed in Chapter 4.

Baseline simulated M9 ground motion pairs were available for 169 locations (stations) within the Cascadia Subduction Zone Model (Chapter 1). In order to obtain the baseline M9 spectral accelerations for the ten representative cities in western Washington, a corresponding Station ID was assigned to each city by selecting the station whose coordinates most closely matched the coordinates of the city. Table 3.1 shows the Station ID that was selected to represent each Washington city as well as the corresponding latitude, longitude, and average closest distance to fault, $R_{cd,avg}$.

Table 3.1. Station ID, Coordinates, and $R_{cd,avg}$ Used to Represent Washington Cities

City Location			**Nearest Station Location**			
City Name	**Latitude**	**Longitude**	**Station ID**	**Latitude**	**Longitude**	$R_{cd,avg}$ **(km)**
Forks	47.9504	-124.3855	Z0FORK	47.9456	-124.5662	25.92
Ocean Shores	46.9737	-124.1563	Z0XOCS	46.9778	-124.1544	23.94
Port Angeles	48.1181	-123.4307	Z0XANG	48.1191	-123.4309	57.61
Olympia	47.0379	-122.9007	Z00CPW	46.9717	-123.1376	75.53
Port Townsend	48.1170	-122.7604	Z0XTWN	48.1146	-122.7561	95.73
Vancouver	45.6272	-122.6727	Z0HUBA	45.6287	-122.6526	109.49
Tacoma	47.2529	-122.4443	Z0TBPA	47.2559	-122.3682	105.61
Seattle	47.6062	-122.3321	Z0XWLK	47.6120	-122.3375	114.56
Graham	47.0529	-122.2943	Z00GHW	47.0395	-122.2737	117.40
Everett	47.9790	-122.2021	Z0EVCC	48.0056	-122.2043	128.53

3.1 BASELINE SIMULATED M9 SPECTRAL ACCELERATIONS

The 30 realizations from the baseline simulated M9 ground motions were used to generate the response spectra for each of the ten representative cities (Figure 3.1 & Appendix C).

The values of the spectral accelerations for the baseline simulated M9 ground motions for each city were obtained by computing the geometric mean (of the 30 realizations) of the geometric mean (of the North-South and East-West acceleration components) for a given period. Figure 3.1 show the response spectra for the ten representative cities, broken up into the four city categories. As expected, the response spectra were qualitatively similar within each category. Table 3.2 shows the baseline M9 spectral acceleration for the ten cities obtained for 0.2 and 1.0 second periods. The table shows that for the cities that were identified as being on sedimentary basins (Port Angeles, Port Townsend, Tacoma, Seattle, and Everett) the ratio of long-period to short period spectral acceleration is greater than 0.7, which indicates that the spectral acceleration at 1s is similar to the spectral acceleration at 0.2s. Once again this can be attributed to the basin amplification effects, which the CSZ 3D model considers, as was mentioned in Chapter 1

One important thing to note when looking at the response spectra from Figure 3.1 for the inland cities on shallow sedimentary basins (Port Angeles, Port Townsend, and Tacoma) is that the response spectra for Tacoma is different from Port Townsend's despite having almost identical $Z_{2.5}$ values. This difference is due to $Z_{2.5}$ being an imperfect measure of the characteristics of a basin as there are three-dimensional effects such as focusing and surface wave conversion that play a role in the amplification of ground motions.

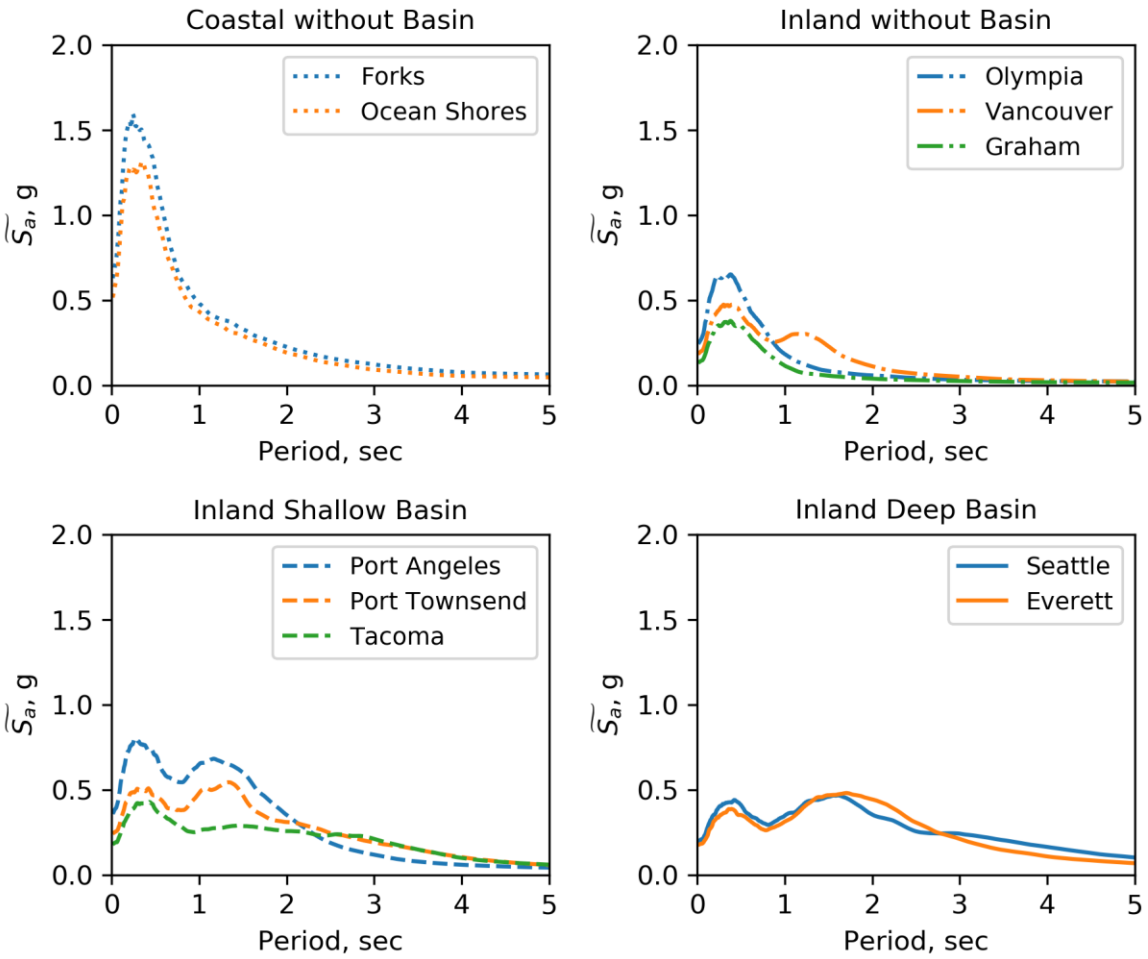

Figure 3.1. Response Spectra from Baseline Simulated M9 Ground Motions for the City Categories

Table 3.2. Geometric Mean S_a of the 30 Baseline Simulated M9 Realizations and Orthogonal Directions for Short (T=0.2s), Long Periods (T=1.0s), and Ratio of Long-period to Short-period

City Name	S_a at T = 0.2 sec (g)	S_a at T = 1.0 sec (g)	Ratio of S_a	Category
Forks	1.523	0.477	0.31	Coastal w/o Basin
Ocean Shores	1.266	0.430	0.34	Coastal w/o Basin
Port Angeles	0.735	0.648	0.88	Inland Shallow Basin
Olympia	0.615	0.183	0.23	Inland w/o Basin
Port Townsend	0.464	0.481	1.04	Inland Shallow Basin
Vancouver	0.411	0.275	0.67	Inland w/o Basin
Tacoma	0.368	0.261	0.71	Inland Shallow Basin
Seattle	0.354	0.348	0.98	Inland Deep Basin
Graham	0.328	0.115	0.35	Inland w/o Basin
Everett	0.320	0.313	0.98	Inland Deep Basin

The response spectra for the cities of Forks, Port Angeles, Seattle, and Graham are shown in Figure 3.2. The response spectra were generated from the geometric mean of both horizontal components (North-South and East-West) for each realization (shown as grey lines) and from the geometric mean of all 30 realizations (shown as the black line) for periods of 0 to 5 seconds. Forks was selected to represent a coastal city without a basin. Graham was selected to represent an inland city without a basin. Port Angeles represents an inland city with a shallow basin, and Seattle represents inland cities on a deep basin.

The figure shows that the response spectra for periods below 1 second is highest for the city of Forks, which is closest to the Pacific coast, next highest for Port Angeles, and smallest for Graham and Seattle (both of which are located at a similar longitudinal coordinate as Seattle). At longer periods the effects of basin amplification are evident for the cities of Seattle and Port Angeles (both located on sedimentary basins), because the spectral acceleration values increase between periods of 1 and 1.5 seconds.

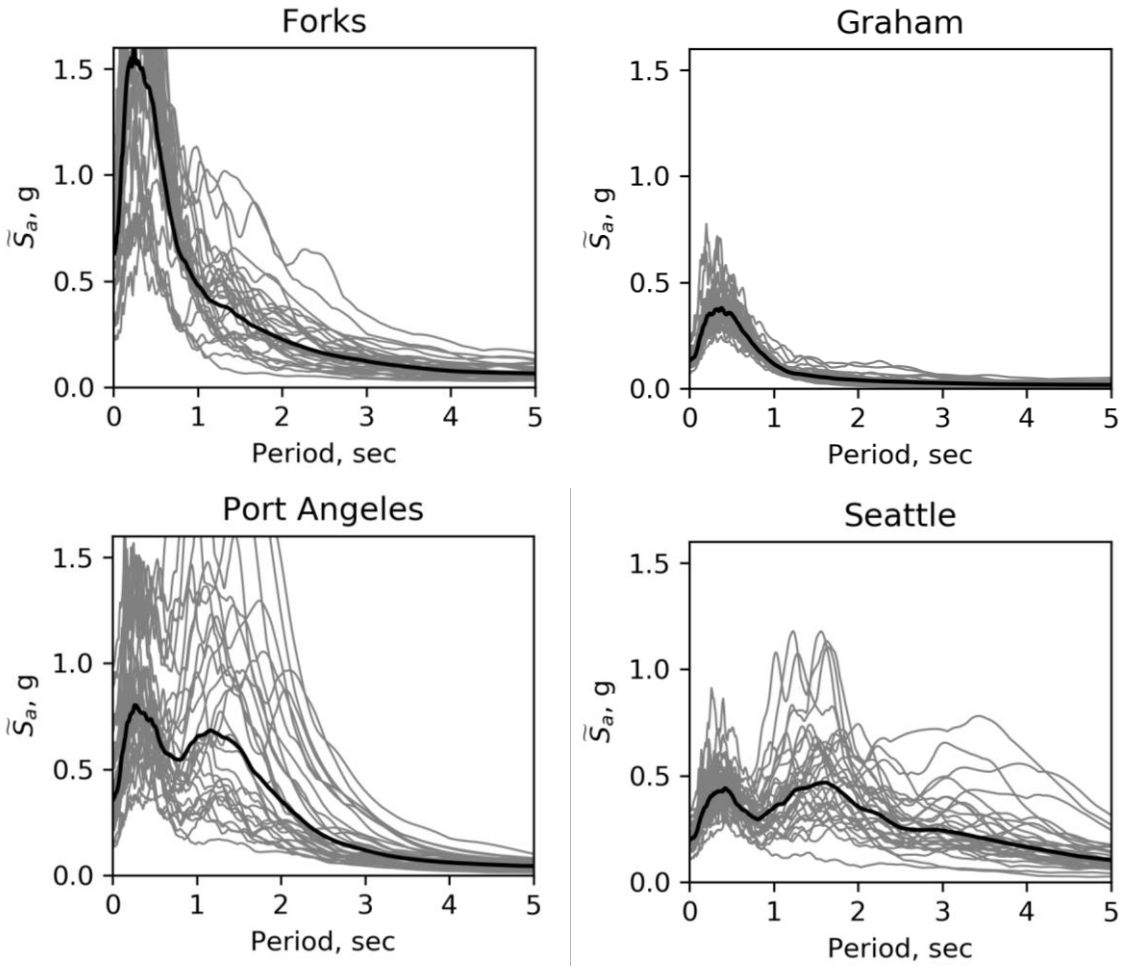

Figure 3.2. Representative Response Spectra from Baseline Simulated M9 Ground Motions

The spectral accelerations for the baseline simulated M9 ground motions were computed for each city at five periods: 0.2, 0.5, 1.0, 2.0, and 3.0 seconds. These accelerations were plotted in the same manner as the bridge design accelerations were plotted in Chapter 2 (with the cities arranged from west to east). Figure 3.3 shows that for periods of 0.2 and 0.5 seconds, the baseline M9 spectral acceleration decreases moving from west to east, with the 0.2-second values decreasing faster than the 0.5-second values.

The coastal cities without basin (Forks and Ocean Shores) experience the largest difference in spectral acceleration values between short periods and long periods, with the 0.2 second acceleration value being 6.8 times greater than the 2.0 second acceleration values for the city of

Forks. This is to be expected because neither one of these cities is on a basin, which means that their high short-period accelerations are attributed solely to their proximity to the fault (they both have an average closest distance to fault, $R_{cd,avg}$ of less than 30 km).

Apart from Port Townsend and Everett, the largest M9 spectral acceleration for the representative cities occurred at short periods (0.2 or 0.5 seconds). For cities west of Port Townsend the 0.2-second acceleration produces the highest baseline M9 spectral acceleration value, but for four out of the five remaining cities east of Port Townsend, the 0.5-second acceleration produces the highest spectral acceleration (Everett being the exception).

For long periods (1.0, 2.0, and 3.0 seconds) the variation in spectral acceleration is smaller, and for nine out of the ten cities the 1.0-second acceleration is the largest of the three. For the city of Everett, however, the largest baseline M9 acceleration occurs at a period of 2.0 seconds. The acceleration values at these three periods are largest for inland cities located in either deep or shallow sedimentary basins and smallest for the three inland without basin cities (Olympia, Vancouver, and Graham).

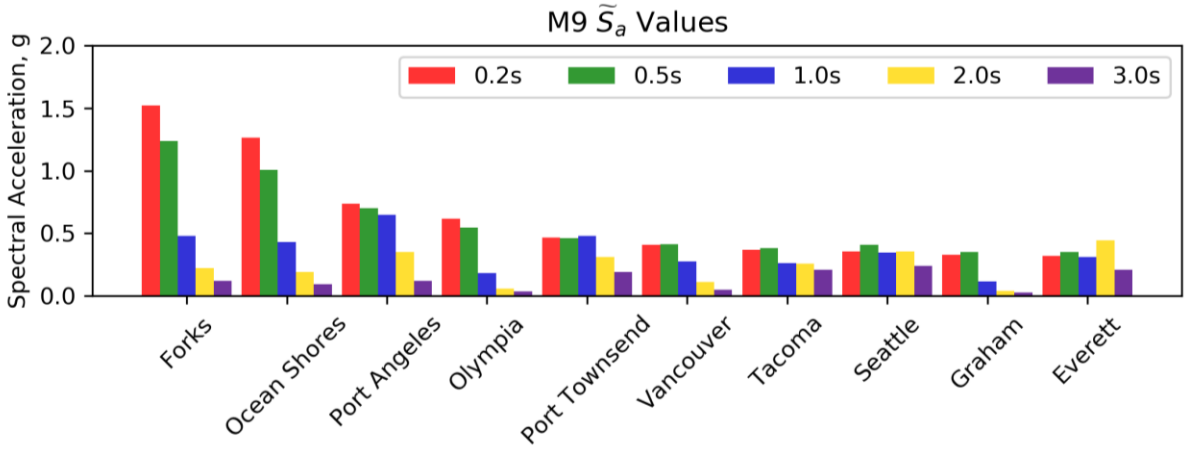

Figure 3.3. Washington Cities Baseline Simulated M9 Spectral Acceleration Values at Different Periods (Site Class C)

3.2 Variation of M9 Spectral Accelerations with Distance to Fault and Depth of Sedimentary Basin

The effect that proximity to the fault and sedimentary basin presence have on the baseline simulated M9 spectral accelerations are shown in Figure 3.4. Figure 3.4a shows how the simulated M9 spectral acceleration values (for V_{s30} = 600 m/s) vary as a function of $R_{cd,avg}$ for periods of 0.5, 1.0, and 2.0 seconds. Similarly, Figure 3.4b shows the baseline M9 spectral acceleration ratio between long period (either 1 or 2 seconds) and short period (0.5 seconds) as a function of $Z_{2.5}$ value. For both types of plots the cities of Seattle, Everett, Tacoma, and Olympia are labeled in order to easily observe what happens to a city that is the furthest away from the fault (Everett), a city that is located on a very deep basin (Seattle), a city that is on a basin with $Z_{2.5}$ less than 3 km (Tacoma), and the Washington state capitol (Olympia).

At a period of 0.5 seconds the M9 spectral accelerations decay in a trend that is similar to that observed for 0.2s in Figure 3.3, with Forks and Ocean Shores having the largest spectral acceleration values and Graham and Everett having the lowest. Because basin amplification effects are not present at this short period, the baseline simulated M9 spectral acceleration values can be represented with the following exponential best-fit line.

$$S_{0.5,Baseline} = 1.3\, e^{-\left(\frac{R_{cd,avg}}{90}\right)} \tag{3.1}$$

where, $S_{0.5,Baseline}$ is the baseline simulated M9 spectral acceleration value at 0.5 seconds, and $R_{cd,avg}$ is the average distance to the fault in km. The data at 1.0 and 2.0 seconds cannot be represented with a best-fit line based on $R_{cd,\text{avg}}$ alone because basin amplification effects occur at these periods.

Figure 3.4b show that the ratio between 2.0 seconds and 0.5 seconds increases faster than the ratio between 1.0 second and 0.5 seconds, which means that there is more sensitivity to value

of $Z_{2.5}$ for the 2.0-second spectral accelerations than the 1.0-second. This indicates that the presence of sedimentary basins has a greater effect in spectral acceleration values at a period of 2.0 seconds than 1.0 second. It is also interesting to note that the 1.0-second ratios are larger than the 2.0-second ratios, which indicate that the 1.0-second spectral accelerations are closer in value to the 0.5-second spectral accelerations (also seen in Figure 3.3).

The effect of sedimentary basins on M9 spectral acceleration ratio can be fit with bilinear relationships. In this case, the logarithmic ratio of long period to short period spectral acceleration increases with $Z_{2.5}$ values until a depth of 3 km is reached at which point the ratios can be assumed to stay constant at a value of 0.9. The best-fit lines for $\ln(S_{a,1.0}/S_{a,0.5})$ and $\ln(S_{a,2.0}/S_{a,0.5})$ are shown in Equation 3.2 and Equation 3.3, respectively.

$$\ln\left(\frac{S_{a,1.0}}{S_{a,0.5}}\right) = \begin{cases} -1.51 + 0.47\,Z_{2.5} & Z_{2.5} < 3 \\ 0.9 & Z_{2.5} \geq 3 \end{cases} \tag{3.2}$$

$$\ln\left(\frac{S_{a,2.0}}{S_{a,0.5}}\right) = \begin{cases} -2.30 + 0.73\,Z_{2.5} & Z_{2.5} < 3 \\ 0.9 & Z_{2.5} \geq 3 \end{cases} \tag{3.3}$$

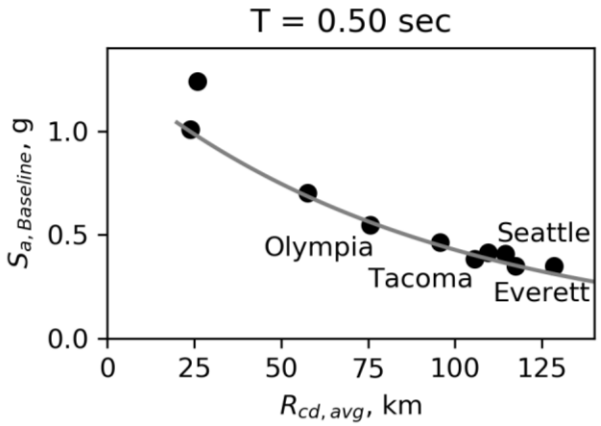

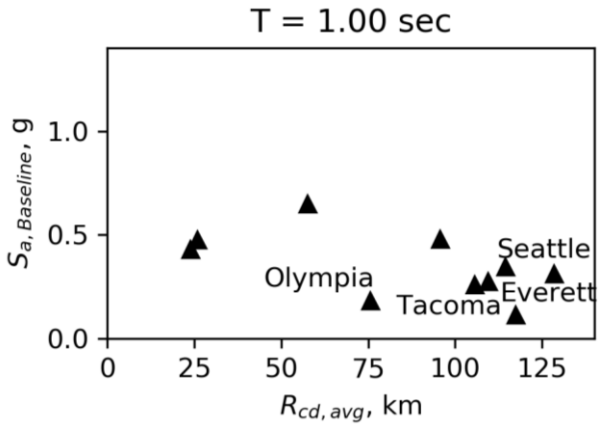

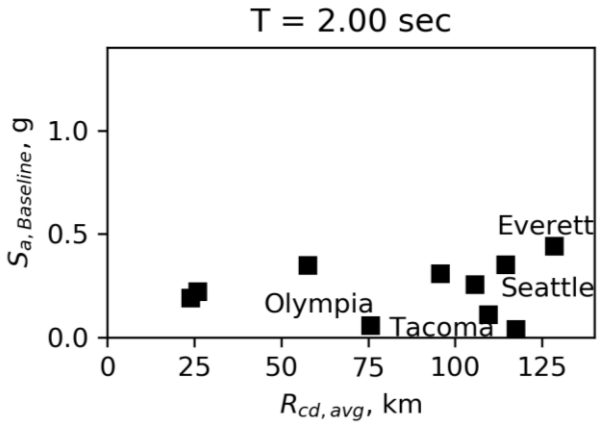

(a) Simulated M9 Spectral Acceleration as Function of Average Closest Distance to the CSZ Fault, $R_{cd.ava}$

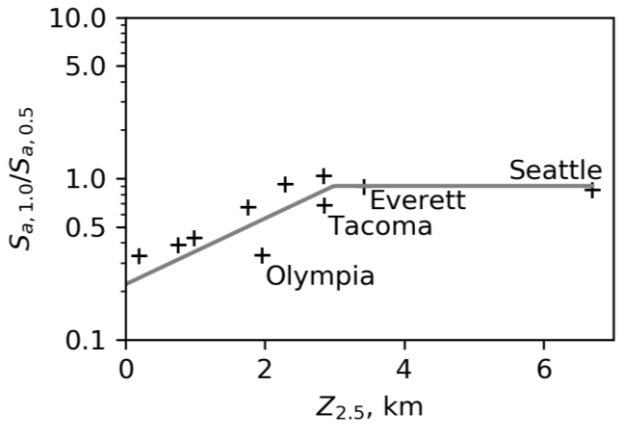

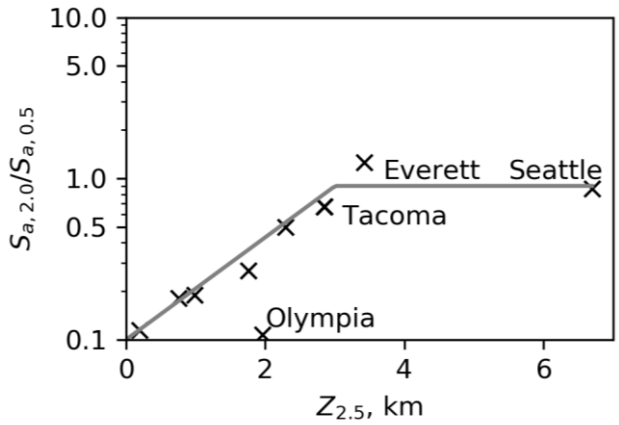

(b) Ratio of Long Period (1 or 2 sec) to Short Period (0.5 sec) Simulated M9 Spectral Acceleration as Function of $Z_{2.5}$ Depth

Figure 3.4. Effect of (a) $R_{cd,avg}$ and (b) $Z_{2.5}$ on Baseline Simulated M9 Spectral Accelerations

3.3 Comparison of M9 Simulations and Bridge Design Spectral Accelerations

The design spectral accelerations obtained from AASHTO-17 and WSDOT-18 specifications, as well as the spectral accelerations obtained from the baseline simulated M9 ground motions are shown in Figure 3.5. The figure compares the spectral accelerations at periods of 0.2, 1.0, and 2.0 seconds.

As a result of the 0.2-second accelerations decreasing moving from east to west, the baseline M9 spectral accelerations go from being greater than both bridge design values to being smaller than both of them. For example, the M9 acceleration for the city of Forks has a value of 1.52g, which is 1.24 times greater than the WSDOT-18 design acceleration and 1.5 times greater than the AASHTO-17 acceleration. In contrast, for the city of Everett, the M9 acceleration has a value of 0.32g, which is approximately 30% of the WSDOT-18 design acceleration and 35% of the AASHTO-17 value.

At a period of 2.0 seconds, a different trend is observed because cities located on basins have higher baseline M9 spectral acceleration values than either of the bridge design values. Here, the city of Everett has the largest difference between M9 and bridge design spectral acceleration values than any of the other cities of study, with the baseline M9 spectral acceleration being 2.4 times and 2.0 times the WSDOT-18 and the AASHTO-17 design accelerations, respectively. This figure highlights the importance of considering basin amplification when computing design spectral accelerations for long periods, because it shows that as of right now many of the long-period bridges located in cities with sedimentary basins are designed for smaller demands than those likely to occur during a M9 CSZ earthquake.

As the period increases, the geographical region in which the baseline M9 spectral acceleration exceeds that of any of the bridge designs accelerations shifts from the Pacific coastal region to the Puget Sound region, due to the basin's amplification of longer period accelerations. For a period of 0.2 seconds, the coastal cities without basin (Forks and Ocean Shores) have a baseline M9 acceleration that surpasses either one or both of the bridge design accelerations. For a period of 1.0 second, the M9 acceleration is higher for two of the three cities located on shallow sedimentary basins (Port Angeles and Port Townsend), but similarly to the trend observed at 0.2 seconds, the M9 accelerations do not surpass both bridge design accelerations for those cities. And for a period of 2.0 seconds, all the cities located on sedimentary basins have baseline M9 spectral acceleration values that are greater than both bridge design accelerations.

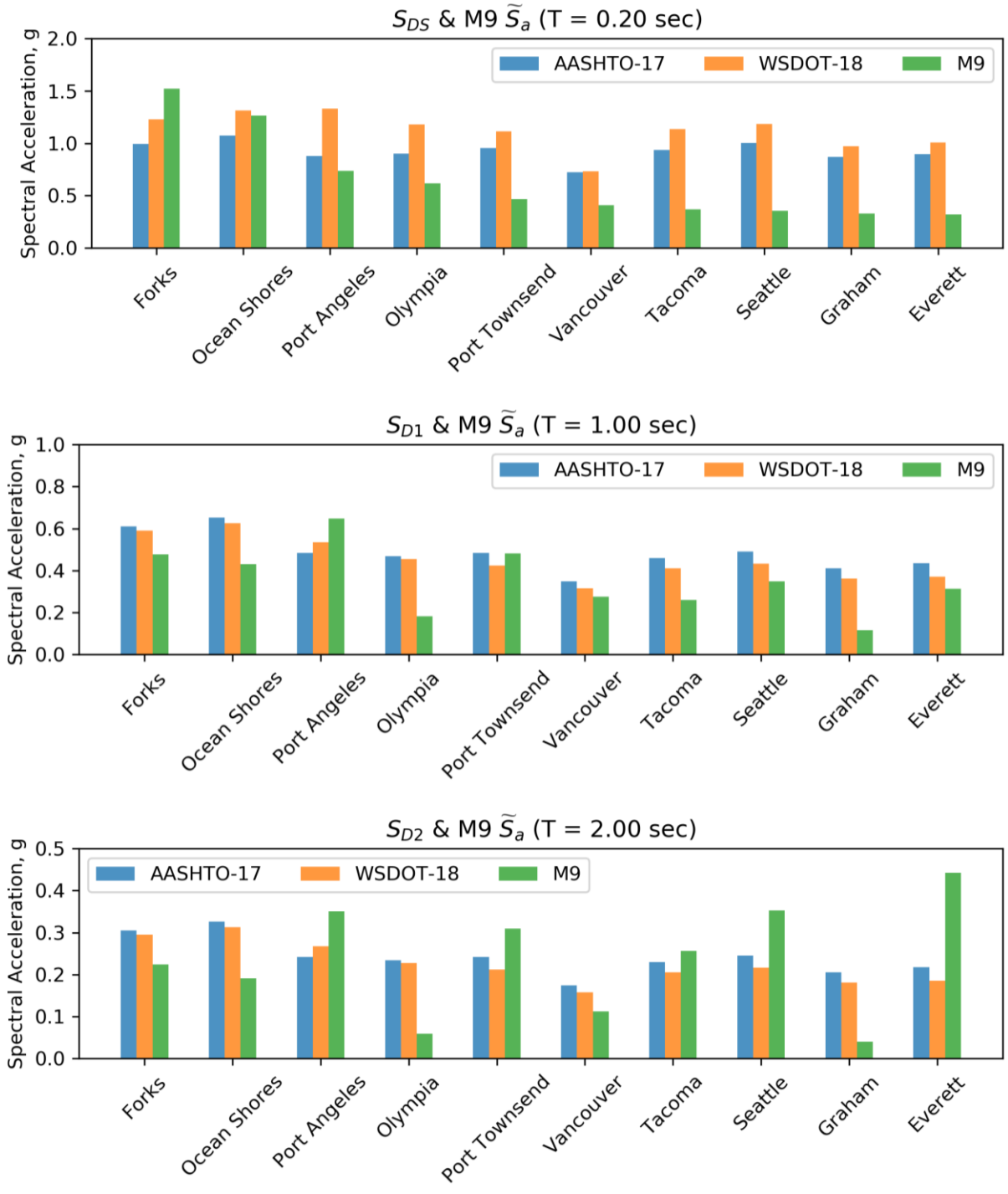

Figure 3.5. Washington Cities Bridge Design S_a and Baseline Simulated M9 $\widetilde{S_a}$ Values (Site Class C)

3.3.1 *Percent Difference*

The percent difference in spectral acceleration between the baseline simulated M9 motions and the AASHTO-17 and WSDOT-18 bridge design values can be seen in Figure 3.6. Positive percent difference indicates that the bridge design code accelerations are lower than the baseline simulated M9 accelerations. Comparing the M9 accelerations to AASHTO-17 shows that for a period of 0.20 seconds the M9 accelerations are approximately 50% smaller than the design accelerations (with the exceptions of Forks and Ocean Shores). For a period of 1.0-second, Port Angeles has a positive percent difference of 34% and Port Townsend has no significant difference, while the remaining cities have negative difference ranging from -22% to -72%. For the 2.0-second period, the M9 accelerations are 12% to 100% larger for the five cities located inside sedimentary basins.

Comparing the M9 accelerations to those obtained from WSDOT-18 show the same trends as the AASHTO-17 comparison. This comparison, however, resulted in more negative and less positive percent difference for 0.2 seconds. At 1.0 second, there is a reduction in the percent difference for the five cities located within sedimentary basins. At 2.0 seconds, the positive percent difference observed for the five basin cities is greater than it was for AASHTO-17, with Everett having a percent difference of +138%.

The side-by-side comparisons from Figure 3.6 show both the AASHTO-17 and WSDOT-18 design accelerations are closer in value to the baseline simulated M9 spectral accelerations at a period of 1.0 second. The comparison also shows that at a short period, AASHTO-17 design values for Forks and Ocean Shores (coastal cities without basin) are smaller than the expected M9 values, which results in large positive percent difference and indicates that short-period bridges in these areas could experience significant damage. The WSDOT-18 comparison shows

that Port Angeles and Port Townsend (inland cities on shallow sedimentary basins) have 1-second baseline simulated M9 spectral accelerations that are at most 30% larger than the design acceleration. Both graphs show that the impact that a magnitude-9 earthquake would have on the state of Washington is most concerning at long periods (2.0 seconds) and for cities that are located in either shallow or deep sedimentary basin areas (Puget Sound Region).

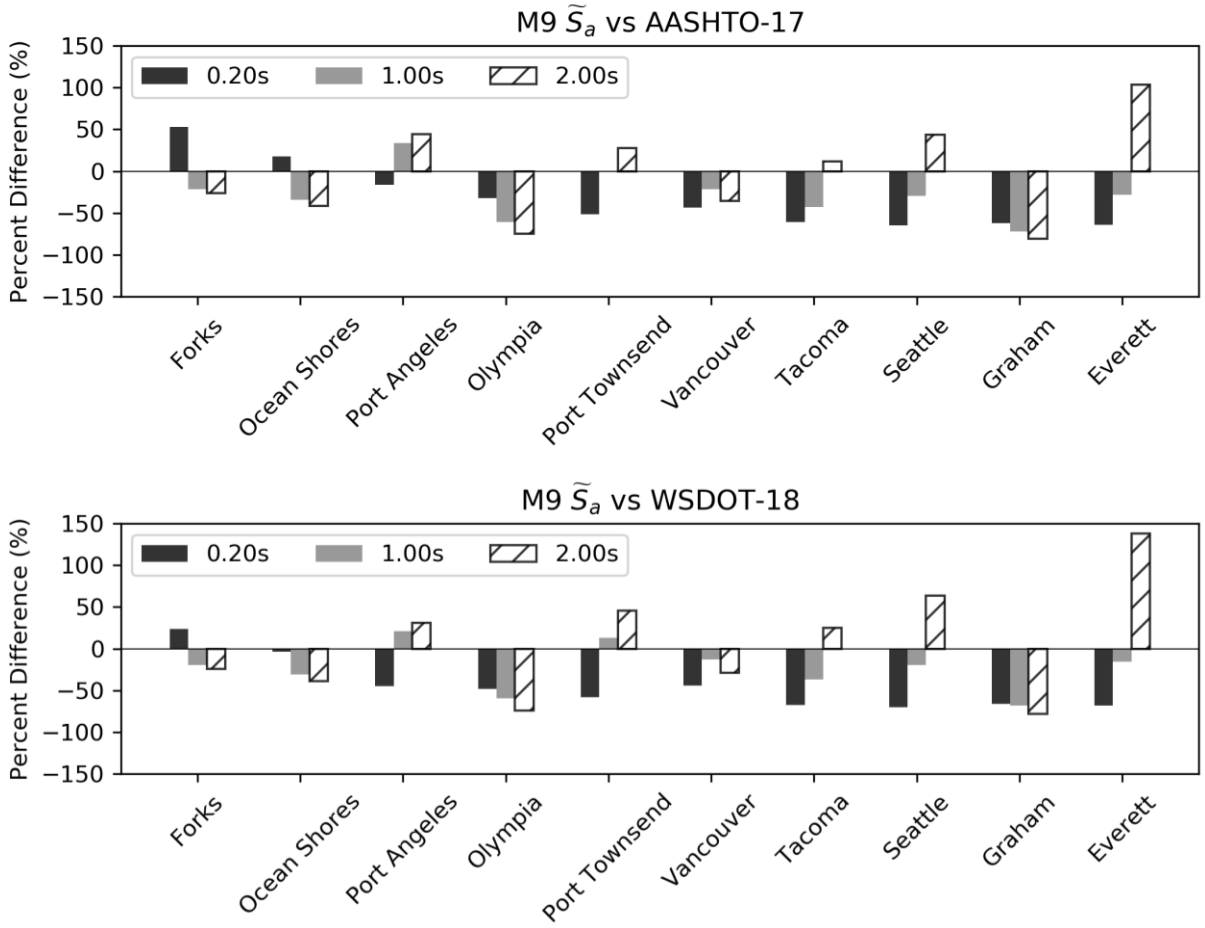

Figure 3.6. Washington Cities Percent Difference Between Baseline Simulated M9 $\widetilde{S_a}$ and Bridge Design *Sa* Values

3.4 Comparison of M9 and Current Washington Bridge Design Spectral Accelerations

The baseline simulated M9 spectral accelerations values for the two orthogonal directions were separated and compared against the spectral accelerations obtained from WSDOT-18 to closely understand the effect that a magnitude-9 earthquake would have on newer bridges and to understand if the direction of the simulated M9 motions differed between the North-South, NS, and East-West, EW, direction. Box-and-whisker plots indicating the 10%, 50%, and 90% percentile spectral acceleration values from the 30 realizations for 0.2, 1.0, and 2.0 seconds can be seen in Figure 3.7. The solid red line seen in each plot represents the WSDOT-18 design spectral accelerations for that period and this value is the same regardless of direction. The plots seen in this figure show similar results to those observed in Figure 3.5 because observing where the red line is in relation to the median of the box-and-whisker indicates if the baseline M9 spectral accelerations surpass the design value.

As mentioned previously, the values for the baseline simulated M9 spectral accelerations are not alarming at a period of 0.2 seconds (except for coastal cities without basin) but do cause concern at a period of 2.0 seconds in the basin areas of the Puget Sound. Figure 3.7 shows that at 2.0 seconds, over 50% of the ground motion realizations are producing M9 values greater than the WSDOT-18 value, and in the most extreme cases, which are seen in Seattle and Everett, 90% of the realizations exceed the design value.

There is an observable difference in baseline M9 spectral acceleration values due to orientation. For all three periods, the values obtained from the North-South direction are greater and have more variability than those obtained from the East-West direction. At 1.0 and 2.0 seconds, the greatest spectral acceleration values and the largest variability can be seen in Port

Angeles. At 2.0 seconds cities that had relatively low variability and similar box-and-whisker plots at 0.2 and 1.0 seconds, such as Tacoma, Seattle, and Everett, exhibit dramatic changes in spectral acceleration and variability, and differ more with direction. The analysis conducted in the following chapters only uses the North-South direction due to this being the stronger direction.

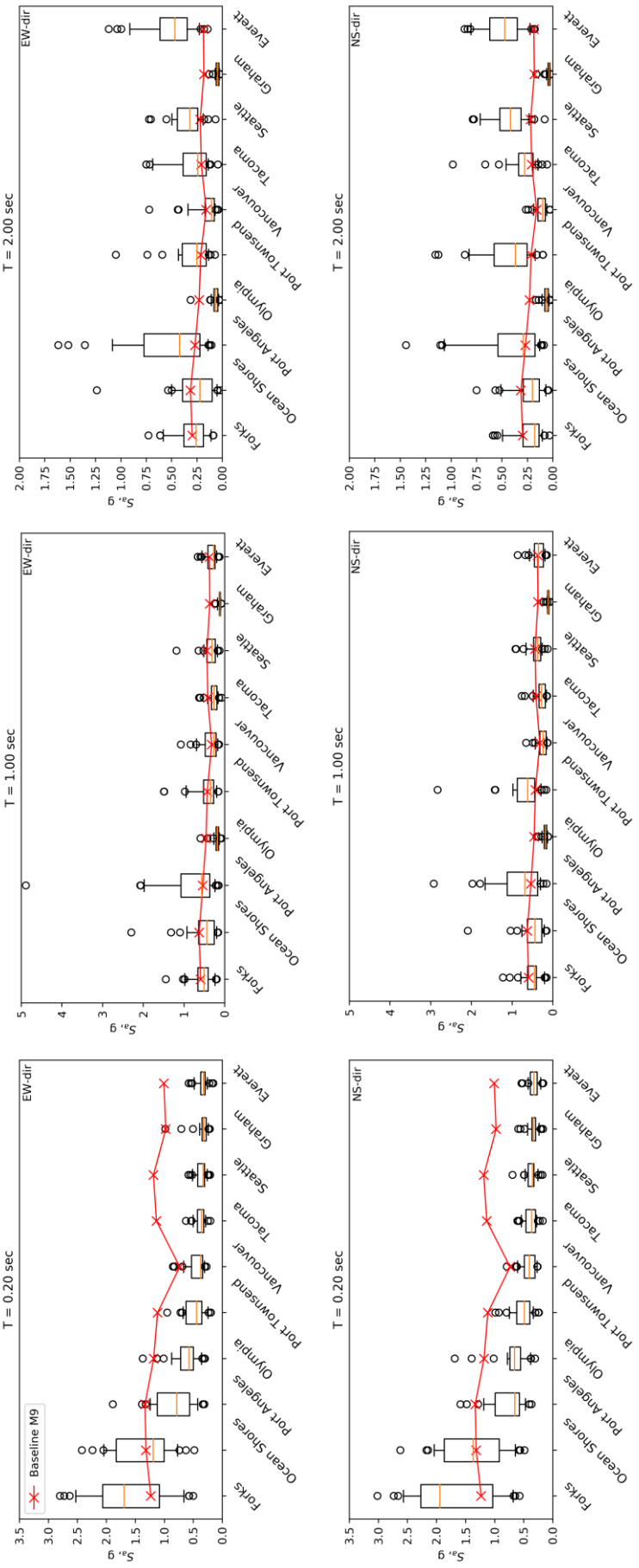

Figure 3.7. Washington Cities WSDOT-18 Design S_a (Site Class C) and Baseline Simulated M9 Accelerations for period of 0.2, 1.0, and 2.0 seconds

Chapter 4. EFFECTS OF SOIL CONDITIONS ON SIMULATED M9 GROUND MOTIONS

The modifications made to the baseline M9 ground motions, described in this chapter, to obtain ground motions that represented local soil conditions were largely done by project collaborator Alex Grant of the USGS. The process is summarized here to provide proper context in subsequent chapters that use the soil-adjusted ground motions.

The soil classes found in the State of Washington range from NEHRP Site Class B to F (Palmer et al. 2007). For this reason, utilizing the baseline simulated M9 ground motions (V_{S30} = 1968 ft./s [600 m/s], Site Class C) from Chapter 3 to study the effects of a magnitude-9 earthquake on different locations throughout Washington state does not reflect the actual variation of local soil conditions. In addition, it is known that many state bridges are founded on poor soils, i.e., site classes D to F. Figure 4.1 shows the site class map for King County, WA. The figure shows that the soil in Seattle is predominantly Site Class C (indicated as light green), but it can also be seen that parts of I-5, I-405, and I-90 are on soils characterized as Site Class D to E (indicated as light orange).

This chapter discusses the methodology followed to adjust the simulated M9 ground motions for softer soil sites, which include four subcategories of Site Class C (C1 – C4), three subcategories of Site Class D (D1 – D3), and one of Site Class E. The chapter also discusses the profiles selected for the parametric study (Chapter 6), and the site amplifications obtained between the soil-adjusted and baseline simulated M9 ground motions for the North-South direction.

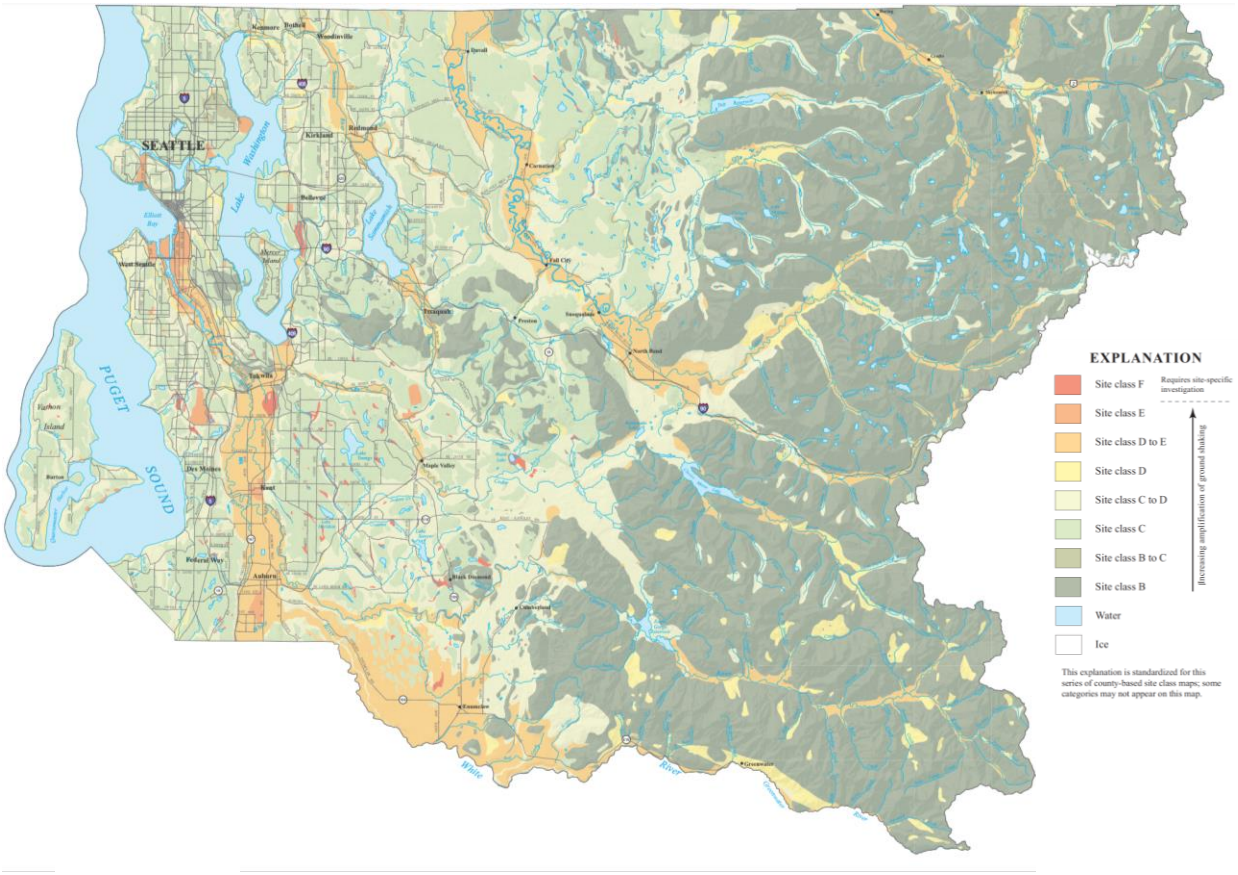

Figure 4.1. Site Class Map of King County, Washington (Figure from Palmer et al. 2007)

4.1 METHODOLOGY

The soil-adjusted simulated M9 ground motions were generated through equivalent linear site response analyses using Pacific Northwest, PNW, shear-wave velocity profiles compiled by Ahdi et al. (2017)[1]. The PNW profile dataset was processed to remove profiles that were shallower than 32.8 ft. [10 m] (due to insufficient data) and deeper than 3281 ft. [1000 m] (due to insufficient resolution). The reduced dataset was analyzed for the two horizontal directions of the thirty baseline simulated M9 ground motions at the ten cities of study. Figure 4.2 shows the number of profiles available for site classes A-E before and after the profile dataset was reduced.

[1] The generation of the soil-adjusted M9 ground motions was performed by Alex Grant from USGS.

The baseline simulated M9 ground motions were input at the base of all the considered soil profiles from a dimensionless linear stiff (rock) layer with 1% damping and an average shear-wave velocity in the upper 30 meters, V_{s30}, of 1968 ft./s [600 m/s]. The reduced profiles were read layer by layer from the ground surface. In order to generate the soil-adjusted simulated M9 ground motions corresponding to sites with V_{S30} less than 2362 ft./s [720 m/s] (part of Site Class C1 and all of C2 – E) the entire profile was used and appended with a rock input base. A shear-wave velocity of 2362 ft./s [720 m/s] was selected as a threshold to prevent very large velocity inversions over the 1968 ft./s [600 m/s] input from the baseline ground motions.

Two Site Class C (C2 and C4) and two Site Class D (D1 and D3) V_{s30} ranges were selected and used to observe the effects of different soil conditions on the simulated M9 ground motions. These four soil classes are used in the parametric study conducted in Chapter 6, and they were selected because they correspond to the common V_{s30} ranges for the State of Washington.

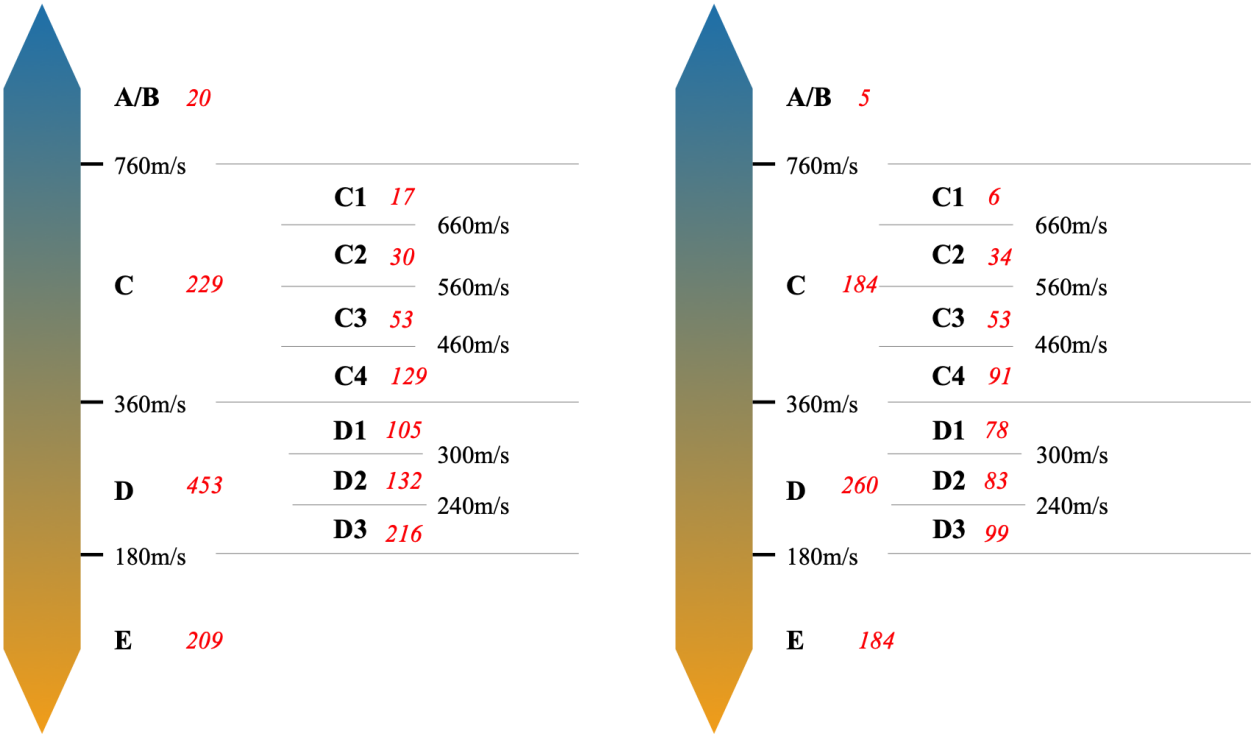

a) Full Set of Profiles b) Reduced Set of Profiles

Figure 4.2. Data Available from Ahdi et al. for PNW Velocity Profiles (Figure by A. Grant)

Due to the different number of profiles available in each soil class (Figure 4.2b), 30 profiles were randomly selected from each of the four soil classes to ensure that the amplification effects observed were not due to differences in the number of profiles. Table 4.1 lists the 30 profiles that were used for each selected site class.

Table 4.1. List of Selected Soil Profiles

SOIL TYPE			
C2	**C4**	**D1**	**D3**
WA-DNR-08_87	7026	WA-DNR-08_210	DOGAMI-13_196
WA-DNR-08_90	WA-DNR-08_69	WA-DNR-08_24	WA-DNR-08_196
WA-DNR-08_41	KIMB-1	WA-DNR-08_68	DOGAMI-13_179
SFER	WA-DNR-08_91	DOGAMI-13_255	SCPT94-1
WA-DNR-08_57	WA-DNR-08_14	DOGAMI-13_74	DOGAMI-13_233
WA-DNR-08_164	PCFR	WA-DNR-08_39	FD86-4
WA-DNR-08_161	DOGAMI-13_132	WA-DNR-08_171	DOGAMI-13_131
ALKI	WA-DNR-08_20	7041	DOGAMI-13_223
GL2	WISH	DOGAMI-13_89	SCP95-24
WA-DNR-08_85	WA-DNR-08_73	LAWT	DOGAMI-13_123
BUCK	DOGAMI-13_79	WA-DNR-08_97	WA-DNR-08_225
HAO	DOGAMI-13_146	7043	DOGAMI-13_180
LTY	WA-DNR-08_12	WA-DNR-08_172	DOGAMI-13_141
DOGAMI-13_102	WA-DNR-08_45	WA-DNR-08_165	WA-DNR-08_190
WA-DNR-08_21	WA-DNR-08_217	ROSS	FD97-5
WA-DNR-08_77	LANE	DOGAMI-13_187	WA-DNR-08_143
WA-DNR-08_231	WA-DNR-08_28	WA-DNR-08_123	WA-DNR-08_5
WA-DNR-08_3	WA-DNR-08_75	DOGAMI-13_106	DOGAMI-13_20
WA-DNR-08_26	WA-DNR-08_187	DOGAMI-13_78	DOGAMI-13_38
BEVT	MRIN	WA-DNR-08_121	WA-DNR-08_232
WA-DNR-08_62	DOGAMI-13_76	WA-DNR-08_65	DOGAMI-13_181
WA-DNR-08_128	WA-DNR-08_175	WA-DNR-08_129	DOGAMI-13_98
WA-DNR-08_176	WA-DNR-08_219	WA-DNR-08_33	DOGAMI-13_31
WA-DNR-08_44	WA-DNR-08_81	WA-DNR-08_208	DOGAMI-13_28
WA-DNR-08_36	DOGAMI-13_114	7027-A	WA-DNR-08_46
WA-DNR-08_6	WA-DNR-08_83	DOGAMI-13_164	WA-DNR-08_199
LYNC	7034	DOGAMI-13_150	WA-DNR-08_115
WA-DNR-08_18	QKTN	2172	WA-DNR-08_234
ERW	WA-DNR-08_151	WA-DNR-08_169	DOGAMI-13_64
BH_DEEPBH	SEW	WA-DNR-08_48	KNEL

4.2 Site Amplification from Spectral Accelerations for Soil-Adjusted M9 Ground Motions

The response spectra generated from the soil-adjusted and baseline simulated M9 ground motions, as well as the amplification ratio, denoted as $S_{a,SoilClass}/S_{a,Baseline}$, obtained between the soil-adjusted, $S_{a,SoilClass}$, and baseline, $S_{a,Baseline}$, M9 ground motions were plotted for periods of 0-4 seconds for all cities of study for the NS direction (Appendix D). The median response spectra obtained from all the ground motion realizations and selected profiles can be seen on the top plot, and the median amplification ratio (with respect to the baseline simulated ground motions) can be seen on the bottom plot.

Figure 4.3 shows the plots obtained for the city of Forks, Port Angeles, Seattle, and Graham. For all cities, the shape of the C2 response spectra is closest to the baseline simulated response spectra. This was to be expected because the V_{S30} for the baseline ground motions is 600 m/s, which falls into the shear-wave velocity range of Soil Class C2. It can also be seen that for all cities the amplification ratios converge to 1.0 as the period increases. This happens because at very long periods, all of the soil profiles behave like rigid bodies regardless of their stiffness.

Figure 4.3 also shows that significant deamplification is present in the D3 ground motions at periods smaller than 0.4 seconds for Forks. Appendix D shows that the same occurs at Ocean Shores, which serves as an indicator that the input motions for coastal cities without basin are rather large and potentially exceed the range of the equivalent linear analysis. Furthermore, Forks has the longest period at which the amplification for the C2, C4, and D1 ground motions begins to converge to 1.0 – approximately 3 seconds.

Port Angeles and Seattle are the two cities shown that are in sedimentary basins and the difference in the response spectra from a shallow sedimentary city and a deep sedimentary city is

most evident in the D3 ground motions. The response spectra for deep basin cities (Seattle) is characterized by slight deamplification for the D3 motions for periods between 0.1 and 0.5 seconds, followed by amplification from 0.5 to 1 second (due to basin amplification effects), and finished by rapid deamplification. The response spectra for shallow basin cities (Port Angeles) have large deamplification between 0.1 and 0.5 seconds for the D3 ground motions, followed by a longer period of amplification, and finished by slow deamplification of the D3 ground motions. Both sedimentary basin groups, however, have the shortest period at which the amplification from the C2, C4, and D1 ground motions begin to stabilize around 1.0 (around 1.5s for deep basin cities and 2.0s for shallow basin cities). Appendix D shows that the response spectra for Tacoma resembles more that of a deep sedimentary basin city despite being categorized as a shallow sedimentary basin city. This is a result of the 3D effects mentioned in Chapter 3, which cause Tacoma to be an outlier of its city classification.

Inland cities without basin, such as Graham, have the highest amplification from the D3 ground motions at periods between 0.5-1.5 seconds despite the response spectra being relatively small. As it can be seen from Figure 4.3, the amplification for the C2, C4, and D1 ground motions begin to converge at around the same period as shallow basin cities, but unlike the shallow basin cities the deamplification for the D3 motions is much faster.

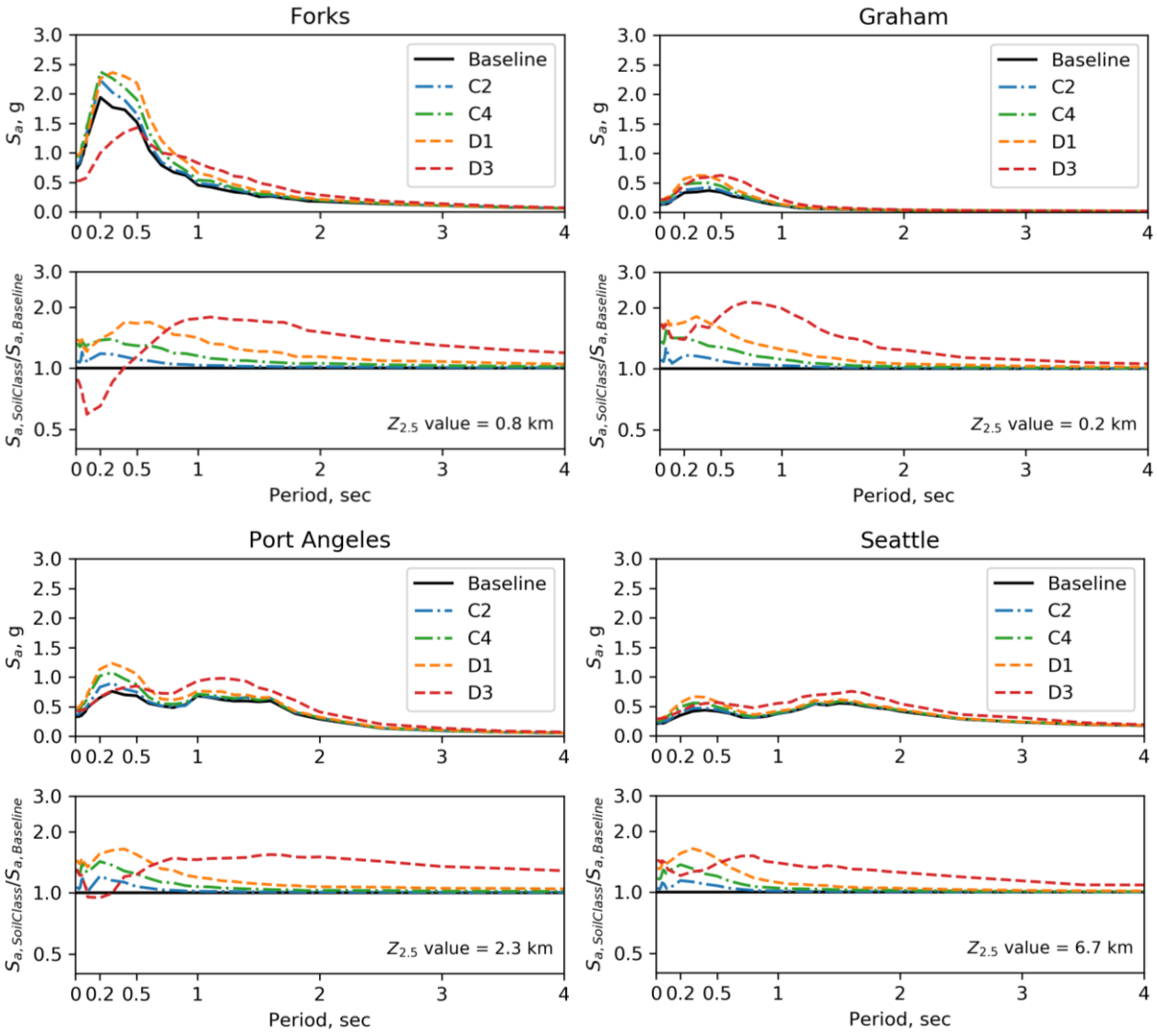

Figure 4.3. Median Response Spectra and Amplification Between Baseline and Soil-Adjusted Simulated M9 Ground Motions

4.3 Effects of Baseline Ground Motion Strength and Shape on Amplification of Soil-Adjusted M9 Motions

The effects of the strength of the baseline simulated ground motions on the soil amplification can be seen on Figure 4.4a for the C2 and D3 soil-adjusted ground motions for

periods of 0.5, 1.0, and 2.0 seconds. For those same soil classes and periods, the effect of the long period to short period baseline ratio, known as the spectral shape, on the amplification in the soil-adjusted ground motions can be seen on Figure 4.4b. Similar to the plots from Chapter 3, both figures label the values corresponding to Seattle, Tacoma, Everett, and Olympia. Neither figure, however, establishes a clear trend between amplification and baseline strength or amplification and baseline spectral shape.

Figure 4.4a shows that the largest amplification variability amongst the ten cities occurs at a short period and for the D3 ground motions. At 0.5 seconds, strong baseline spectral accelerations result in the lowest amplifications for the D3 simulated ground motions and the highest amplifications for C2. Increasing the period from 0.5 to 1.0 second, minimally changes the amplifications for the D3 motions for the two deep basin cities – Everett remains the same, but Seattle increases slightly – while the other eight cities increase in amplification. At 1.0 second, the amplifications for the C2 ground motions decrease slightly as the baseline spectral acceleration increases, but for all ten cities the ratios are essentially 1.0. For the amplifications for the D3 motions, their values also decrease as baseline acceleration increases. At a period of 2.0 seconds, however, the amplification for the D3 ground motion drops for all four cities labeled, and the two deep basin cities (along with Tacoma) have the lowest amplification values. In this case, the amplifications for the D3 motions increase for baseline spectral accelerations between 0 – 0.25g and decrease for greater spectral accelerations. Furthermore, the C2 amplifications are stable around 1.0, which indicates that there are no amplification effects between the soil-adjusted and baseline spectral accelerations.

The amplification trend for the C2 soil-adjusted ground motions with respect to the baseline spectral shape is very similar to the trend observed in Figure 4.4a. Figure 4.4b shows that as the

period increases, the amplification for the C2 motion has a reduction in variability (for all cities) and stabilizes around 1.0 at a period of 2.0 seconds for all baseline spectral shape values. For the D3 soil-adjusted ground motions, the largest range of amplification values occurs at a period of 0.5 seconds, where all four of the indicated cities have values higher than 1.4. At 1.0 second the amplification values for all representative cities are between 1.4 and 2.0. At this period, the smallest amplifications occur at Seattle and Everett (the two deep basin cities), and one of the highest amplifications occurs at Olympia (an inland with no basin city). However, because the amplification for Tacoma is higher than that for Seattle and Everett it is not possible to establish a trend between amplification and spectral shape in terms of how it affects cities located inside deep sedimentary basins and those located outside basin areas. At the longest period, 2.0 seconds, the two deep basin cities (and Tacoma) have the largest spectral shape values, but some of the lowest amplifications. The low amplifications are a result of the quick convergence to 1.0 from deep basin cities that was observed in Figure 4.3.

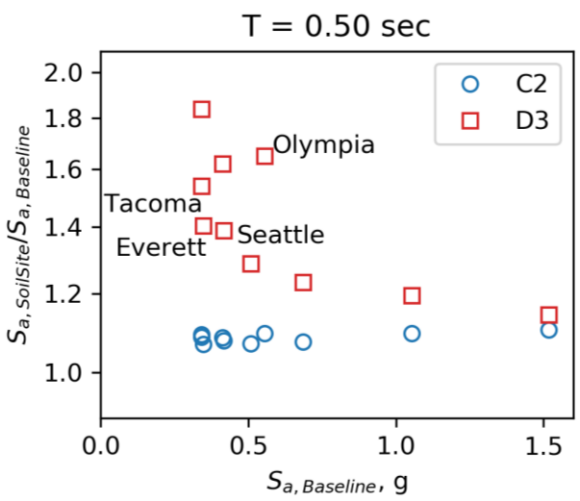

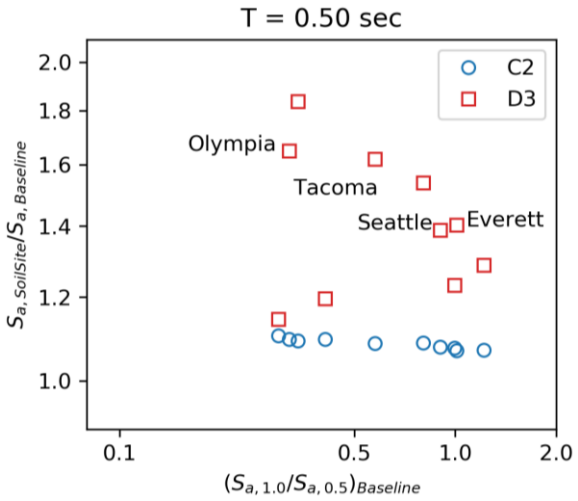

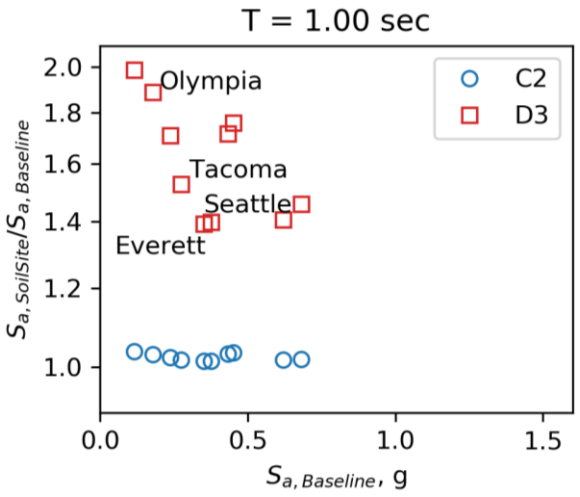

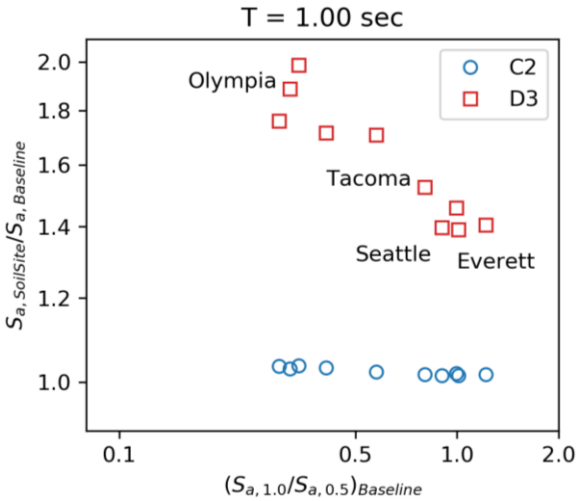

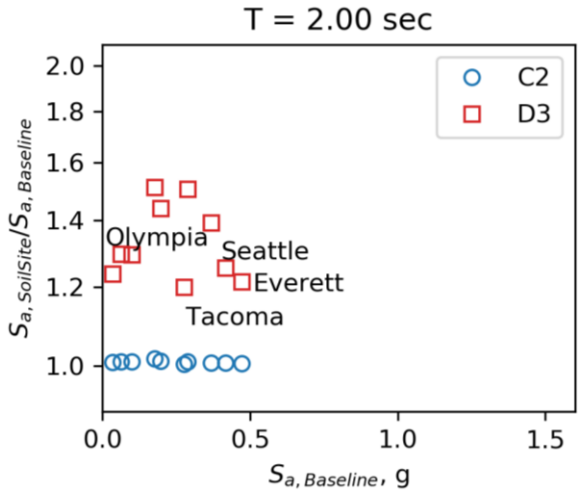

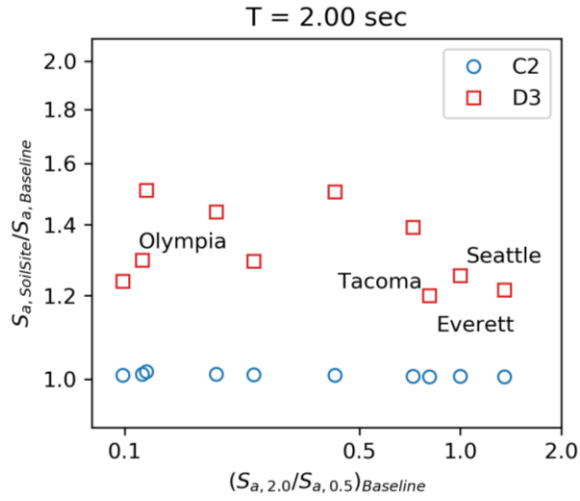

(a) Amplification of Soil-Adjusted M9 Ground Motions as Function of Baseline M9 $\widetilde{S_a}$

(b) Amplification of Soil-Adjusted M9 Ground Motions as Function of Ratio of Long Period to Short Period M9 $\widetilde{S_a}$

Figure 4.4. Soil-Adjusted Amplifications due to Baseline M9 (a) Strength and (b) Shape

Chapter 5. METHODOLOGY FOR SINGLE-DEGREE-OF-FREEDOM OCSILLATOR PARAMETRIC STUDY

This chapter discusses the methodology for conducting the single-degree-of-freedom, SDOF, parametric study, for which results are described in Chapter 6. The parametric study considered the following parameters:

- 30 M9 ground motion realizations (Chapter 1);
- 1 ground motion direction: NS;
- 10 locations (Table 2.1);
- 4 soil classes: C2, C4, D1 and D3 (Chapter 4);
- 30 soil profiles per site class (Chapter 4);
- 3 types of SDOF oscillators: Elastic Perfectly-Plastic, IMK without degradation and IMK with degradation (Section 5.2); and
- 4 oscillator natural periods (0.2s, 0.5s, 1.0s, and 2.0s).

Considering all combinations of the above parameters, the parametric study consisted of 432,000 outcomes. The results of each analysis were summarized in terms of:

- The displacement ductility demand, D/D_y, where D is maximum deformation and D_y is deformation at yield;
- The normalized SDOF force, F/F_y, where F is maximum force and F_y is force at yield;
- The yield force, F_y;
- The deformation at yield, D_y; and

- In the case of the IMK SDOF systems information on whether the system collapsed under the ground motion.

Section 5.1 describes the three types of oscillators and how the properties of the oscillators were determined, and Section 5.2 gives examples of the behavior of each oscillator. The parametric study was performed using the computational resources of the Stampede2 supercomputer at The University of Texas at Austin's Texas Advanced Computer Center (TACC). A fourth SDOF system, a linear oscillator, is described in Appendix E.

5.1 OSCILLATOR PROPERTIES

Three types of single-degree-of-freedom, SDOF, systems were used in the parametric study. The three systems modeled were: (1) Elastic Perfectly-Plastic, abbreviated as EPP, (2) Modified Ibarra-Medina-Krawinkler without cyclic deterioration, hereby abbreviated as IMK – No Cyclic Det., and (3) Modified Ibarra-Medina-Krawinkler with cyclic deterioration, hereby abbreviated as IMK – Cyclic Det. Both Modified Ibarra-Medina-Krawinkler oscillators utilized the same backbone, but with different cyclic deterioration parameters.

Figure 5.1 shows the backbone curves and defining properties of each spring system, and Section 5.2 explains each of the backbones and provides examples of the spring force versus displacement curves obtained for a particular city, realization, period, direction, and soil type.

For each model, the elastic stiffness of the spring, k, was determined from the period, T, and mass, m (Equation 3.1).

$$k = \left(\frac{2\pi}{T}\right)^2 \cdot m \tag{5.1}$$

The yield force, F_y, and the deformation at yield, D_y, were determined by Equation 5.2 and Equation 5.3, respectively.

$$F_y = \Omega \cdot m \cdot g \cdot S_{a,DBE} = \Omega \cdot m \cdot g \cdot \frac{C_{sm}}{R} \quad (5.2)$$

$$D_y = \frac{F_y}{k} \quad (5.3)$$

where g is the gravitational constant, and Ω is the design and material overstrength factor, taken as 1.5 (Marafi et al. 2019). Because the focus of the parametric study is to determine the impact of the simulated M9 ground motions on modern bridges, $S_{a,DBE}$ is calculated according to WSDOT-18 (Chapter 2), and it is dependent on site class. $S_{a,DBE}$ is equal to the quotient of the elastic seismic response coefficient, C_{sm}, (AASHTO 2017 ∮ 3.10.42) and the force reduction factor, R, taken to be a typical value 5 for bridge bents (WSDOT BDM 2018).

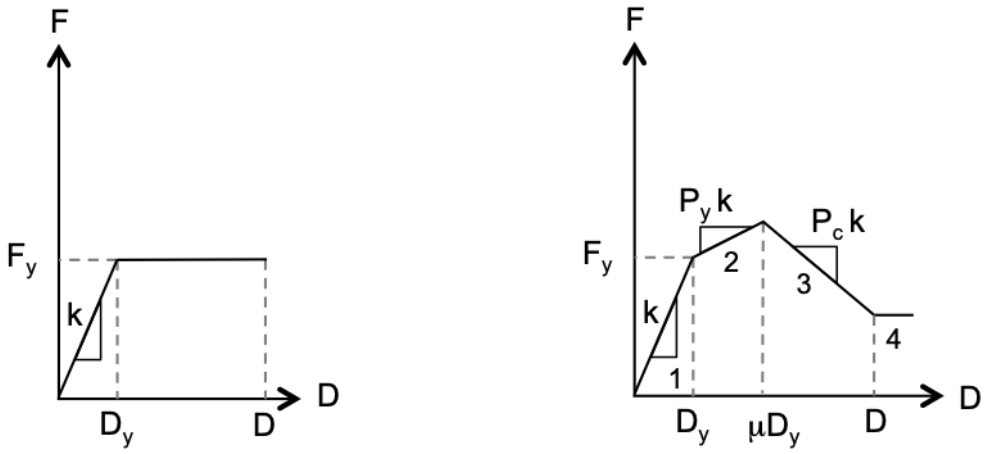

a) EPP b) IMK

Figure 5.1. SDOF Spring System Backbones

All three systems were assigned a nominal mass of 1, but the strength of the oscillator, F_y, varied depending on the location, period, and soil conditions being analyzed. Table 5.1 shows the normalized base-shear strength, F_y/W, values for all ten representative cities for periods of 0.2, 0.5, 1.0, and 2.0 seconds for Site Class C and Site Class D soils. The four periods were selected

because, as Chapter 3 explained, at short periods (0.2 and 0.5 seconds) cities closer to the Pacific coast are expected to have high M9 spectral accelerations, and at periods of 1.0 second or longer cities located on sedimentary basins are expected to experience basin amplification effects. Note that when analyzing oscillator response for the baseline M9 ground motions, Site Class C was used to determine the oscillator strength because the V_{S30} used to generate those motions (1968.5 ft./s [600 m/s]) is within the V_{S30} range for Site Class C.

Table 5.1. F_y/W for Washington Cities at Four Periods of Interest

City	S_s	S_1	Site Class C 0.2s	Site Class C 0.5s	Site Class C 1.0s	Site Class C 2.0s	Site Class D 0.2s	Site Class D 0.5s	Site Class D 1.0s	Site Class D 2.0s
Forks	1.025	0.394	0.369	0.355	0.177	0.089	0.335	0.335	0.225	0.113
Ocean Shores	1.096	0.416	0.394	0.375	0.187	0.094	0.349	0.349	0.235	0.117
Port Angeles	1.110	0.357	0.400	0.321	0.160	0.080	0.352	0.352	0.208	0.104
Olympia	0.984	0.303	0.354	0.272	0.136	0.068	0.327	0.327	0.181	0.091
Port Townsend	0.930	0.283	0.335	0.255	0.127	0.064	0.315	0.315	0.173	0.086
Vancouver	0.578	0.210	0.220	0.189	0.095	0.047	0.232	0.232	0.137	0.069
Tacoma	0.945	0.274	0.340	0.247	0.123	0.062	0.318	0.318	0.169	0.084
Seattle	0.988	0.288	0.356	0.259	0.129	0.065	0.327	0.327	0.175	0.087
Graham	0.811	0.241	0.292	0.217	0.108	0.054	0.286	0.286	0.075	0.076
Everett	0.837	0.247	0.301	0.223	0.111	0.056	0.293	0.293	0.156	0.078

5.2 OSCILLATOR BEHAVIOR

5.2.1 *Elastic Perfectly-Plastic System*

The Elastic Perfectly-Plastic, EPP, system introduces some nonlinear behavior into the spring. The spring material model used for this system was the Elastic-Perfectly Plastic Material (OpenSees, McKenna, 2012). Figure 5.1.a shows that the spring starts off with an elastic stiffness, but after F_y is reached, the strength in the system plateaus and remains constant at F_y,

independent of level of deformation. This type of system typically resulted in slightly higher ductility demand values than the linear system (Appendix E).

Figure 5.2 shows the oscillator results for the City of Seattle, for Site Class C, at a period of 1.0 second, in the North-South direction, and for a single realization (csz005). The figure shows the time history plot of the input acceleration, a_g, the acceleration of the mass, a, normalized spring force, f_s/f_y, and displacement ductility demand, d/d_y. It also shows the normalized spring force versus ductility demand curve.

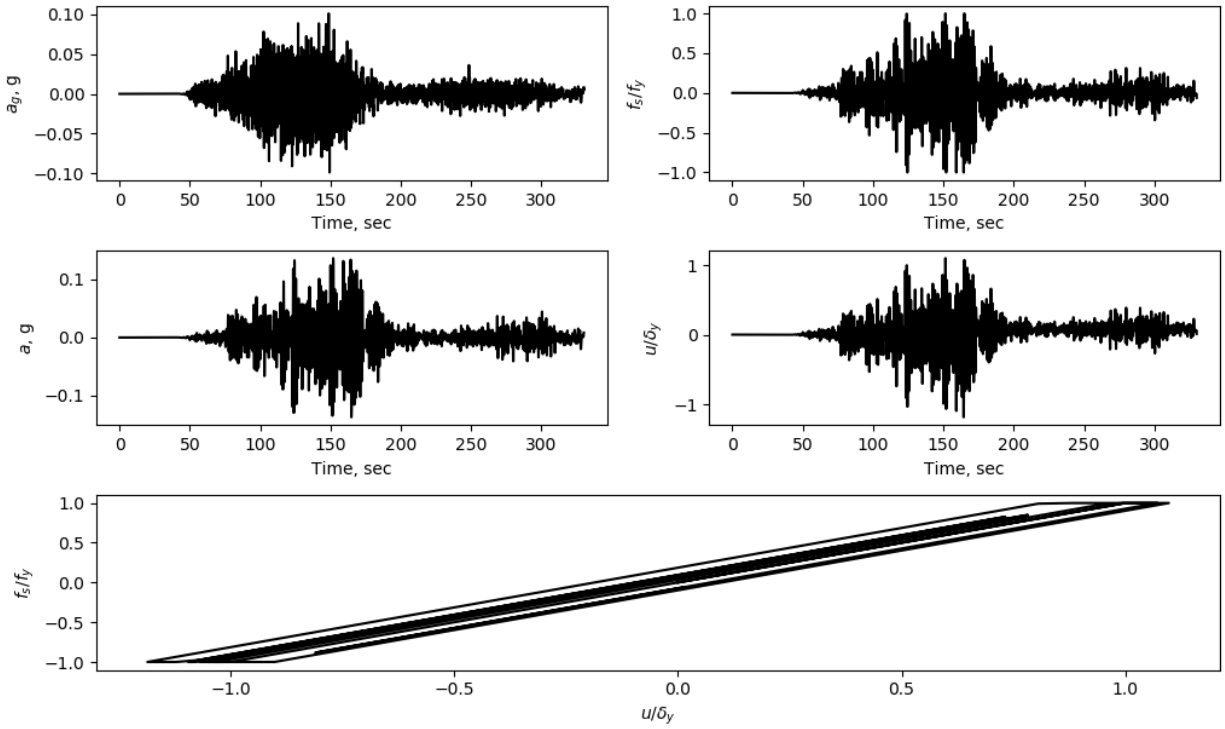

Figure 5.2. EPP SDOF Results (Seattle, csz005, T=1.0 sec, EW direction, Site Class C)

5.2.2 *Modified Ibarra-Medina-Krawinkler System*

The IMK Cyclic Det. and IMK No Cyclic Det. better approximate the response of real structures. SDOFs with these behaviors were modeled using 5% Rayleigh damping and their backbone and spring material model was the Ibarra-Medina-Krawinkler Deterioration Model

with Peak-Oriented Hysteretic Response, abbreviated as IMK (OpenSees, McKenna, 2017). The ductility at maximum force, μ, of the systems was set equal to 5 because WSDOT Bridge Design Manual has a maximum value of 6 for the displacement ductility demand value of Normal Bridges (WSDOT BDM 2018).

Figure 5.1.c shows that the backbone for this system is composed of four regions. Region 1 is the elastic portion, with stiffness equal to k and strength equal to F_y. Region 2 characterizes the post-yield stiffness and it was set to equal 5% of the elastic stiffness, denoted as $P_y k$. The strength at the end of this region is the capping strength, which occurs at μD_y, and corresponds to the system's maximum strength. Region 3 is the descending branch of the system and it has a negative stiffness of 10% of the elastic stiffness, denoted as $P_c k$. This region ends when the descending branch reaches 1% of the yield strength, denoted as κF_y. The last region, Region 4, is where the backbone 'flattens', which represents the zero-stiffness portion of the curve.

The parameters that the IMK model behavior uses to characterize the cyclic deterioration are λ_s, λ_c, and λ_a and they were set to equal $1000000 D_y$ for the IMK – No Cyclic Det. system and $100 D_y$ for IMK – Cyclic Det system. A fourth parameter, λ_k, also contributes to the deterioration and it was given a value equal to $2\lambda_s$ for both systems. For these systems, a pushover analysis was conducted in order to determine the average stiffness of the oscillator after it had been subjected to the ground motion. In this analysis if the average stiffness was found to be near zero then the oscillator was classified as having collapsed. A second check for collapse was performed in which the final recorded ductility demand value was compared against a threshold value. The threshold value corresponded to the displacement at the end of Region 3 in the IMK backbone, denoted as D, normalized by the displacement at yield; if the final recorded ductility demand value was found to be larger than the threshold value then the oscillator was classified as

having collapsed. Table 5.2 lists the threshold values for the representative cities, for all periods of study, and for both soil classes.

Table 5.2. Washington Cities Ductility Demand Threshold Values

	Site Class C				Site Class D			
Period	**0.2s**	**0.5s**	**1.0s**	**2.0s**	**0.2s**	**0.5s**	**1.0s**	**2.0s**
Forks	16.90	16.91	16.88	16.94	16.89	16.89	16.88	16.93
Ocean Shores	16.89	16.90	16.88	16.93	16.90	16.90	16.89	16.84
Port Angeles	16.91	16.89	16.86	16.86	16.91	16.91	16.90	16.90
Olympia	16.89	16.89	16.88	16.88	16.91	16.91	16.88	16.93
Port Townsend	16.91	16.91	16.87	16.95	16.91	16.91	16.92	16.86
Vancouver	16.90	16.88	16.93	16.82	16.90	16.90	16.86	16.93
Tacoma	16.90	16.91	16.87	16.95	16.90	16.90	16.91	16.85
Seattle	16.91	16.89	16.85	16.93	16.88	16.88	16.90	16.85
Graham	16.90	16.91	16.90	16.86	16.89	16.90	16.89	16.83
Everett	16.88	16.91	16.87	16.96	16.91	16.91	16.88	16.88

Figures 5.3 and 5.4 show the results for a motion that does not cause collapse. The results for a motion that does cause the system to collapse can be seen in Appendix F. The IMK – Cyclic Det. model was calibrated by reproducing the ductility demand values for the same force reduction factor and ductility at maximum force combinations observed in Marafi et al. (2019). The results for this calibration can be seen in Appendix G.

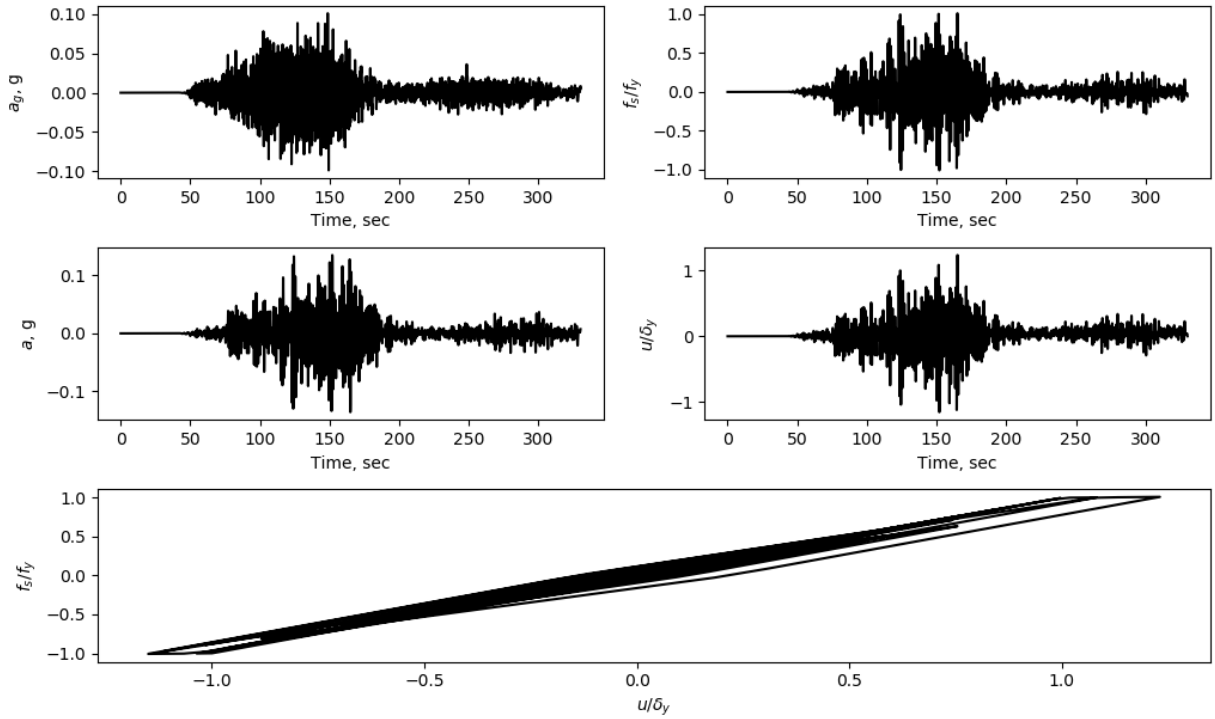

Figure 5.3. IMK – No Cyclic Det. SDOF Results (Seattle, csz005, T=1.0 sec, EW direction, Site Class C)

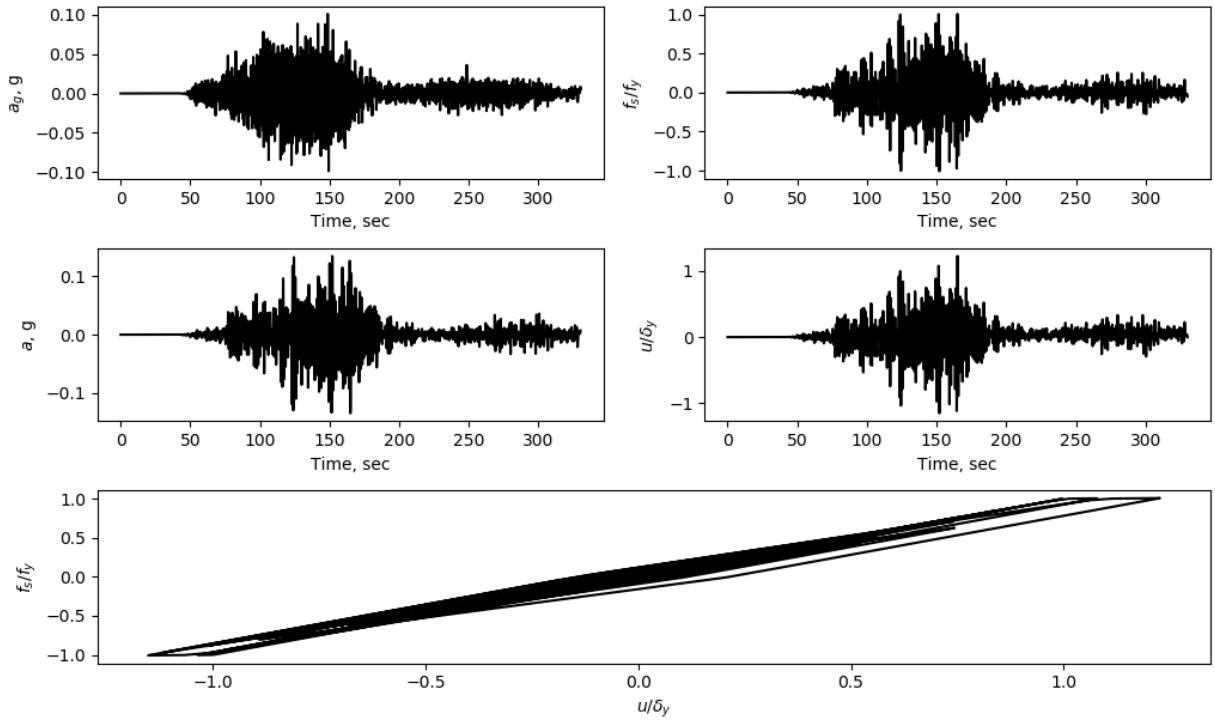

Figure 5.4. IMK – Cyclic Det. SDOF Results (Seattle, csz005, T=1.0 sec, EW direction, Site Class C)

Chapter 6. RESULTS OF PARAMETRIC STUDY

The results from the single-degree-of-freedom oscillators parametric study (Chapter 5) are discussed in this chapter. These results are summarized in terms of the normalized base-shear strength, normalized spectral acceleration, and median displacement ductility demand.

6.1 Normalized Base-Shear Strength and Normalized Spectral Acceleration

The normalized base-shear strength, F_y/W, is the value obtained when the oscillator's yield force, F_y, is normalized by the oscillator's weight, W. This value is related directly to the design response spectra, because the yield force depends on the elastic seismic response coefficient, C_{sm}, which is determined with the use of the design spectral acceleration (Equation 5.2).

Figure 6.1 shows the normalized base-shear strengths for the four representative cities of Forks, Graham, Port Angeles, and Seattle. The black and grey lines from the top plots for each of the four cities in Figure 6.1 represent the normalized base-shear strength for Site Class C and D. For all four cities, F_y/W is smaller for Site Class D than Site Class C at short periods but larger at long periods. This difference is due to Site Class D being softer than Site Class C, which results in larger long-period site coefficients (Appendix B).

The bottom plots in Figure 6.1 represents the normalized spectral acceleration, denoted as $S_{a,SoilClass}/(F_y/W)$. This value comes from normalizing the spectral acceleration from a given ground motion by the normalized base-shear strength. In this case, the normalized spectral acceleration represents the ratio of the median simulated M9 spectral acceleration, $S_{a,M9}$, to design basis earthquake spectral acceleration, $S_{a,DBE}$, $(S_{a,M9}/\Omega S_{a,DBE})$, including the assumed

overstrength factor. It is important to note that similar to F_y, the design basis earthquake spectral acceleration includes the seismic response coefficient, C_{sm}, and overstrength factor, Ω.

Figure 6.1 shows the normalized base-shear strength and normalized spectral acceleration plots for the city of Forks, Port Angeles, Seattle, and Graham. The plots for all ten cities are provided in Appendix H. The difference among the four cities' normalized base-shear strength plots is a result of their geographic location and site coefficient values, and not the presence or absence of a sedimentary basin. This is because, as discussed in Chapter 2, the 2002 and 2014 National Seismic Hazard Maps utilized to obtain design spectral accelerations do not take into account the amplification of long-period ground motions in deep sedimentary basins. Consequently, the design spectral acceleration values are largest for cities that are located close to the Pacific coast (e.g., Forks and Ocean Shores) and smallest for cities located on the interior of the state (e.g., Graham), as seen in Figure 2.2.

Because the soil-adjusted simulated M9 ground motions do consider basin amplification effects, the normalized spectral acceleration plots for the four cities look different from one another. For the city of Forks, at periods smaller than 0.5 seconds the $S_{a,SoilClass}$ /(F_y/W) values for the four soil classes are arranged in the same order as they are in the soil-adjusted response spectra plot shown in Chapter 4 (Figure 4.3), with D1 having the largest value and D3 the smallest. This occurs because at short periods, D1 has the highest spectral acceleration and smallest normalized base-shear strength value. While the normalized base-shear strength value for C2 and C4 is larger than the D3 value, both C-type ground motions have higher spectral acceleration values and, therefore, a greater normalized spectral acceleration than D3. It is because of this relationship between response spectra and normalized base-shear strength values

that the D3 normalized spectral acceleration values are similar to the values for the other three site classes at long periods.

Graham is one of the inland cities without basin and as a result has the lowest $S_{a,SoilClass}$ /(F_y/W) values out of the four cities shown. The absence of a sedimentary basin and its distance from the fault cause it to have small response spectra, which produces low normalized spectral acceleration values for all site classes.

Port Angeles represents shallow sedimentary basin cities and similarly to Forks, at periods smaller than 0.5 seconds, D1 has the largest $S_{a,SoilClass}$ /(F_y/W) values and D3 has the smallest. Unlike Forks, however, the normalized spectral acceleration values increase at long periods. This increase is attributed to the spectral shape of the soil-adjusted M9 motions due to the basin amplification effects. The higher spectral acceleration value at 1.0 second compared to 0.5 second causes the normalized spectral acceleration to increase. The same thing happens for deep basin cities, such as Seattle, but in this case the $S_{a,SoilClass}$ /(F_y/W) values increase with period because the response spectra of deep basin cities has a longer range of periods with positive spectral shape. For the two cities on sedimentary basins, the D1 values are the smallest for long periods because the spectral acceleration values are similar to the C2 and C4 values; however, the normalized spectral acceleration value is greater for Site Class D, which causes a larger reduction.

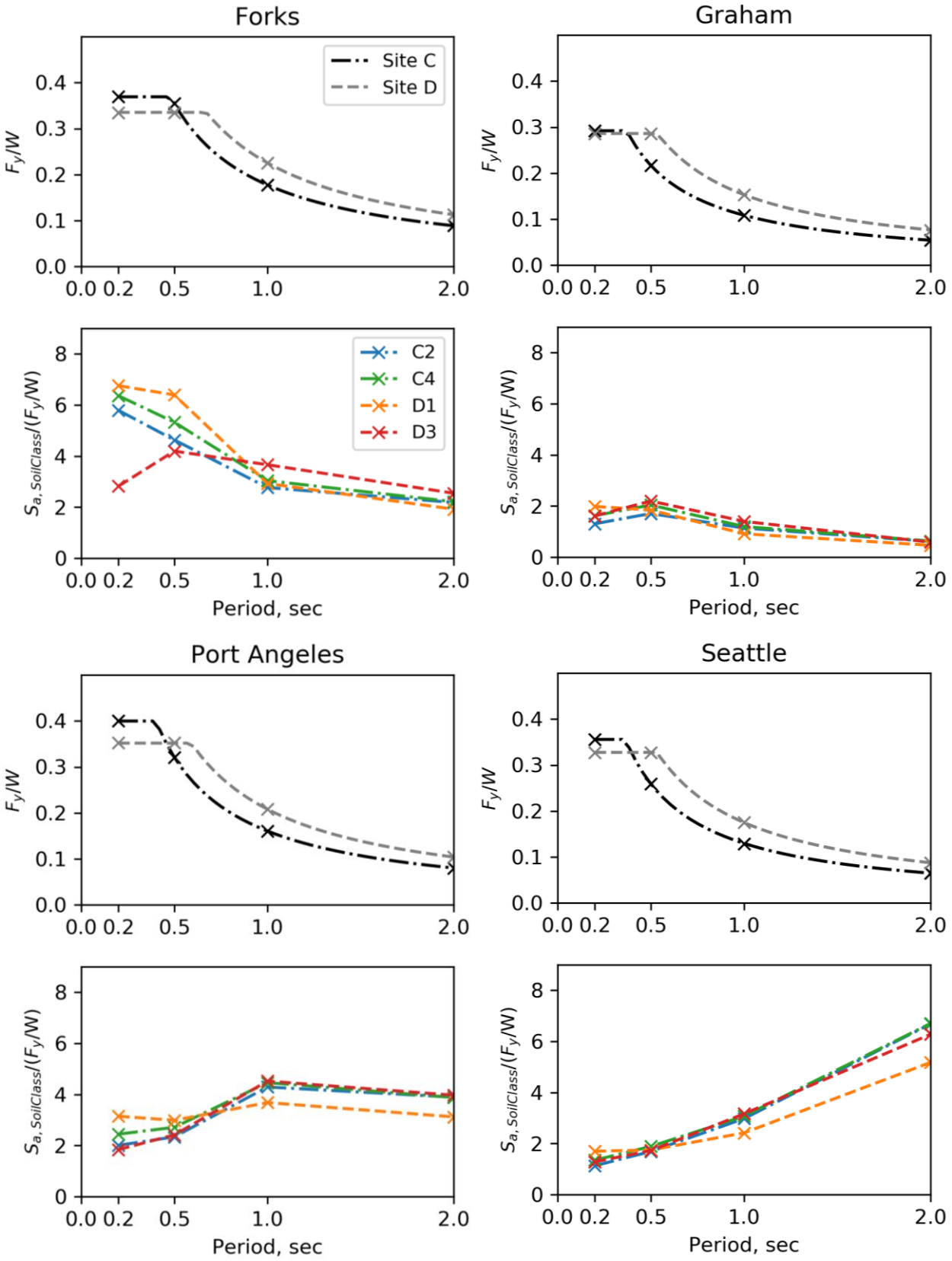

Figure 6.1. Normalized Base-Shear Strength, F_y/W, and Normalized Spectral Acceleration, $S_{a,SoilClass}/(F_y/W)$

6.2 DISPLACEMENT DUCTILITY DEMAND

Displacement ductility demand is the ratio of the maximum oscillator displacement, *D*, to the yield displacement, D_y. Figure 6.2 shows the displacement ductility demand values, denoted as $\widetilde{\delta_{M9}}/\delta_Y$, for the EPP oscillator, the IMK – No Cyclic Deterioration oscillator, and the IMK – Cyclic Deterioration oscillator for the same four cities discussed in the previous section. The values shown for the two IMK oscillators are either the median displacement ductility demand or collapse, denoted as 'Col'. A value of collapse is obtained when more than 50% of the ground motion realizations and profile combinations analyzed caused the oscillator to collapse. There was no pushover analysis or threshold value for the EPP system, so in the cases where the median displacement ductility demand value exceeded 10, the results were plotted as '10+'. The displacement ductility demand plots for the three SDOF oscillators include the results from the baseline ground motion to highlight the effects that different soil conditions have on the system's response.

For the non-basin coastal city of Forks, the three curves tell similar stories. The plots show that more than 50% of structures with a period of 0.2 seconds (stiff structures) collapse for all soil types. The collapse or very large displacement ductility demand values at a period of 0.2 seconds was to be expected for Forks because of its proximity to the rupture plane. The impact that proximity to the fault has on a city has been noted previously in Chapter 3 and Chapter 4, but it is now evident that short-period structures in this area are at greatest risk, even if they are designed considering ground-motion intensities that are consistent with the 2014 USGS NSHM. The median displacement ductility demand for all other periods and oscillator types (except for the EPP system located on D1 soil) is lower than WSDOT's displacement ductility demand value of 6 (Section 5.2.2). This indicates that new intermediate and long-period structures (flexible

structures) are not as much of a concern in coastal cities without sedimentary basins. Of course, older structures designed to lower standards are likely to suffer damage for all periods, because these older structures were likely designed to have lower strengths.

The $\widetilde{\delta_{M9}}/\delta_Y$ results for Graham indicate that there is no collapse concern for neither stiff nor flexible structures located in inland cities without basins. For Forks, the median ductility demand values for all types of soils and oscillator systems (Figure 6.2) have a maximum value of 3. This maximum value occurs at 0.2 seconds and results from the combination of no basin amplification effects, low response spectra, and small normalized base-shear strength values causes a decrease in $\widetilde{\delta_{M9}}/\delta_Y$ as the period increases.

In Port Angeles the effect of basin amplification is evident in the increase in displacement ductility demand at a period of 1.0 second, compared the demand at 0.5 second. Although the $\widetilde{\delta_{M9}}/\delta_Y$ value does not exceed the WSDOT displacement ductility demand limit, it is approximately 2 times larger than the displacement ductility demand value at a period of 0.5 seconds. In addition, at a period of 0.2 seconds the two softer soils, D1 and D3, the EPP and IMK – No Cyclic Det. oscillators have median $\widetilde{\delta_{M9}}/\delta_Y$ values that exceed the WSDOT limit, and the median demand in the IMK – Cyclic Det system is collapse. This is not a result of fault proximity, but rather oscillator behavior due to the presence of soft soils. Stiff structures located on Site Class D soils in shallow sedimentary basin cities are at risk of collapse in the M9 Cascadia earthquake.

The negative effects that deep sedimentary basins have on structural response can be seen from the results obtained for Seattle. These plots show that the long-period basin amplification effects cause a drastic increase in median displacement ductility demand at longer periods. There is no evidence of collapse at any period, but it can be seen that long-period structures are a

concern in these types of cities because the displacement ductility demand for all oscillators exceed a value of 6 for the Baseline, C2, and C4 soil types (see Appendix I for Everett results). While the median displacement ductility demand for D1 and D3 soils is not as high, the 2.0 second $\widetilde{\delta_{M9}}/\delta_Y$ values are much higher for deep basin cities than the 2.0 second values seen at any of the other three cities shown. This is attributed to the long range of periods with positive spectral shape and the slow rate of spectral acceleration decrease observed at long periods, which causes the $\widetilde{\delta_{M9}}/\delta_Y$value at periods over 1.0 second to decrease slowly.

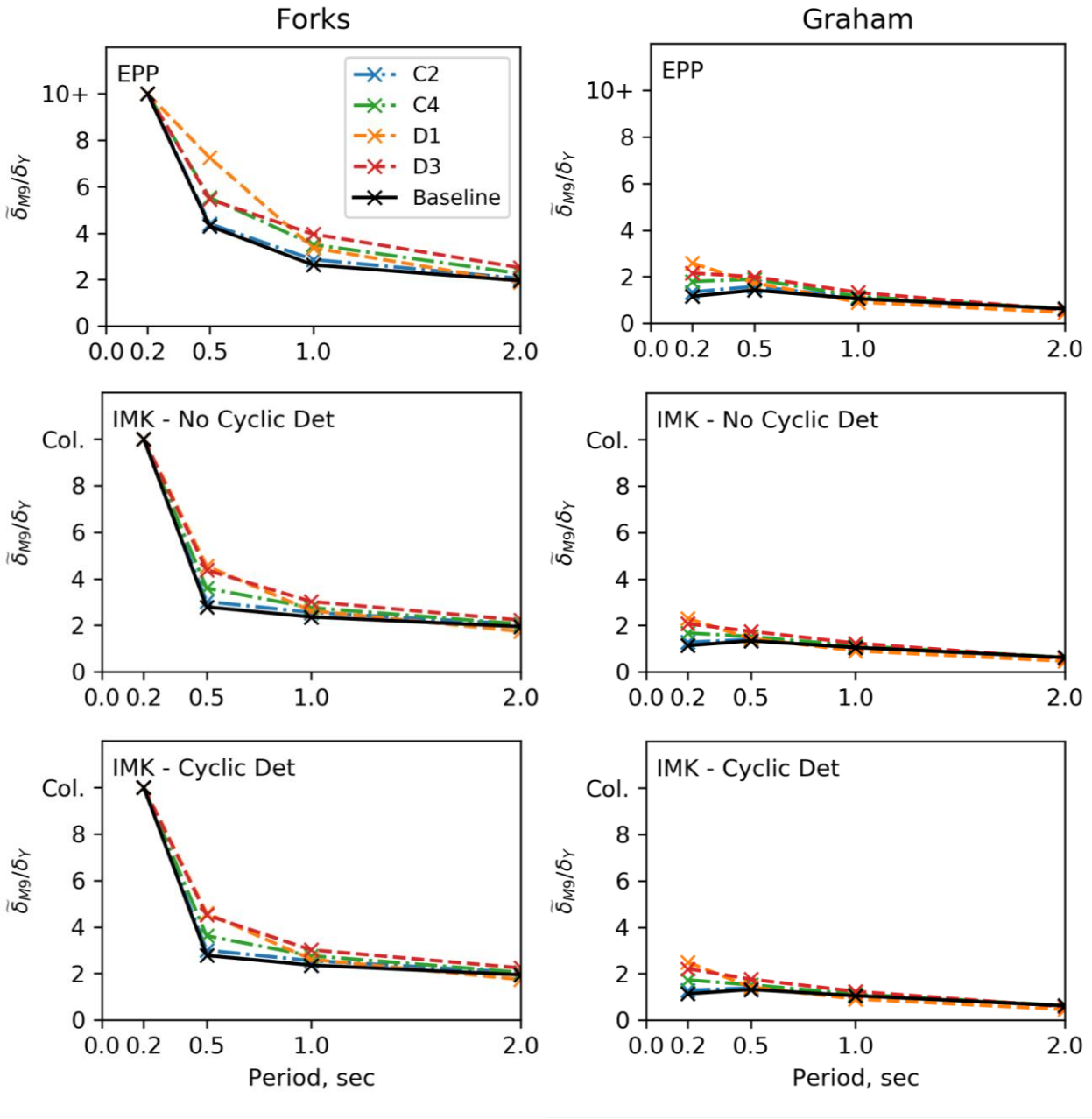

Figure 6.2. Displacement Ductility Demand, D/D_y

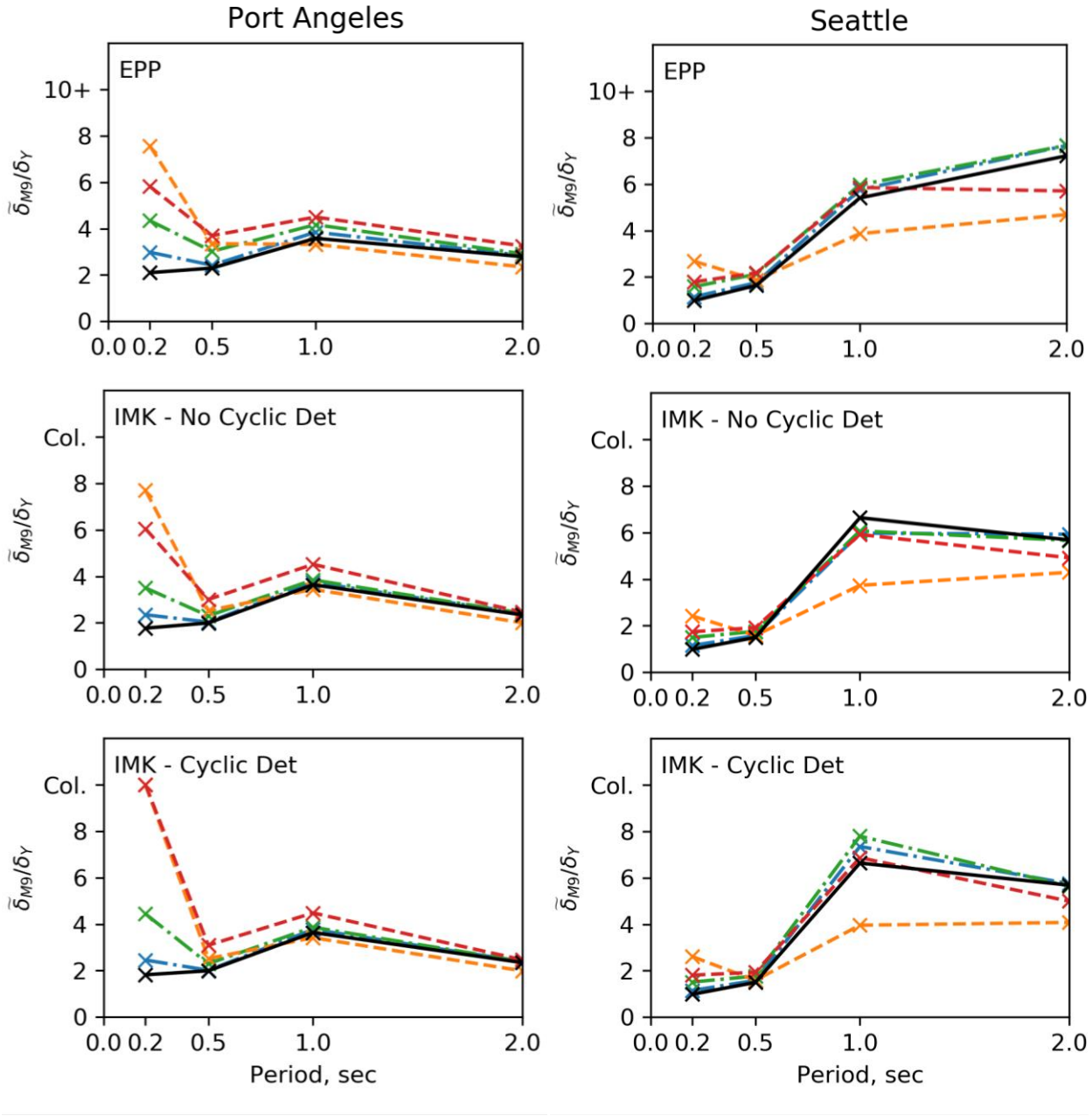

Figure 6.2. Displacement Ductility Demand, D/D_y (continued)

6.3 Distance to Fault and Sedimentary Basin Effects on Displacement Ductility Demand

The effect of proximity to the fault and $Z_{2.5}$ depth on the median displacement ductility demand, μ, of the IMK – Cyclic Deterioration oscillator can be seen on Figure 6.3 for soil types

C2 and D3. Figure 6.3.a shows the relationship between average closest distance to the fault, $R_{cd,avg,}$ and displacement ductility demand. Due to the presence of basin amplification effects at 1.0 and 2.0 seconds, the only significant relationship between $R_{cd,avg}$ and μ can be seen at a period of 0.5 seconds. At this period, the displacement ductility demand decreases as the distance from the fault increases. For cities that are located 30 km or less from the fault (Forks and Ocean Shores), the C2 and D3 median displacement ductility demand decreases as the period increases. At periods over 1.0 second, however, there is no relationship between median displacement ductility demand and $R_{cd,avg,}$ because cities that are located more than 50 km away from the fault have μ values that either increase or decrease as the distance from the fault increases. Increasing the period from 1.0 to 2.0 seconds, however, shows that the displacement ductility demand values from C2 and D3 soils converge. This occurs because the response spectra at long periods are similar for all soil-adjusted ground motions.

Plotting the long period to short period displacement ductility demand ratio as a function of $Z_{2.5}$ depth shows that the ductility demand ratio increases as $Z_{2.5}$ increases. Figure 6.3b shows that cities located in deep sedimentary basins have the highest displacement ductility demand ratios and that for all cities the ratios are higher when the ductility at 0.5 seconds is compared against that from 1.0 seconds. The reason as to why the1.0 second ratios are larger than the 2.0-second ratios is because the change in response spectra shape that occurs in shallow and deep sedimentary cities as a result of basin amplification begins at approximately 1.0 second and by 2.0 seconds the shape decreases once again. These plots show that there is more difference in the displacement ductility demand ratio between C2 and D3 soils when a larger long period is used.

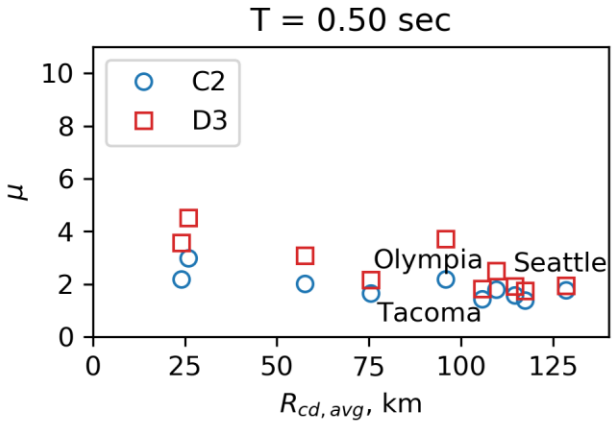

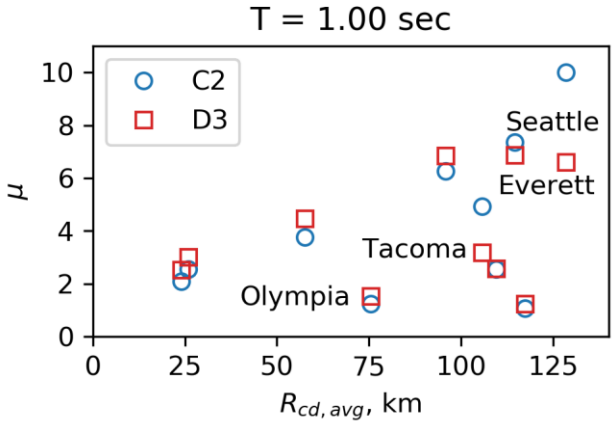

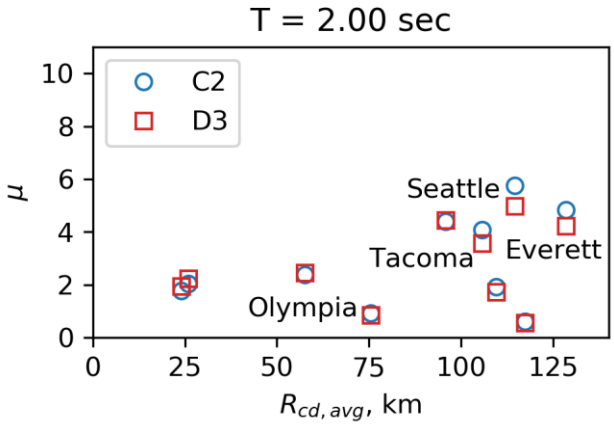

(a) Displacement Ductility Demand as a Function of Average Closest Distance to CSZ Fault, $R_{cd,avg}$

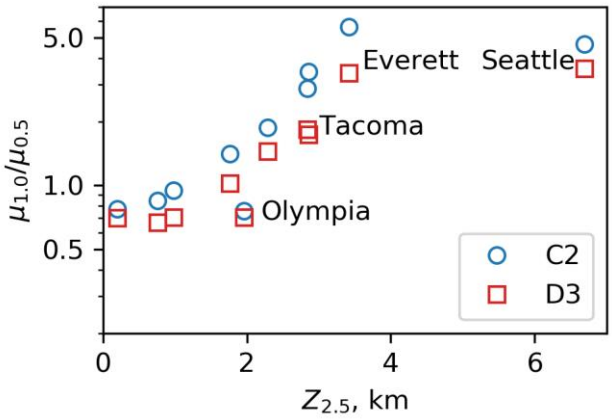

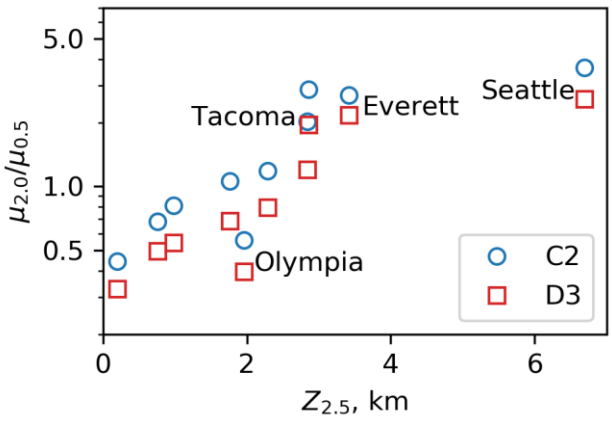

(b) Ratio of Long Period (1 or 2 sec) to Short Period (0.5 sec) Displacement Ductility Demand as Function of $Z_{2.5}$ Depth

Figure 6.3. Effect of (a) $R_{cd,avg}$ and (b) $Z_{2.5}$ on Displacement Ductility Demand

Chapter 7. CONCLUSIONS

The ground motions produced by a large-magnitude Cascadia Subduction Zone, CSZ, earthquake are expected to have long durations and undergo long-period amplifications due to the presence of shallow and deep sedimentary basins. Bridge design spectral acceleration values obtained from national design code, AASHTO-17 and Washington's current bridge design code, WSDOT-18, are calculated without taking into account the effects of basin amplification. These effects need to be understood in order to observe the response of generalized structural systems and determine the effects that a magnitude-9 seismic event would have on bridges located throughout Western Washington.

Ten representative cities from the State of Washington were selected and categorized into one of four groups based on its geographic location and the depth at that location to a shear-wave velocity of 2.5 km/s, $Z_{2.5}$ depth. The four groups were (1) coastal cities without basin [Forks and Ocean Shores], (2) inland cities without basin [Olympia, Vancouver, and Graham], (3) inland cities on shallow sedimentary basins [Port Angeles, Port Townsend, and Tacoma], and (4) inland cities on deep sedimentary basins [Seattle, and Everett]. The discussions in Chapters 3, 4, and 6 analyze one representative city from each of the four categories and explain the effect that location and sedimentary basin presence have on the simulated response spectra, soil-adjusted amplification, and median displacement ductility demand. Appendices C, D, H, and I contain the detailed results for all 10 cities.

Although the ten representative cities were categorized based on geographic location and $Z_{2.5}$ depth, many of the results show that there are outliers within the categories as certain cities have spectral accelerations or oscillator demand that is more indicative of cities in another

category. Tacoma is an example of such outliers because it was categorized as a shallow sedimentary basin city, but it actually has a ground motions that are more likes a deep sedimentary city. This difference in classification and behavior occurs because $Z_{2.5}$ is a one-dimensional measure, which means that it is an imperfect way of categorizing because in reality there are three-dimensional effects that play a role in the response spectra and ground motion characteristics of cities located over sedimentary basins.

7.1 BASELINE SIMULATED M9 GROUND MOTIONS

The CSZ model used to generate the baseline simulated M9 ground motions incorporates deep sedimentary basins from the Pacific Northwest, which results in long-period basin amplification effects for cities located in shallow or deep sedimentary basins. These effects are evident in the response spectra for such cities, because the spectral acceleration values for periods between 1-2 seconds have a positive response spectra shape (Chapter 3). The increase in spectral acceleration values of shallow and deep sedimentary basin cities as a result of basin amplification effects produces 2.0-second baseline simulated M9 spectral accelerations that are larger than the WSDOT-18 design accelerations. These large M9 spectral accelerations are a first indicator that flexible structures located in sedimentary basins might be currently under-designed.

The relationship between the baseline spectral acceleration and average closest distance to the fault, $R_{cd,avg}$, for a period of 0.5 seconds can be represented with the following relationship.

$$S_{0.5,Baseline} = 1.3\, e^{-\left(\frac{R_{cd,avg}}{90}\right)} \tag{7.1}$$

No relationship can be established at longer periods because basin amplification effects cause the spectral acceleration values to no longer be a function of $R_{cd,avg}$ only. The long-period

accelerations are best represented when the ratio of long period to short period spectral acceleration is plotted as a function of $Z_{2.5}$ depth. The results show that the presence of a sedimentary basin has more effect on the 2.0-second spectral accelerations than at 1.0 second. The two bilinear relationships are given as follows.

$$\ln\left(\frac{S_{a,1.0}}{S_{a,0.5}}\right) = \begin{cases} -1.51 + 0.47\,Z_{2.5} & Z_{2.5} < 3 \\ 0.9 & Z_{2.5} \geq 3 \end{cases} \tag{7.2}$$

$$\ln\left(\frac{S_{a,2.0}}{S_{a,0.5}}\right) = \begin{cases} -2.30 + 0.73\,Z_{2.5} & Z_{2.5} < 3 \\ 0.9 & Z_{2.5} \geq 3 \end{cases} \tag{7.3}$$

7.2 Effects of Site Conditions

Pacific Northwest shear-wave velocity profiles were used by USGS Research Scientist Alex Grant to perform equivalent linear site response analyses and generate soil-adjusted ground motions with an average shear-wave velocity in the upper 30 meters, V_{s30}, representative of the soil conditions of the State of Washington. Two Site Class C (denoted C2 and C4) and two Site Class D (denoted D1 and D3) V_{s30} ranges were selected and used in Chapter 4 and Chapter 6.

The response spectra documented in Chapter 4 show that the soil-adjusted response spectra for coastal cities not on basins have large deamplification for the D3 soil-adjusted ground motions at periods smaller than 0.4s. This finding indicates that the range of the equivalent linear analysis was potentially exceeded because of the large input motions for cities in this category. The cities located on shallow or deep sedimentary basins also have deamplification for the D3 motions, with the deamplification for shallow basin cities being greater than that for deep basin cities.

No relationship can be established between amplification of the soil-adjusted ground motions with respect to the strength of the baseline simulated M9 ground motions and baseline spectral acceleration or baseline spectral shape. The results of the amplification of the soil-

adjusted motions as a function of baseline spectral acceleration show that the amplifications for the C2 ground motions stabilize around 1.0 at periods of 1.0 and 2.0 seconds. This occurred because the V_{s30} of the baseline simulated M9 motions fell within the V_{s30} range of the C2 ground motions. In this case, the amplifications for the D3 motions either increased or decreased as the baseline spectral acceleration increased.

The variability in the results of the amplification as a function of baseline spectral shape changes depending on the period being analyzed, with 0.5 seconds having the largest amplification range. Similarly to the results from the baseline strength, the amplification for the D3 motions either increases or decreases as the baseline spectral shape increases, which indicates that it is not possible to establish a trend between amplification and spectral shape.

7.3 Impact of Simulated M9 Ground Motions on Single-Degree-of-Freedom Systems

The normalized spectral acceleration values for coastal cities without basins are large for periods smaller than 0.5 seconds, and moderate for periods greater than 1.0 second. The high values for short periods and moderate long-period values are a result of high spectral accelerations due to the city's proximity to the rupture plane, and absence of basin amplification effects, respectively. Inland cities without basins have low normalized spectral acceleration values for all soil-adjusted ground motions as a result of distance to the fault and absence of a sedimentary basin.

Cities that are categorized as being in either shallow or deep sedimentary basins have small normalized spectral acceleration values for periods smaller than 0.5 seconds, but much larger values for periods greater than 1.0 seconds. The increase in values is an attribute of the positive spectral shape due to basin amplification effects of the soil-adjusted motions.

Even for new structures, the results from the parametric study indicate that stiff structures (T = 0.2 seconds) located near the Pacific coast and flexible structures (T ≥1.0 second) located on deep sedimentary basins are at risk of collapse due to the high displacement ductility demands obtained for all four soil types (Chapter 6). These values exceeded the WSDOT displacement ductility demand limit of 6 and in some scenarios caused the oscillators to collapse. Furthermore, the results also show that stiff structures in shallow basin cities have high displacement ductility demand values when Site Class D soils are present. It is expected that regardless of the city classification, older structures would have even larger likelihoods of damage and potential collapse.

The only significant relationship between average closest distance to the fault and displacement ductility demand occurs at a period of 0.5 seconds, in which the displacement ductility demand increases as the distance from the fault increases. At higher periods, basin amplification effects cause the displacement ductility demands values to fluctuate between increasing and decreasing as the average closest distance to the fault increases. The results of long period to short period displacement ductility demand values as a function of $Z_{2.5}$ depth show that the ductility demand ratio increases as $Z_{2.5}$ depth increases. This indicates that cities located on sedimentary cities have larger displacement ductility demand ratios than cities located outside basin areas.

7.4 FUTURE WORK

There are many opportunities to expand on the work presented in this thesis. One possibility is to utilize a nonlinear single-degree-of-freedom system whose properties are more representative of a wider range of ‘typical’ Washington state bridges, including older ones. Because the research findings discussed here only take into account four periods, the response of

structures with periods between 0.5 and 1.0 second has not been investigated. Utilizing a wider range of periods would provide more information on the structural response of intermediate structures.

In addition, the results from the East-West direction as well as the combination of the two directions (with the use of geometric mean) can be further analyzed and used to obtain a more comprehensive understanding of the effects of a magnitude-9 earthquake on bridge systems located in various soil conditions and geographic locations.

BIBLIOGRAPHY

[1] AASHTO. 2017. *LRFD Bridge Design Specifications.* American Association of State Highway and Transportation Officials.

[2] Ahdi, S.K et al. 2017. "Development of VS Profile Database and Proxy-based Models for VS30 Prediction in the Pacific Northwest Region of North America." *Bulletin of the Seismological Society of America* 107: 1781-1801.

[3] ASCE. 2017. *Minimum Design Loads And Associated Criteria for Buildings and Other Structures, ASCE/SEI 7-16.* Reston, VA: American Society of Civil Engineers.

[4] Changramohan, Reagan, Jack W. Baker, and Gregory G.Deierlein. 2016. "Quantifying the Influence of Ground Motion Duration on Structural Collapse Capacity Using Spectrally Equivalent Records." *Earthquake Spectra* 32(2): 927-950.

[5] Encyclopædia Britannica. "Ring of Fire." https://www.britannica.com/place/Ring-of-Fire (May 20, 2019)

[6] FEMA (Federal Emergency Management Agency). 1995. *NEHRP Recommended Seismic Provisions for Seismic Regulations for New Buildings (FEMA 222A and 223A).*

[7] FEMA (Federal Emergency Management Agency). 2015. *NEHRP Recommended Seismic Provisions for New Buildings and Other Structures (FEMA P-1050-1).* Volume I: Part 1 Provisions, Part 2 Commentary. https://www.fema.gov/media-library-data/1440422982611-3b5aa529affd883a41fbdc89c5ddb7d3/fema_p-1050-1.pdf

[8] FHWA (Federal Highway Administration). 2014. *LRFD Seismic Analysis and Design of Bridges Reference Manual.* https://www.fhwa.dot.gov/bridge/seismic/nhi130093.pdf

[9] Frankel, Arthur et al. 2018. "Broadband Synthetic Seismograms of Magnitude 9 Earthquakes on the Cascadia Megathrust Based on 3D Simulations and Stochastic Synthetics, Part 1: Methodology and Overall Results." *Bulletin of the Seismological Society of America.* http://pubs.geoscienceworld.org/ssa/bssa/article/544772/Broadband-Synthetic-Seismograms-for-Magnitude-9

[10] Khaleghi, Bijan. 2017. *Memo to All Design Section Staff.* Washington State Department of Transportation Bridge and Structures Office.

[11] Liu, Pengcheng, and Archuleta, R.J. 2002. "The Effect of a Low-Velocity Surface Layer on Simulated Ground Motion." *Seismological Research Letters.* 73(2), 195-272. https://doi.org/10.1785/gssrl.73.2.195

[12] Marafi, Nasser et al. 2017. "Effects of Deep Basins on Structural Collapse during Large Subduction Earthquakes." *Earthquake Spectra.* 33(3), 963-997.

[13] Marafi, Nasser et al. 2019a. "Impacts of Simulated M9 Cascadia Subduction Zone Motions on Idealized Systems." *Earthquake Spectra.* https://earthquakespectra.org/doi/10.1193/052418EQS123M

[14] Marafi, Nasser et al. 2019b. "Performance of RC Core-Wall Buildings during Simulated M9 Cascadia Subduction Zone Earthquake Scenarios." *Journal of Structural Engineering, In Review.*

[15] McKenna, F. "OpenSees." http://opensees.berkeley.edu/

[16] Pacific Northwest Seismic Network. "Cascadia Subduction Zone." https://pnsn.org/outreach/earthquakesources/csz (May 20, 2019)

[17] Palmer, Stephen P. et al. 2007. "Liquefaction Susceptibility and Site Class Maps of Washington State, By County." *Washington Division of Geology and Earth Resources. Open File Report 2004-20*. ftp://ww4.dnr.wa.gov/geology/pubs/ofr04-20/ (June 4, 2019).

[18] Petersen, M.D. et al. 2014. "Documentation for the 2014 National Seismic Hazard Maps." *USGS. Open File Report, 2014-1091, 243 p.* https://dx.doi.org/10.3133/ofr20141091

[19] Petersen, M.D. et al. 2018. "Preliminary 2018 Update of the U.S National Seismic Hazard Model: Overview of Model, Changes, and Implications." *USGS.* https://earthquake.usgs.gov/hazards/hazmaps/2018_NSHM_Overview_Documentation_public_v1.pdf

[20] Stephenson, William. et al. 2017. "P- and S-wave Velocity Models Incorporating the Cascadia Subduction Zone for 3D Earthquake Ground Motion Simulations." Update for OFR 2007-1348. *USGS. Open File Report, 2017-1152, 17 p.* https://doi.org/10.3133/ofr20171152

[21] USGS. 2018a. "2002 US Hazard Data." https://earthquake.usgs.gov/hazards/hazmaps/conterminous/2002/data.php (February 2, 2018).

[22] USGS. 2018b. "Seismic Design Web Service Documentation." https://earthquake.usgs.gov/ws/designmaps/ (April 14, 2018).

[23] USGS. "Cascadia Subduction Zone." https://earthquake.usgs.gov/data/crust/cascadia.php (May 20, 2019).

[24] USGS. "USGS FAQs." https://web.archive.org/web/20140805134145/http://www.usgs.gov/faq/categories/9831/3342 (May 20, 2019)

[25] Wirth, Erin A. et al. 2018. "Broadband Synthetic Seismograms for Magnitude 9 Earthquakes on the Cascadia Megathrust Based on 3D Simulations and Stochastic Synthetics, Part 2: Rupture Parameters and Variability." *Bulletin of the Seismological*

Society of America. https://pubs.geoscienceworld.org/ssa/bssa/article/544767/Broadband-Synthetic-Seismograms-for-Magnitude-9

[26] WSDOT. 2018. *Bridge Design Manual (LRFD)*

APPENDIX A

Chapter 2 discusses the effect that different versions of the USGS National Seismic Hazard Maps (USGS 2002 and USGS 2014) have on bridge design spectral acceleration values. This appendix discusses the design spectral acceleration values obtained for building design codes and directly compares them to the bridge design values from Chapter 2. The comparison illustrates the effect that changing the return period has on design spectral acceleration values.

Older and newer building design codes utilize the same USGS Maps as older and newer bridge design codes, but building codes utilize a return period of 2475 years (2% probability of exceedance in 50 years). Similarly to bridge design codes, older building codes (ASCE 7-05) utilize site coefficient from NEHRP 1994 and newer codes (ASCE 7-16) utilize NEHRP 2015 coefficients. For building design, however, the accelerations obtained from the hazard maps are multiplied by a factor of 2/3 to obtain the design spectral acceleration values. Table A.1 provides information regarding the map version, return period used, and site coefficient source for the comparison made between design codes.

Table A.1. Reference Building Codes Information

	Bridge Code		**Building Code**	
	AASHTO-17	WSDOT-18	ASCE 7-05	ASCE 7-16
Return Period (years)	975	1000	2475	2475
USGS Map Version	2002	2014	2002	2014
Site Coefficient Source	NEHRP 1994	NEHRP 2015	NEHRP 1994	NEHRP 2015

The design spectral values for ASCE 7-05 and ASCE 7-16 were obtained from the USGS web service software (https://earthquake.usgs.gov/ws/designmaps/) for risk category I, Site Class C, and the specified latitude and longitude. As done in Chapter 2, contour maps and bar graphs

for design spectral acceleration at a period of 0.2 second (5 Hz), S_{DS}, and design spectral accelerations at a period of 1.0 second (1 Hz), $S_{D1,}$ were created, Figures A.1 – A.2. These contour maps and bar graphs do not include PGA values because neither one of the building codes explicitly utilize PGA in design. Figures A.1 and A.2 show that the western part of the state has higher design accelerations than the eastern part, and that utilizing USGS 2014 maps results in higher spectral accelerations.

Figure A.2 shows that increasing the return period (utilizing building codes) for any map version decreases the S_{DS} values by approximately 0.10g in the West and 0.15g in the East for the 2002 map, and approximately 0.15g and 0.05g in the West and East, respectively, for the 2014 map. Similarly, the S_{D1} values decrease approximately 0.05g in the West and 0.07g in the East for the 2002 map, but increase approximately 0.1g in the West and 0.07g in the East for the 2014 map.

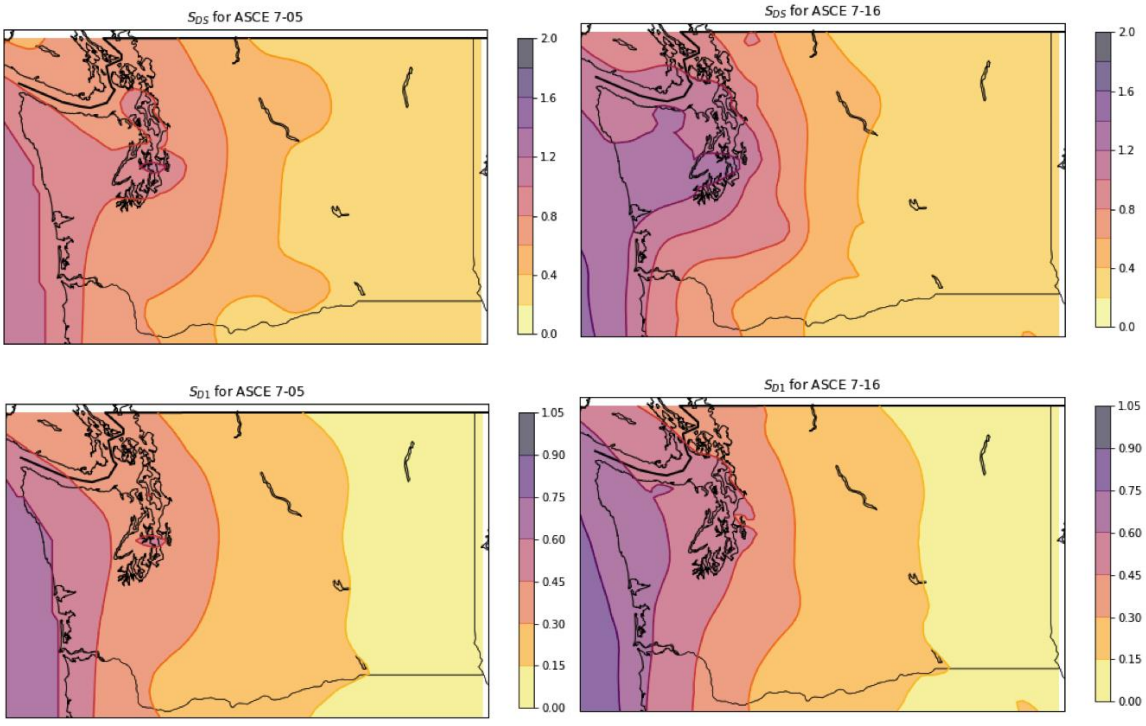

Figure A.1. Washington State Design S_a Contour Maps for ASCE 7-05 & ASCE 7-16 (Site Class C)

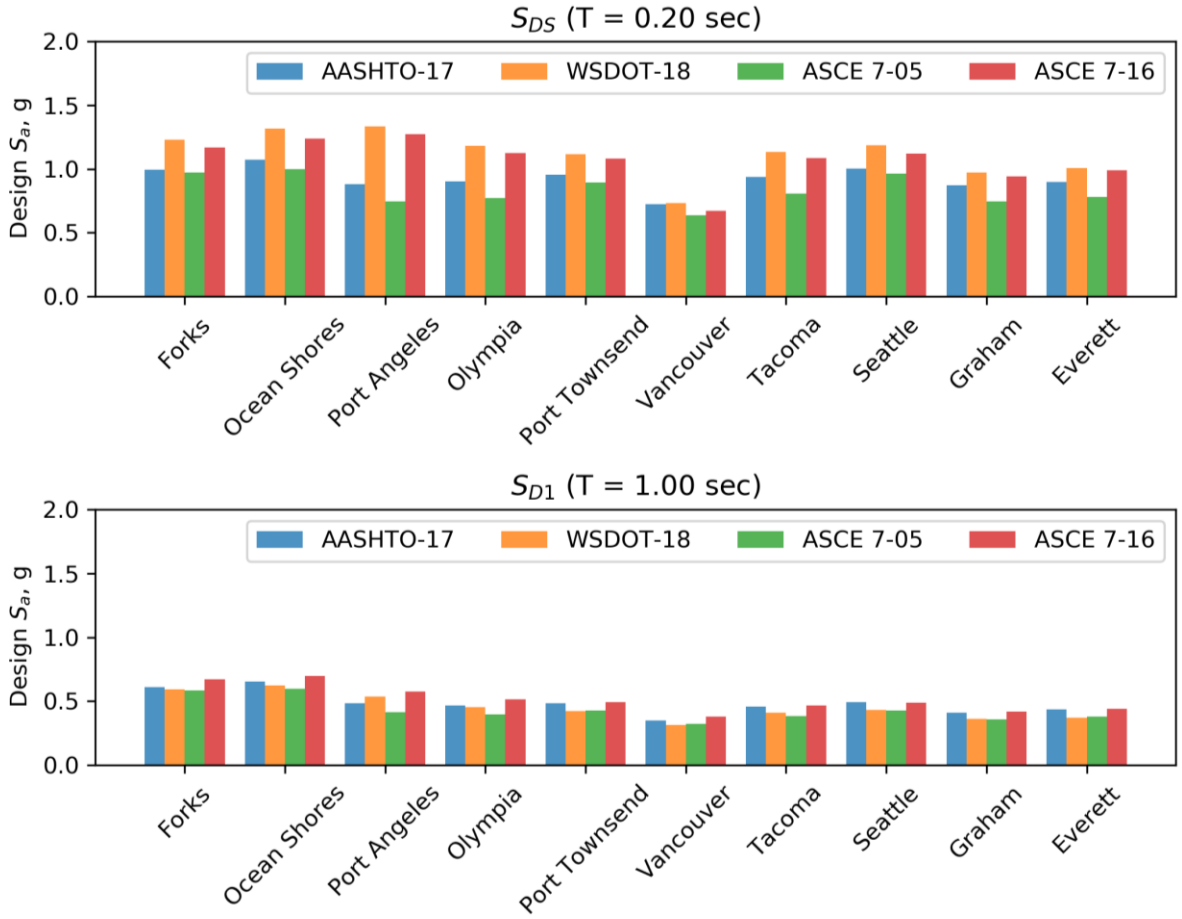

Figure A.2. Washington Cities Design S_a Values According to Design Code (Site Class C)

Effect of USGS Map Version

For a return period of 2475-years (building design), the region located between the Olympic Peninsula and the Puget Sound Region has high positive percent change values for both S_{DS} and S_{D1}. Within this region are the cities of Port Angeles and Olympia, and Figure A.4 shows that these cities have the largest percent changes out of the ten cities of study with +70% and +46% for S_{DS}, and +40% and +30% for S_{D1}, respectively. The 2475-year S_{DS} contour map has the most negative percent change located in the mid-portion of the Eastern border. But unlike the 1000-

year contour map (bridge design), the 2475-year contour map shows that the entire Eastern border has a negative S_{D1} percent change between 0% and -5%.

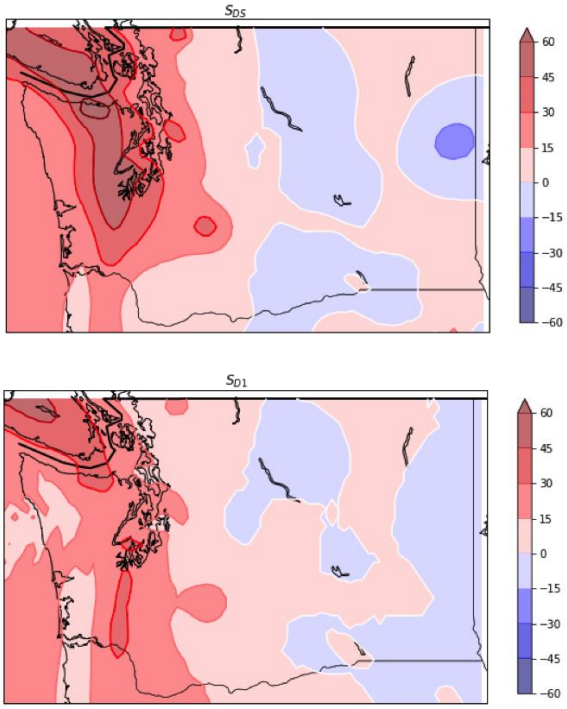

Figure A.3. Washington State Design S_a Percent Change Contours Caused by Changing USGS Map Version (ASCE7-16/ASCE7-05, 2475-year Return Period, Site Class C)

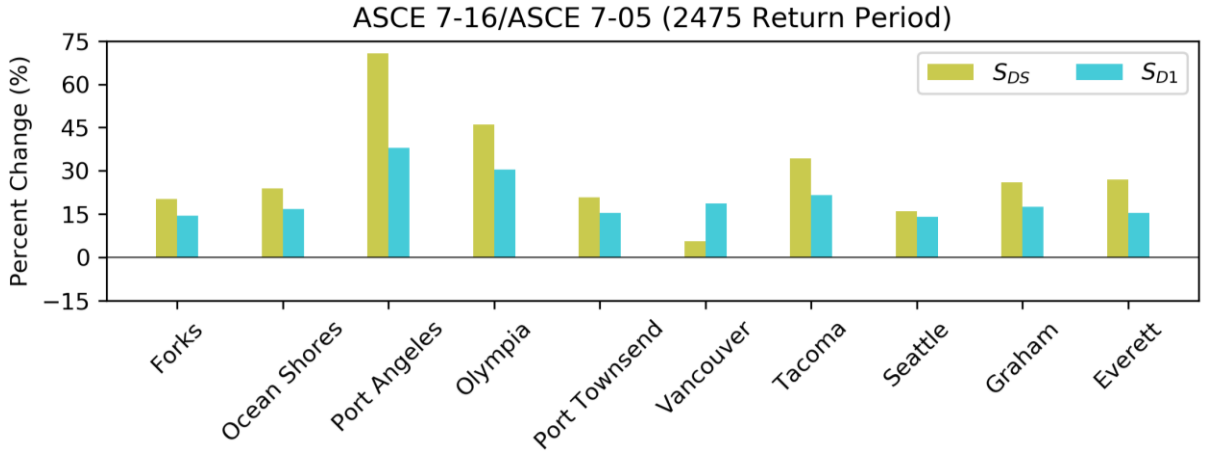

Figure A.4. Washington Cities Design S_a Percent Change Values Caused by Changing USGS Map Version (ASCE7-16/ASCE7-05, 2475-year Return Period, Site Class C)

EFFECT OF RETURN PERIOD

The maps shown in Figure A.5 show the percentage change in PGA, S_{DS}, and S_{D1} caused by changing the return period from approximately 1000 years to 2475 years and then applying a factor of 2/3. Increasing the return period (but maintaining the USGS map version) decreases the design values on the western part of the state and increases them on the eastern part for the 2002 USGS map. For the 2014 USGS map, the western part of the state S_{DS} values decrease, while in the eastern part the S_{DS} values increase. The S_{D1} values increase for the whole state.

Figures A.5 and A.6 show that for the 2002 map version, the cities located along the Western coast and central region of the state (Forks, Ocean Shores, and Vancouver) have the smallest percent change. These figures also show that for S_{D1} there is a concentration of large percent change observed inside parts of the Olympic Peninsula and Puget Sound Region, in which cities located in this area (Port Angeles, Olympia, and Tacoma) have a percent change range between -20% to -15% (0% – 10% more negative than its immediate surroundings). Figure A.5 also shows that both the S_{DS} and S_{D1} contours have a 'low region' in which the percent change goes more positive than its immediate surroundings. This region is located near the city of Seattle and has a percent change range from -10% to +2.5% (0% – 5% more positive) for $S_{DS,}$ and a range from -10% to -5% (0% – 5% more positive) for S_{D1}. Figure A.6 shows that for the 2002 map the absolute value difference in percent change values between S_{DS} and S_{D1} is small as it ranges between 0.5 % – 9%, with this difference being the smallest for the city of Everett.

For the 2014 map version, the accelerations increase more than they did for the 2002 map. Furthermore, the smallest statewide percent change occurred inside the Puget Sound Region. Here, the overall percent change ranged between 0% to -5% for S_{DS}, which is 0% – 5% smaller (more positive) than the percent change observed directly to the East and West. Figure A.6

shows that the cities of Port Townsend, Tacoma, Graham, and Everett have an S_{DS} percent change ranging between -2% to -4.5%. Figures A.5 and A.6 show that amongst all the cities of study, there is less variation in the S_{DS} percent change as they all lie within the -7.5% to 0% contours. As it was previously mentioned, increasing the return period increases the S_{D1}, which results in the all-around positive percent change observed. Figures A.5 and A.6 show that the Puget Sound Region is where the smallest values of percent change are concentrated, but there is no longer uniformity in the values. From this region, the cities of Olympia, Tacoma, and Seattle have the smallest S_{D1} percent change with approximately +14%, +13%, and +12%, respectively. For both map versions, the largest percent change increases in design spectral acceleration occurred in Eastern Washington.

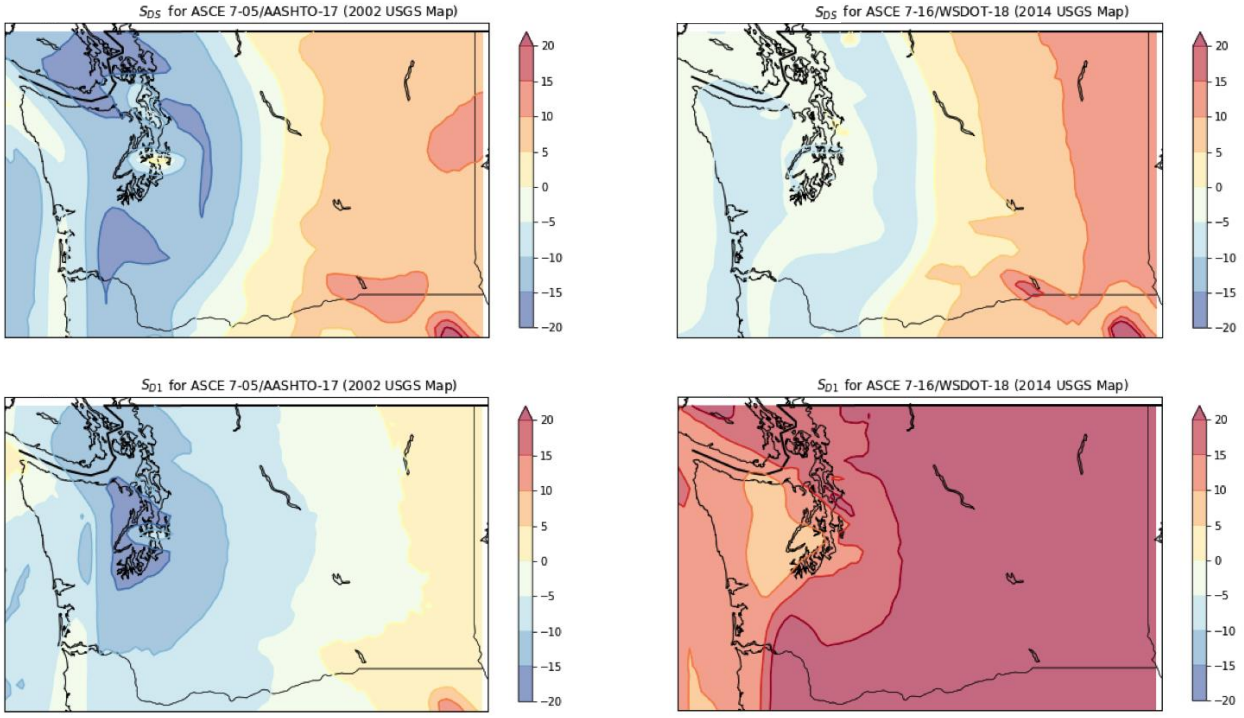

Figure A.5. Washington State Design S_a Percent Change Contours Caused by Changing Return Period (Site Class C)

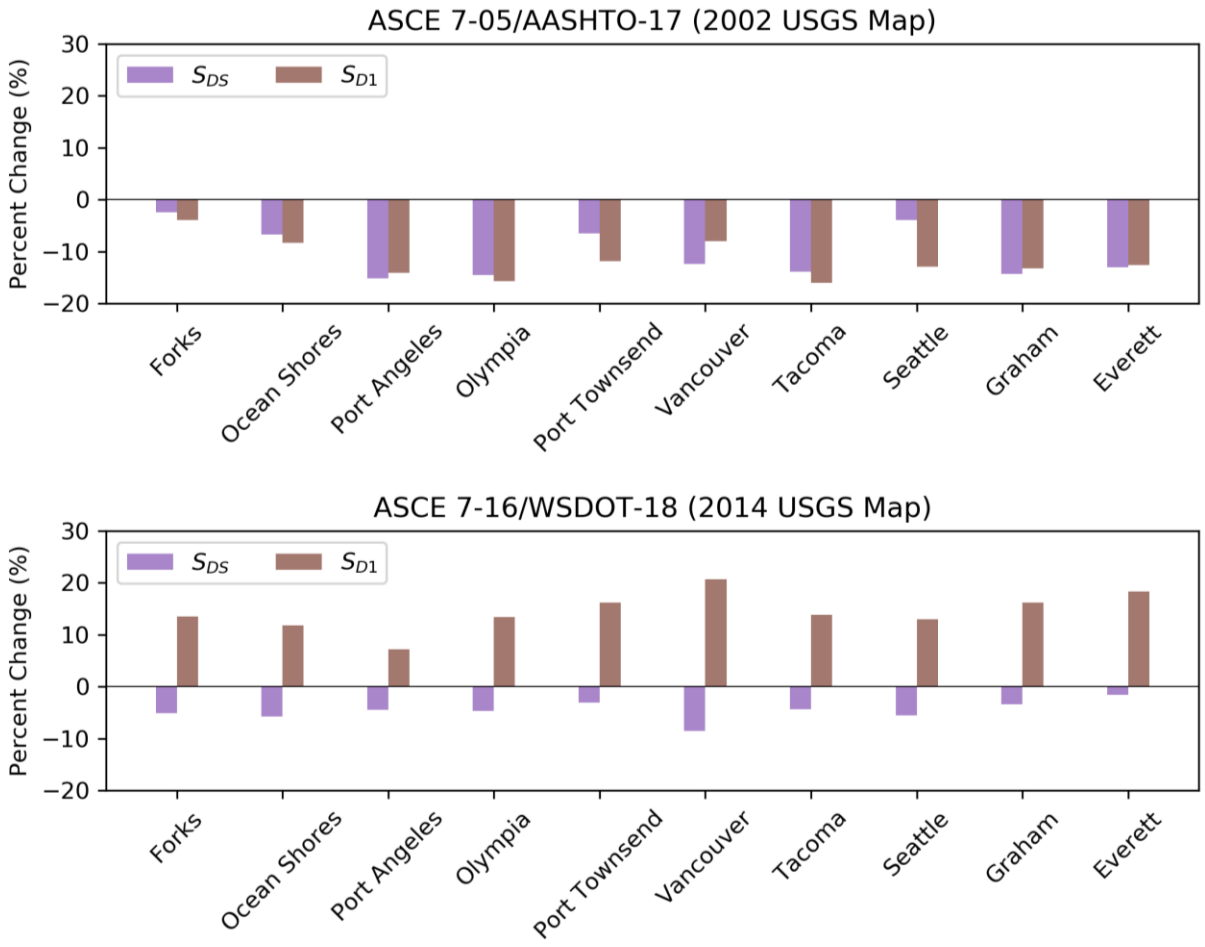

Figure A.6. Washington Cities Design S_a Percent Change Values Caused by Changing Return Period (Site Class C)

APPENDIX B

2002 SITE-CLASS COEFFICIENTS

Table B.1 Values of F_{pga} as Function of Site Class and Mapped Peak Ground Acceleration

Site Class	Mapped Peak Ground Acceleration				
	PGA ≤ 0.10	PGA = 0.20	PGA = 0.30	PGA = 0.40	PGA ≥ 0.50
A	0.8	0.8	0.8	0.8	0.8
B	1.0	1.0	1.0	1.0	1.0
C	1.2	1.2	1.1	1.0	1.0
D	1.6	1.4	1.2	1.1	1.0
E	2.5	1.7	1.2	0.9	0.9
F	Obtained from site-specific analysis				

Table B.2 Values of F_a as Function of Site Class and Mapped Short Period Spectral Acceleration Coefficient

Site Class	Mapped Spectral Response Acceleration Coefficient at Short Periods				
	$S_s \leq 0.25$	$S_s = 0.50$	$S_s = 0.75$	$S_s = 1.00$	$S_s \geq 1.25$
A	0.8	0.8	0.8	0.8	0.8
B	1.0	1.0	1.0	1.0	1.0
C	1.2	1.2	1.1	1.0	1.0
D	1.6	1.4	1.2	1.1	1.0
E	2.5	1.7	1.2	0.9	0.9
F	Obtained from site-specific analysis				

Table B.3 Values of F_v as Function of Site Class and Mapped Long Period Spectral Acceleration Coefficient

Site Class	Mapped Spectral Response Acceleration Coefficient at 1-Second Periods				
	$S_1 \leq 0.10$	$S_1 = 0.2$	$S_1 = 0.3$	$S_1 = 0.4$	$S_1 \geq 0.50$
A	0.8	0.8	0.8	0.8	0.8
B	1.0	1.0	1.0	1.0	1.0
C	1.7	1.6	1.5	1.4	1.3
D	2.4	2.0	1.8	1.6	1.5
E	3.5	3.2	2.8	2.4	2.4
F	Obtained from site-specific analysis				

Table B.4 Values of F_{pga} as Function of Site Class and Mapped Peak Ground Acceleration

Site Class	Mapped Peak Ground Acceleration					
	PGA ≤ 0.10	PGA = 0.20	PGA = 0.30	PGA = 0.40	PGA = 0.50	PGA ≥ 0.60
A	0.8	0.8	0.8	0.8	0.8	0.8
B Measured	0.9	0.9	0.9	0.9	0.9	0.9
B Unmeasured	1.0	1.0	1.0	1.0	1.0	1.0
C	1.3	1.2	1.2	1.2	1.2	1.2
D	1.6	1.4	1.3	1.2	1.1	1.1
E	2.4	1.9	1.6	1.4	1.2	1.1
F	Obtained from site-specific analysis					

Table B.5 Values of F_a as Function of Site Class and Mapped Short Period Spectral Acceleration Coefficient

Site Class	Mapped Spectral Response Acceleration Coefficient at Short Periods					
	$S_s \leq 0.25$	$S_s = 0.50$	$S_s = 0.75$	$S_s = 1.00$	$S_s = 1.25$	$S_s \geq 1.50$
A	0.8	0.8	0.8	0.8	0.8	0.8
B Measured	0.9	0.9	0.9	0.9	0.9	0.9
B Unmeasured	1.0	1.0	1.0	1.0	1.0	1.0
C	1.3	1.3	1.2	1.2	1.2	1.2
D	1.6	1.4	1.2	1.1	1.0	1.0
E	2.4	1.7	1.3	Obtained from site-specific analysis		
F	Obtained from site-specific analysis					

Table B.6 Values of F_v as Function of Site Class and Mapped Long Period Spectral Acceleration Coefficient

Site Class	Mapped Spectral Response Acceleration Coefficient at 1-Second Periods					
	$S_1 \leq 0.10$	$S_1 = 0.2$	$S_1 = 0.3$	$S_1 = 0.4$	$S_1 = 0.50$	$S_1 \geq 0.60$
A	0.8	0.8	0.8	0.8	0.8	0.8
B Measured	0.8	0.8	0.8	0.8	0.8	0.8
B Unmeasured	1.0	1.0	1.0	1.0	1.0	1.0
C	1.5	1.5	1.5	1.5	1.5	1.4
D	2.4	2.2*	2.0*	1.9*	1.8*	1.7*
E	4.2	3.3*	2.8*	2.4*	2.2*	2.0*
F	Obtained from site-specific analysis					

APPENDIX C

COASTAL CITIES WITHOUT BASIN

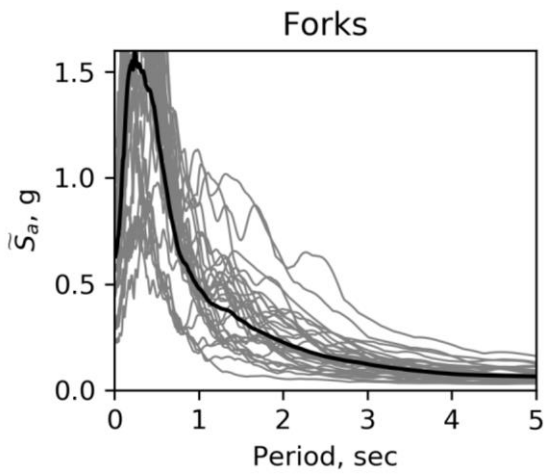

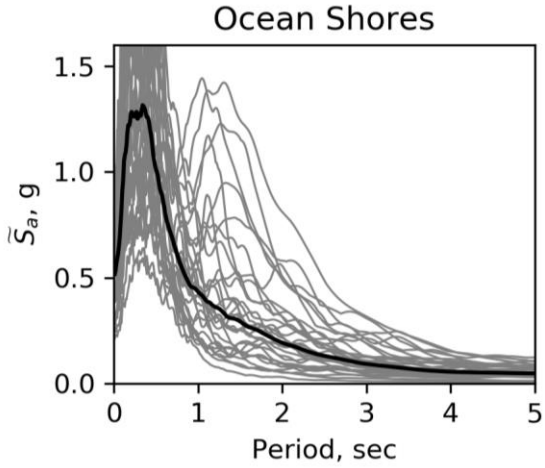

INLAND CITIES WITHOUT BASIN

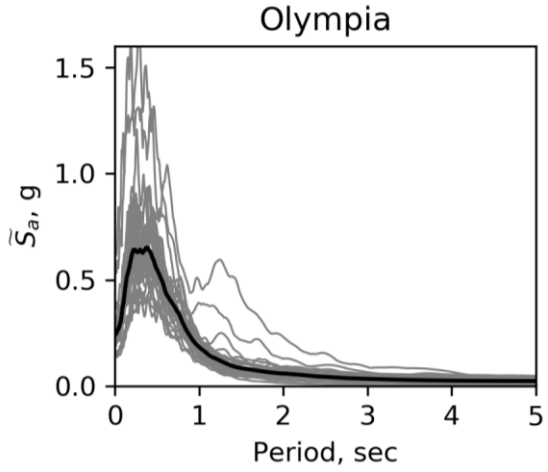

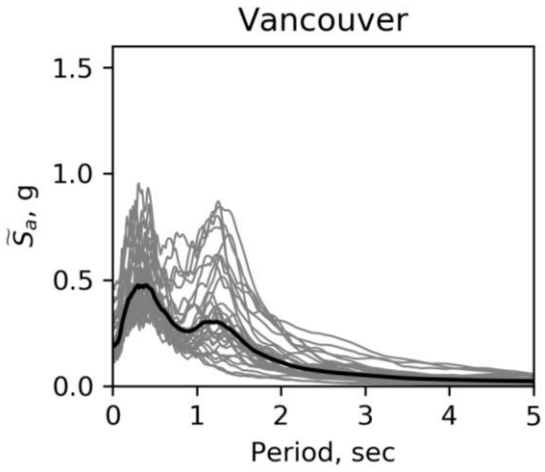

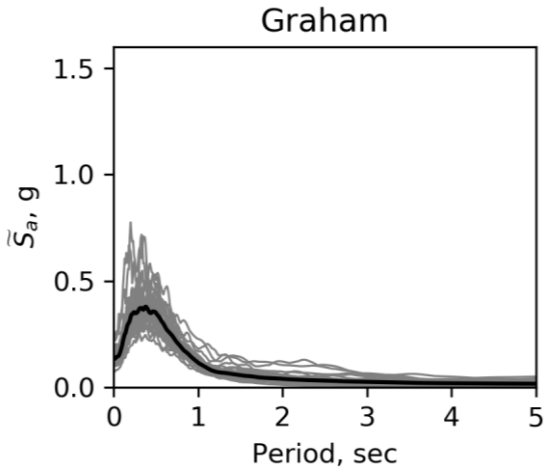

INLAND CITIES ON SHALLOW SEDIMENTARY BASINS

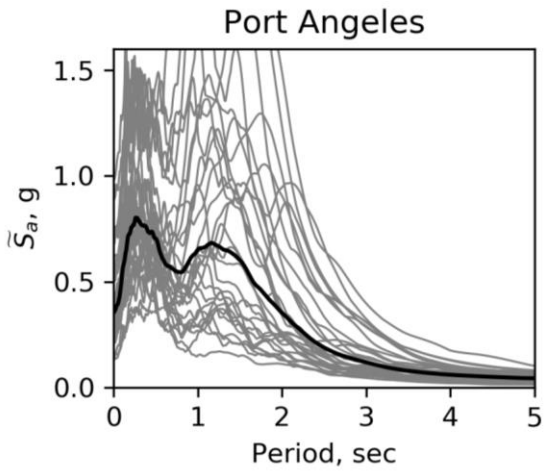

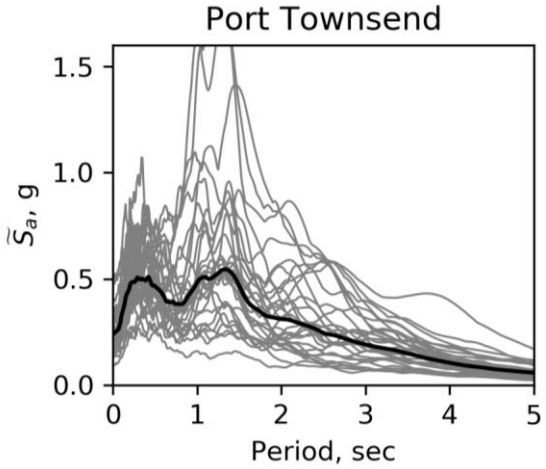

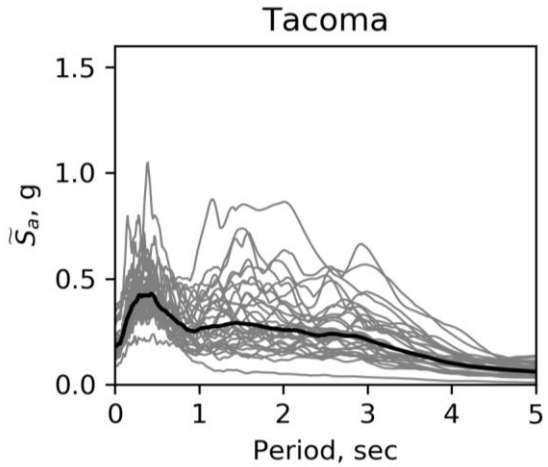

INLAND CITIES ON DEEP SEDIMENTARY BASINS

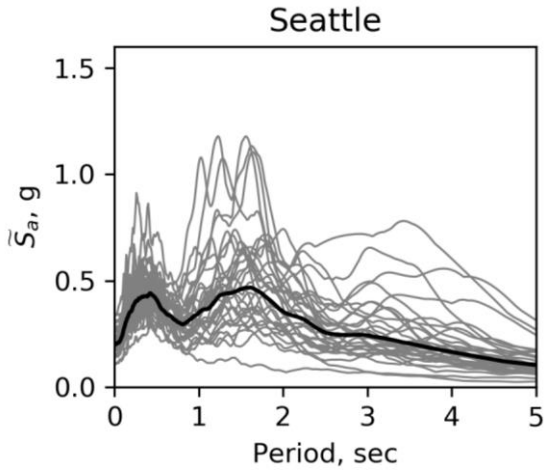

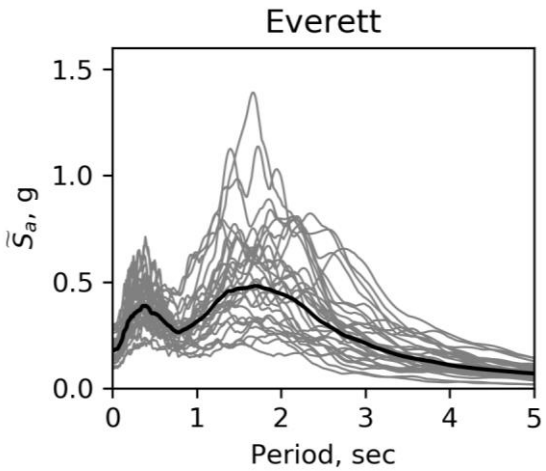

APPENDIX D

COASTAL CITIES WITHOUT BASIN

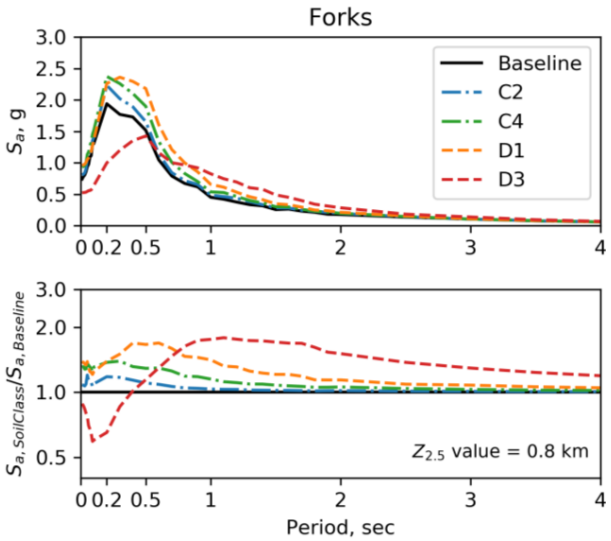

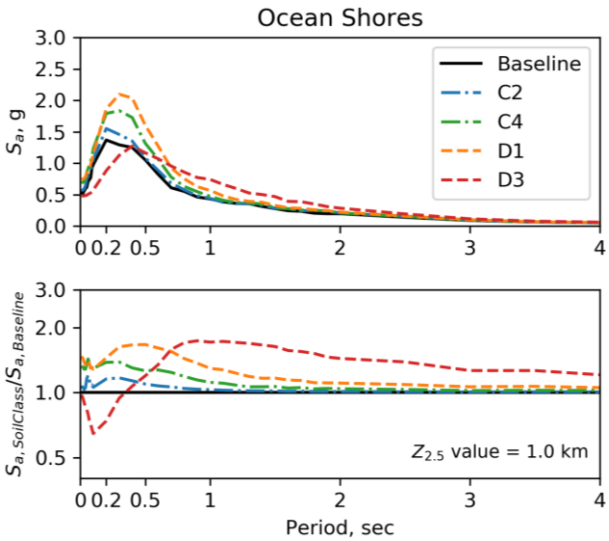

INLAND CITIES WITHOUT BASIN

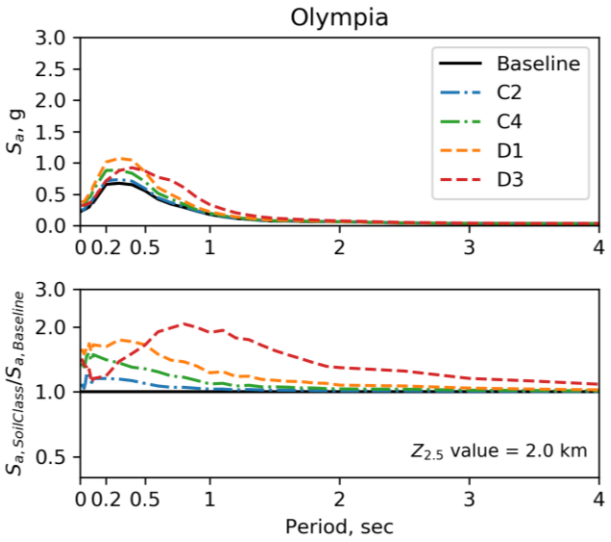

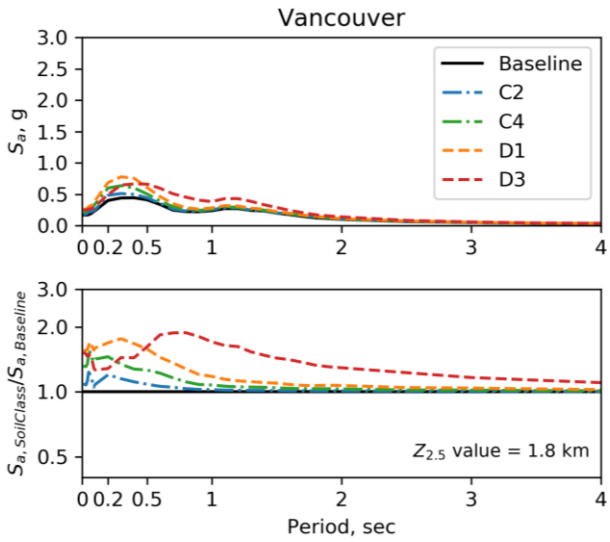

INLAND CITIES WITHOUT BASIN (CONTINUED)

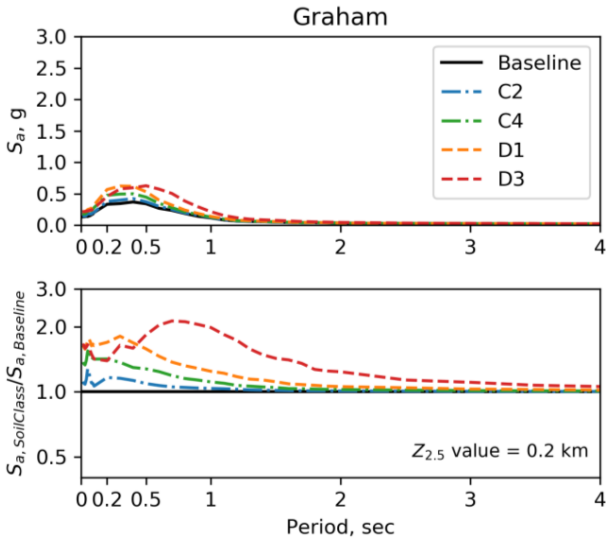

INLAND CITIES ON SHALLOW SEDIMENTARY BASINS

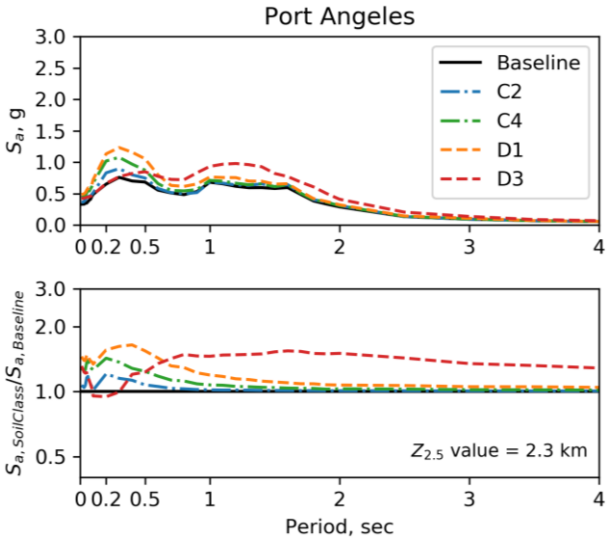

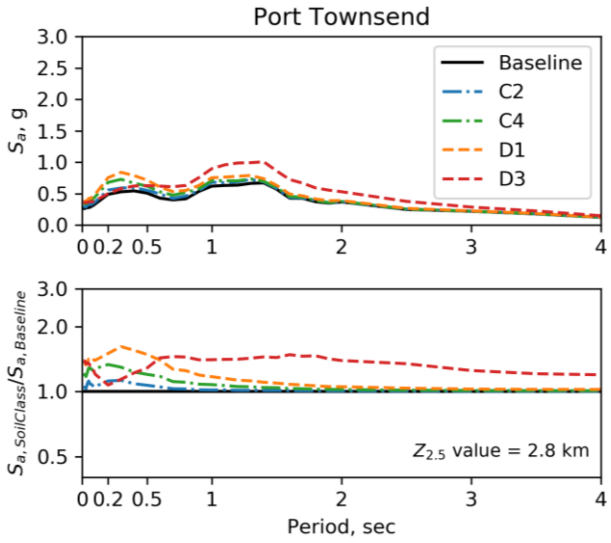

INLAND CITIES ON SHALLOW SEDIMENTARY BASINS (CONTINUED)

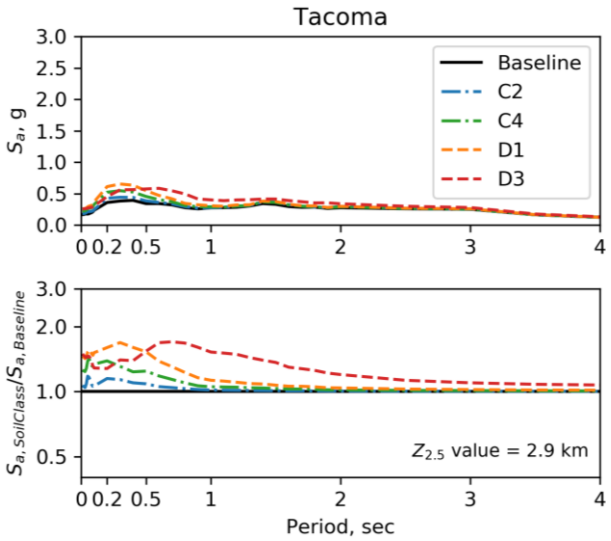

INLAND CITIES ON DEEP SEDIMENTARY BASINS

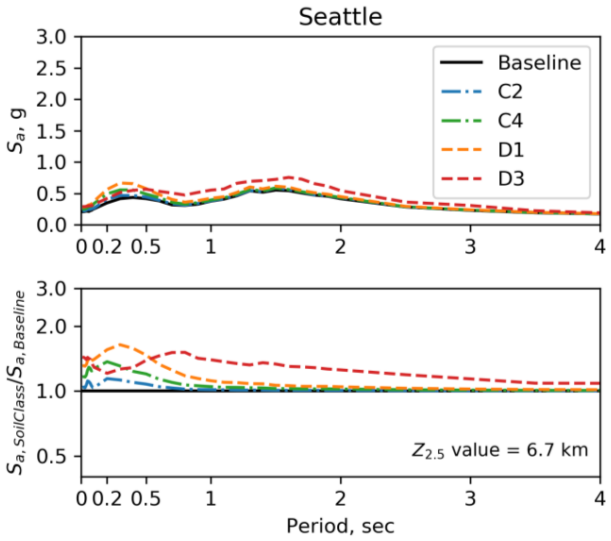

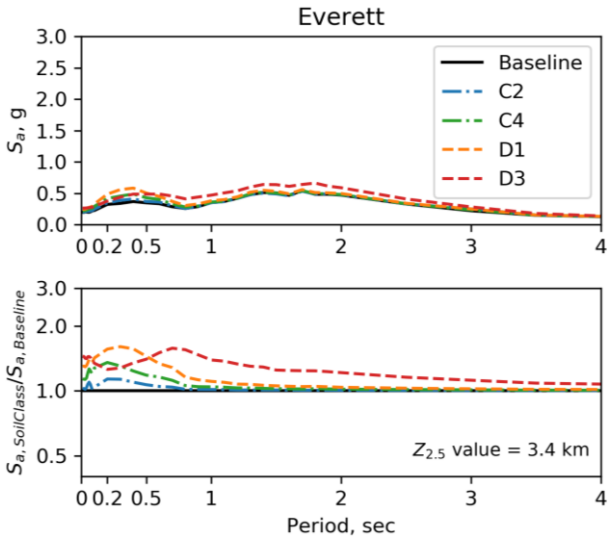

APPENDIX E

An additional fourth single-degree-of-freedom oscillator was created to supplement the three discussed in Chapter 5. This fourth oscillator was a linear oscillator and it was developed in order to ensure that the displacement ductility demand values being recorded by the open-source computational analysis program were correct. The linear oscillator allowed for this check to be made because for linear springs the displacement ductility demand equals the ratio of simulated M9 spectral acceleration to design spectral acceleration ($S_{a,M9}/S_{a,DBE}$). This system served as the control system because once the displacement ductility demand values had been compared to the ratio of M9 spectral acceleration to design spectral acceleration, the remaining three systems were created and the results obtained from those systems were deemed as correct. Figure E.1 shows an example of the backbone utilized for a linear SDOF.

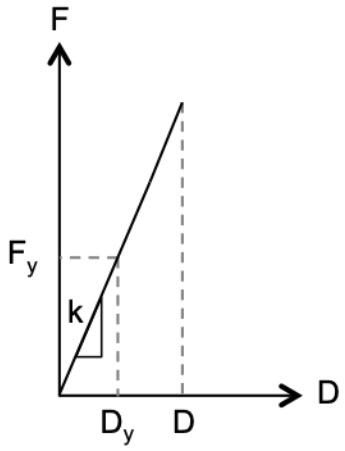

Figure E.1. Linear SDOF Spring System Backbone

The spring material model used was the Elastic Uniaxial Material (OpenSees, McKenna, 2013). The stiffness of the curve shown in Figure E.1 is the elastic stiffness of the spring, *k*, the yield force is F_y, and the deformation at yield is D_y. Figure E.2 shows the oscillator results for the city of Seattle, for Site Class C, at a period of 1.0 second, in the North-South direction, and for a

single realization (csz005). The figure shows the time history curve of the input acceleration, a_g, the recorded acceleration, a, normalized spring force, f_s/f_y, and displacement ductility demand, d/d_y. It also shows the normalized spring force versus ductility demand curve. The figure shows that the normalized spring force versus ductility demand curve is exactly the same as that of the system backbone. This indicates that the system behaved exactly as it was designed to behave under both loading and unloading scenarios.

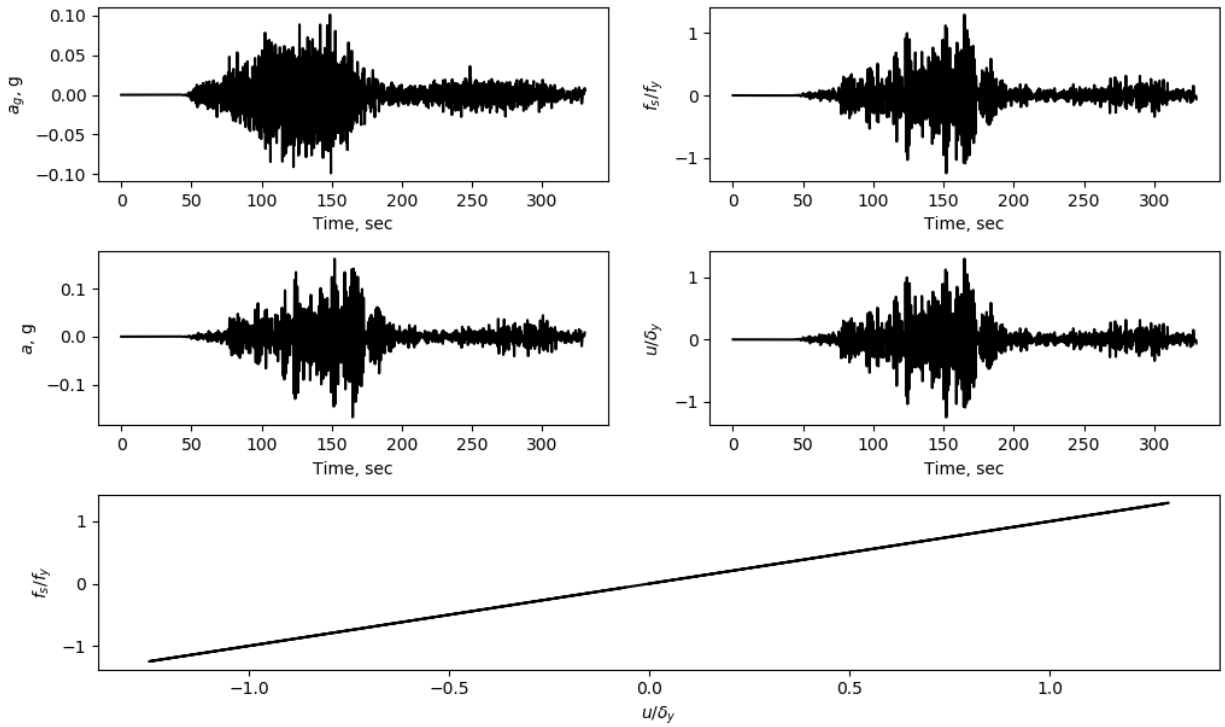

Figure E.2. Linear SDOF Results (Seattle, csz005, T=1.0 sec, EW direction, Site Class C)

APPENDIX F

Chapter 5 shows the results for acceleration time history curve, a_g, recorded acceleration, a, normalized spring force, f_s/f_y, ductility demand, d/d_y, and normalized spring-displacement curve for the four SDOF types and for a simulated baseline M9 motion that does not cause the fully nonlinear oscillators to collapse. The figures in this appendix show the results for the same city, period, direction, and soil classification, but for a motion that does cause collapse (csz003).

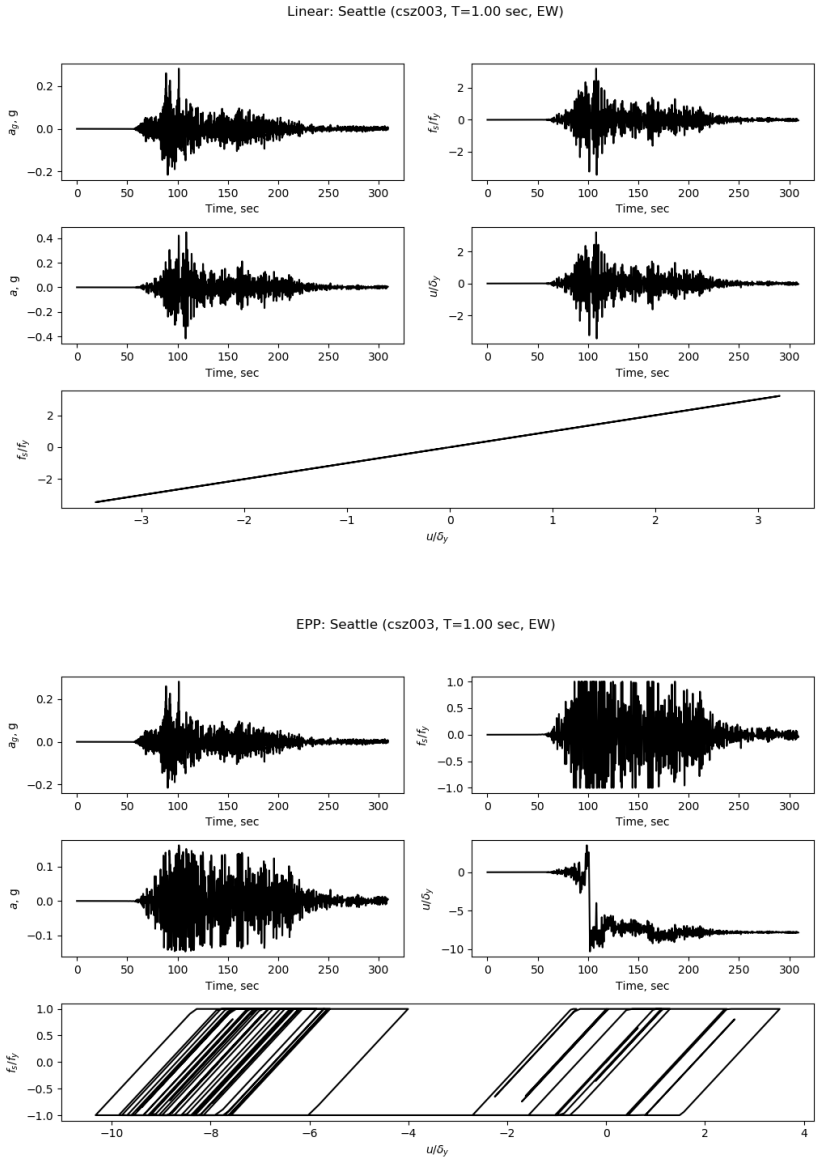

Figure F.1. SDOF Spring Systems for Seattle, csz003, T=1.0 sec, EW direction, Site C

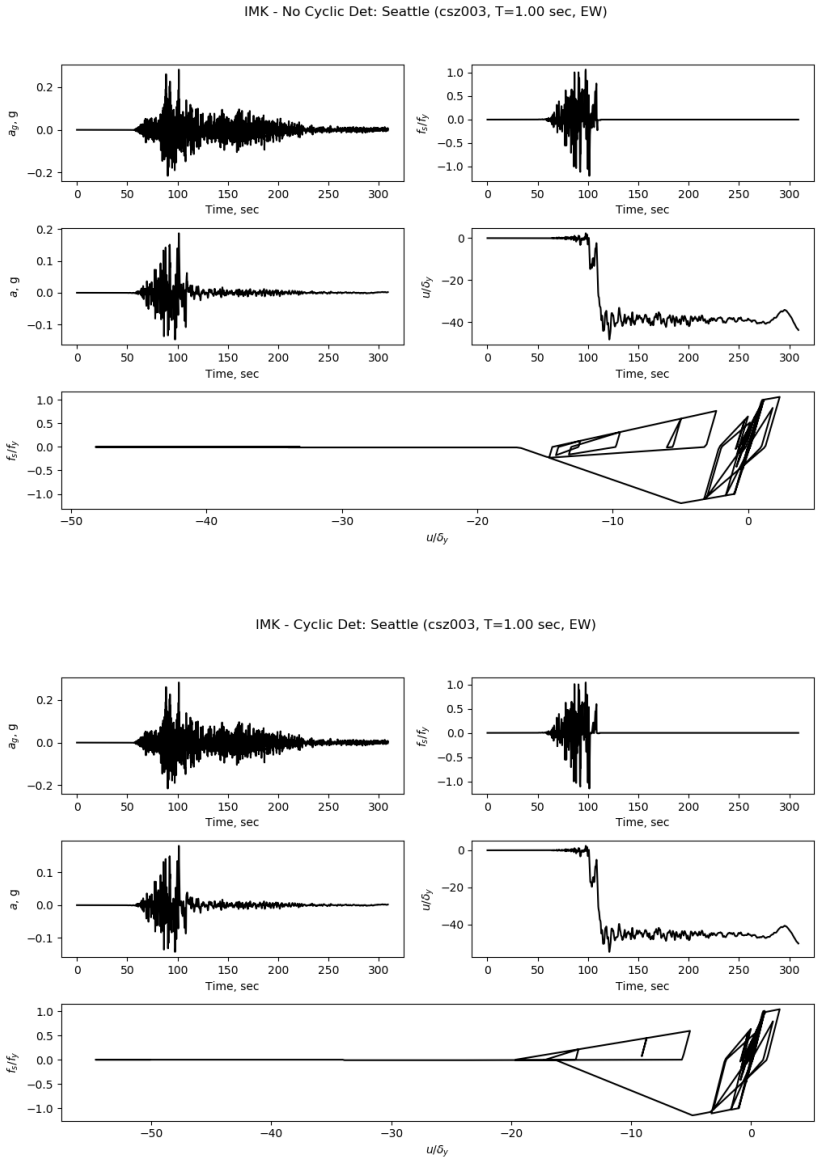

Figure F.1. SDOF Spring Systems for Seattle, csz003, T=1.0 sec, EW direction, Site C Class (continued)

APPENDIX G

The IMK – Cyclic Det. SDOF system from Chapter 5 was used in a calibration study that calculated the probability of collapse and demand ductility for the cities of Seattle and La Grande at periods of 0.5, 1.0, 2.0, 3.0, 4.0, and 5.0 seconds, and for the same four combinations of reduction factor and ductility at maximum force observed in Marafi et al. (2019). The four combinations represented (1) low strength and low ductility [R=3, μ=3], (2) high strength and low ductility [R=8, μ=3], (3) low strength and high ductility [R=3, μ=8], and (4) high strength and high ductility [R=8, μ=8].

In this case, the values for $S_{a,DBE}$ were determined with the use of ASCE 7-16 and they corresponded to Site C. Figures G.1 – G.2 show the probability of collapse and median ductility demand values obtained at the six periods for each orthogonal direction (dashed grey line) and the combination of the two directions (solid black line). The dashed red line seen in the probably of collapse plot indicates 50% probability of collapse. This meant that if 50% or more of the ground motions resulted in collapse then the ductility demand value for that period would be discarded and plotted as ‘Col’ to indicate that the system collapses. The dashed black line seen in the ductility demand plot indicates the μ value being used. The figures show the same ductility demand values and collapse that Marafi et al. (2019) observed.

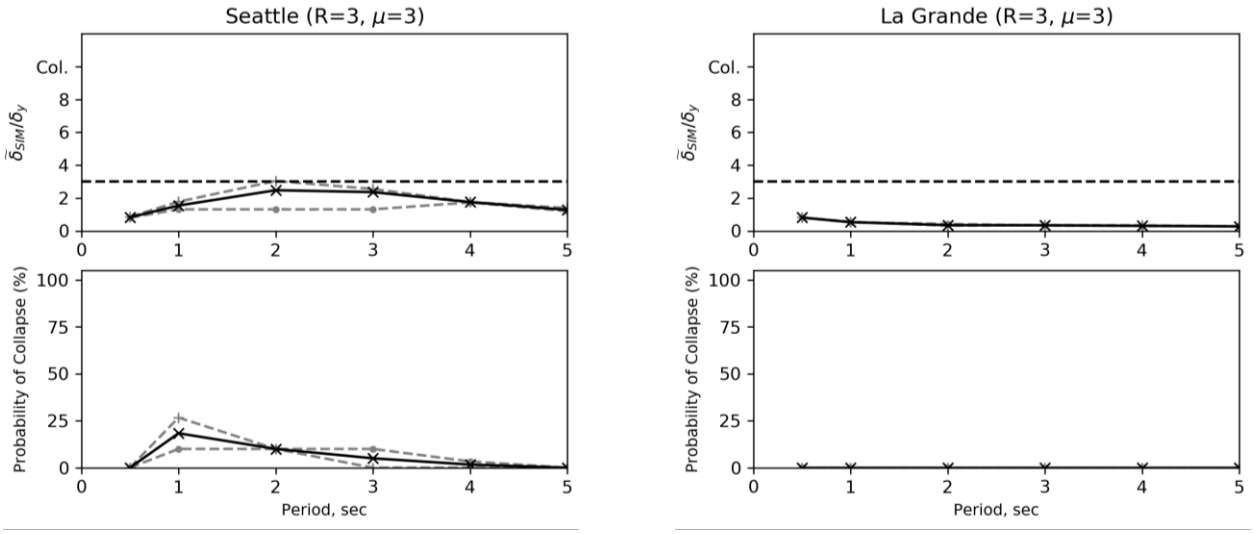

(a)

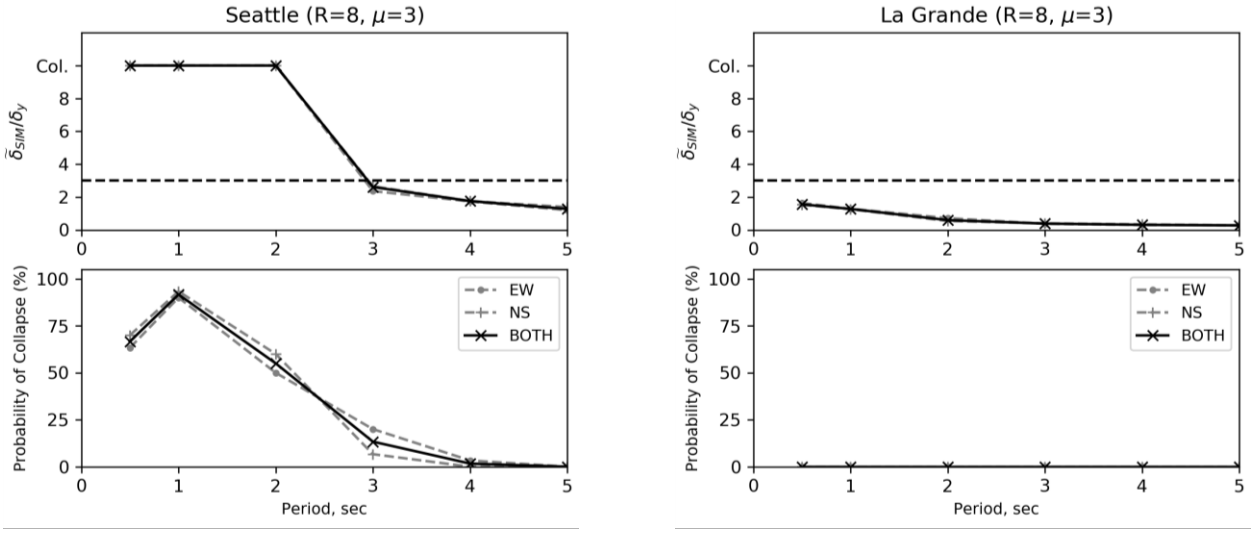

(b)

Figure G.1. Demand Ductility and Probability of Collapse for IMK – Cyclic Det. SDOF System with (a) Low-Strength and Low-Ductility, and (b) High-Strength and Low-Ductility

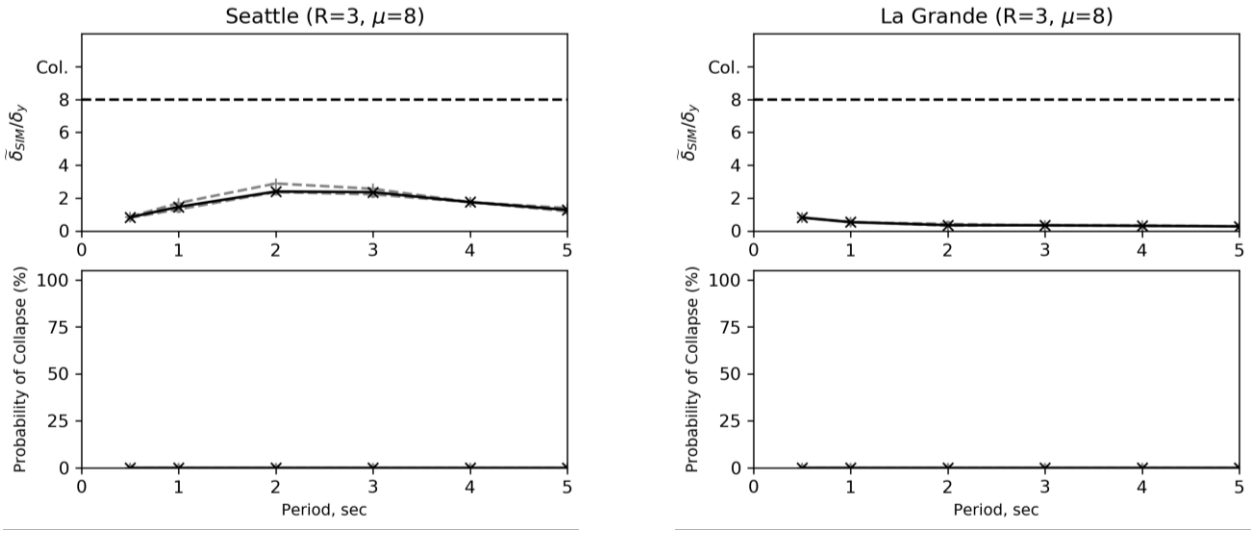

(a)

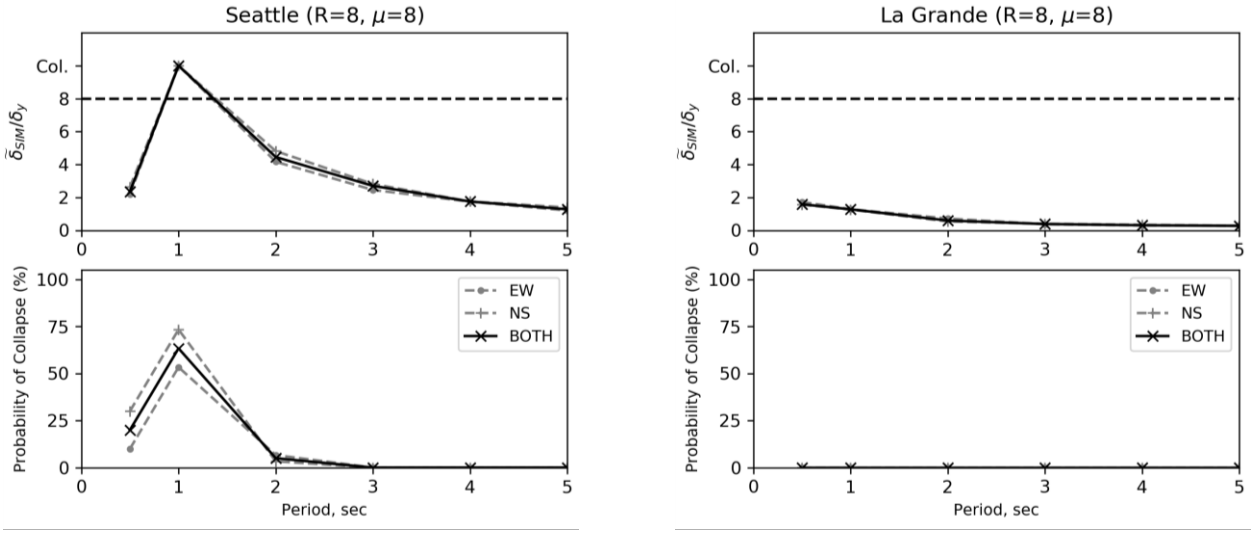

(b)

Figure G.2. Demand Ductility and Probability of Collapse for IMK – Cyclic Det. SDOF System with (a) Low-Strength and High-Ductility, and (b) High-Strength and High-Ductility

APPENDIX H

COASTAL CITIES WITHOUT BASIN

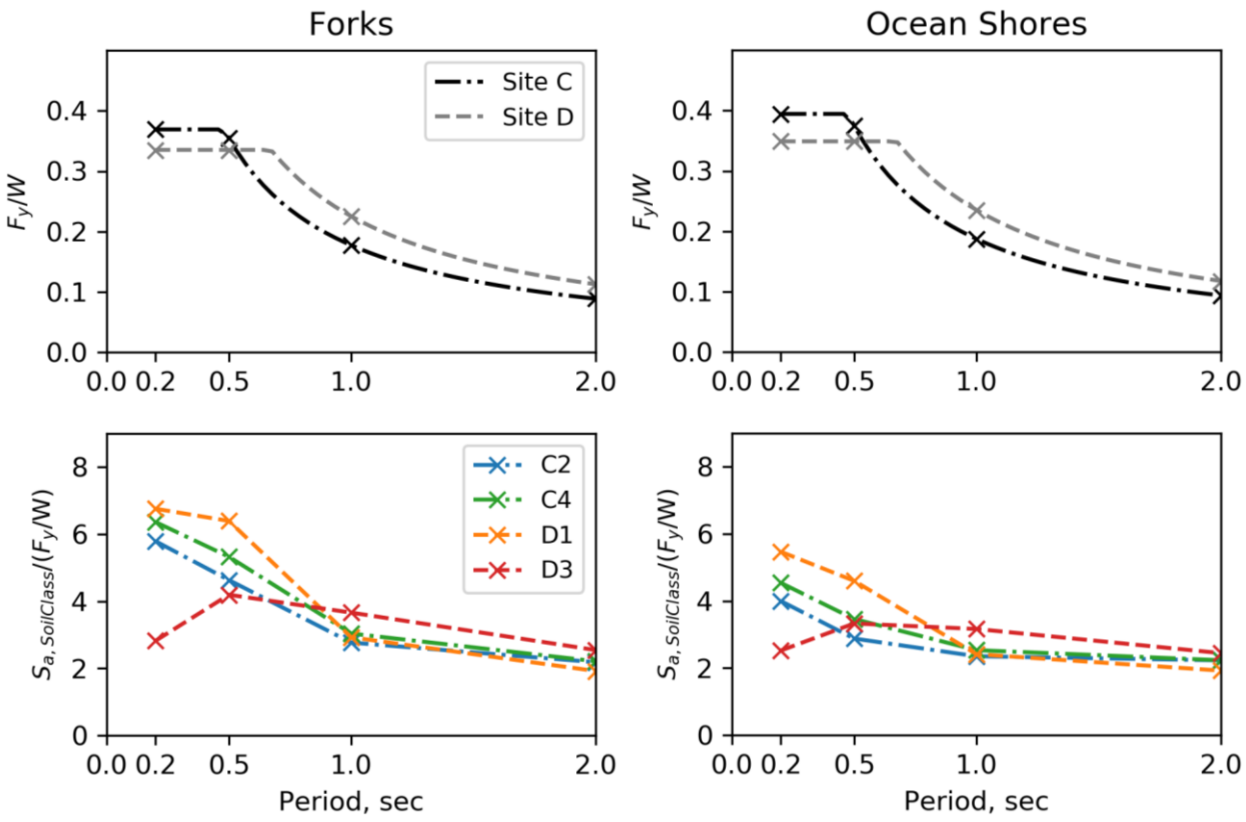

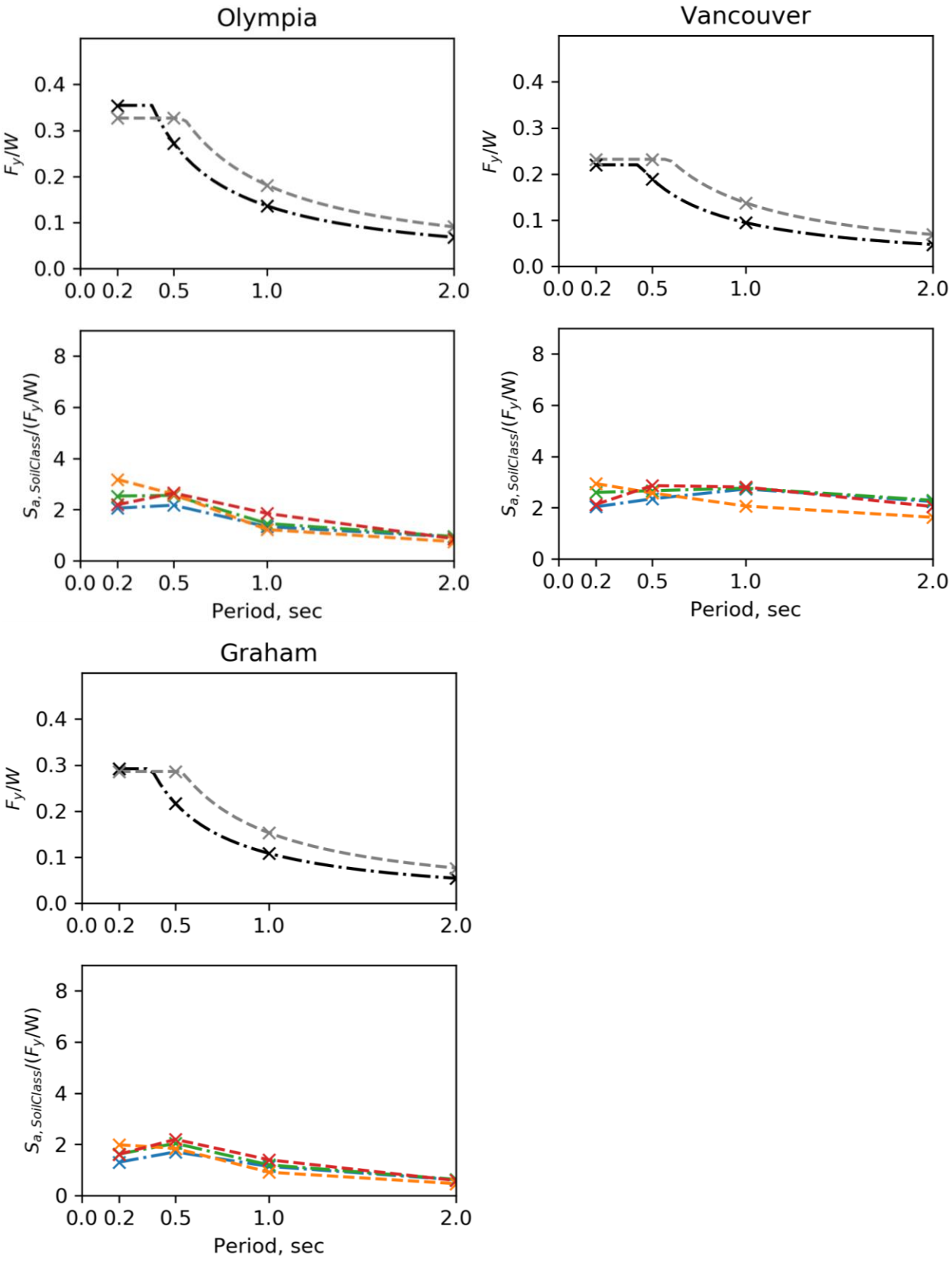
Olympia
Vancouver
Graham
F_y/W
$S_{a,SoilClass}/(F_y/W)$
0.0
0.1
0.2
0.3
0.4
0
2
4
6
8
0.0
0.2
0.5
1.0
2.0
Period, sec

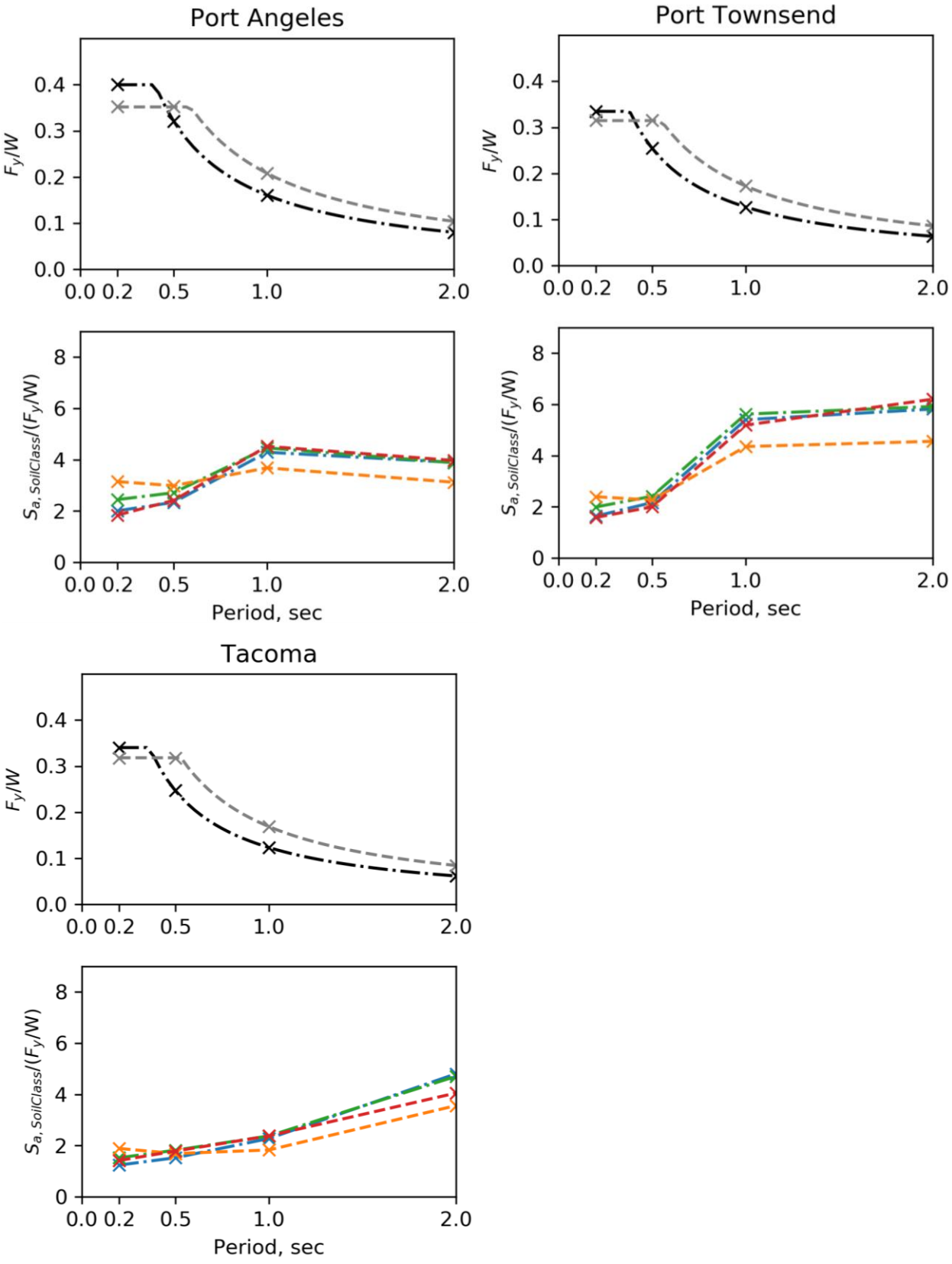
Port Angeles
Port Townsend
Tacoma
F_y/W
$S_{a,SoilClass}/(F_y/W)$
0.0
0.1
0.2
0.3
0.4
0
2
4
6
8
0.0 0.2 0.5 1.0 2.0
Period, sec

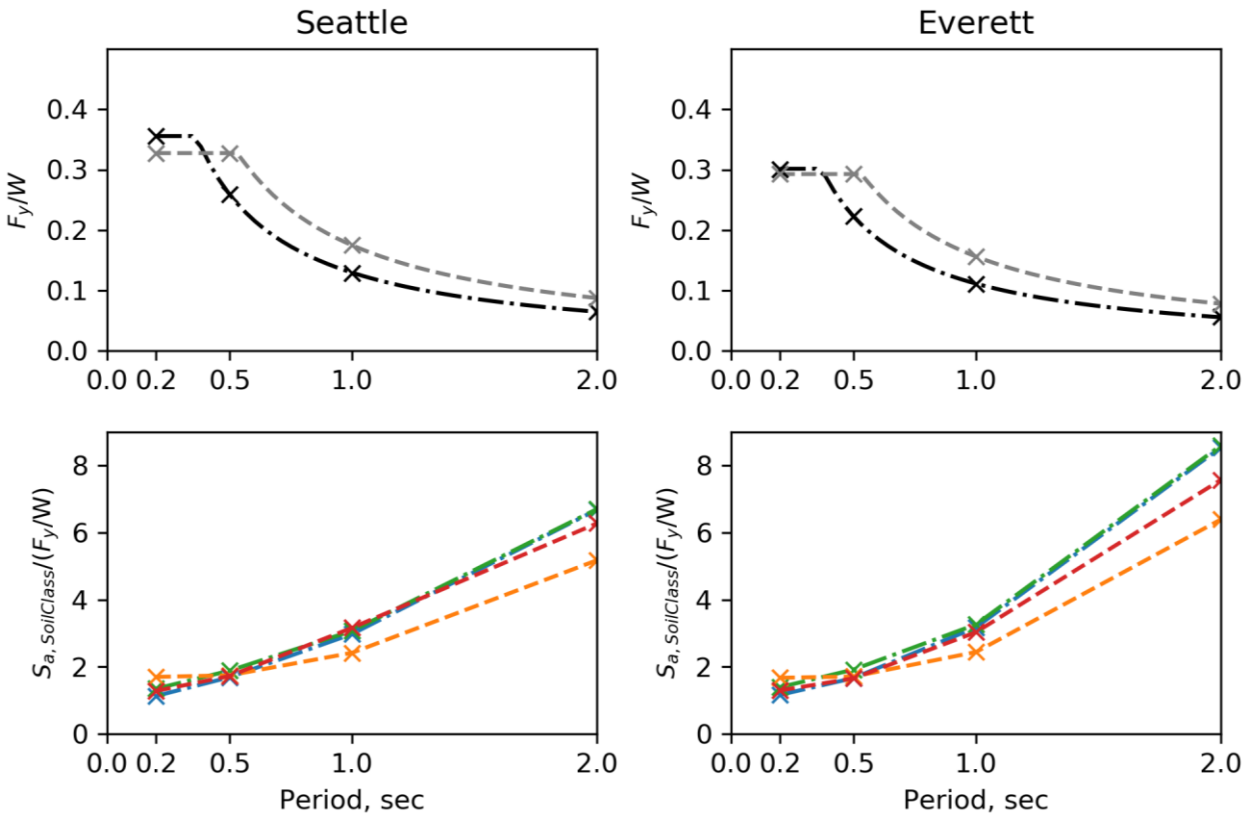
Seattle
Everett
F_y/W
$S_{a,SoilClass}/(F_y/W)$
0.0
0.1
0.2
0.3
0.4
0
2
4
6
8
0.0 0.2 0.5 1.0 2.0
Period, sec

APPENDIX I

COASTAL CITIES WITHOUT BASIN

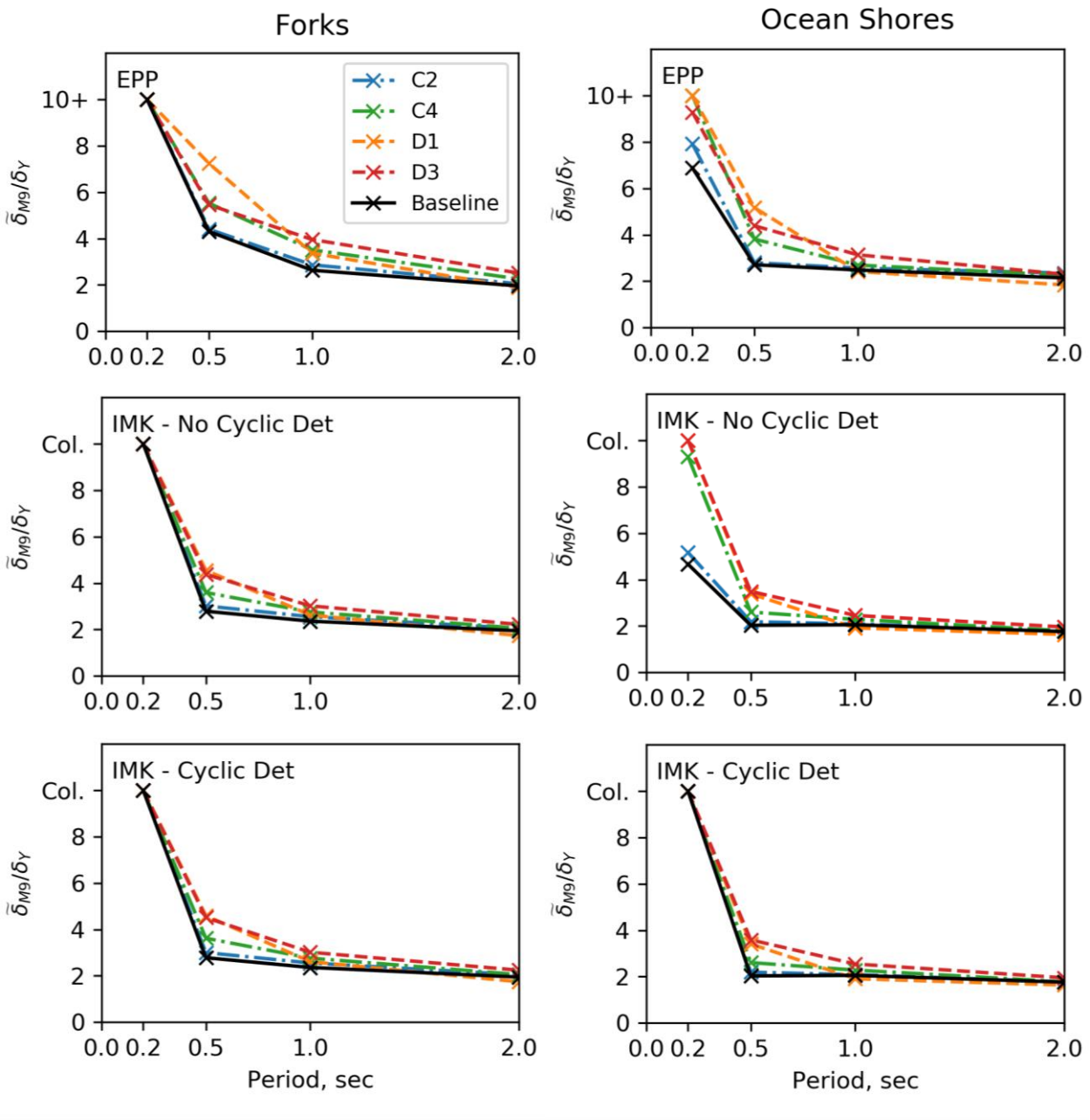

INLAND CITIES WITHOUT BASIN

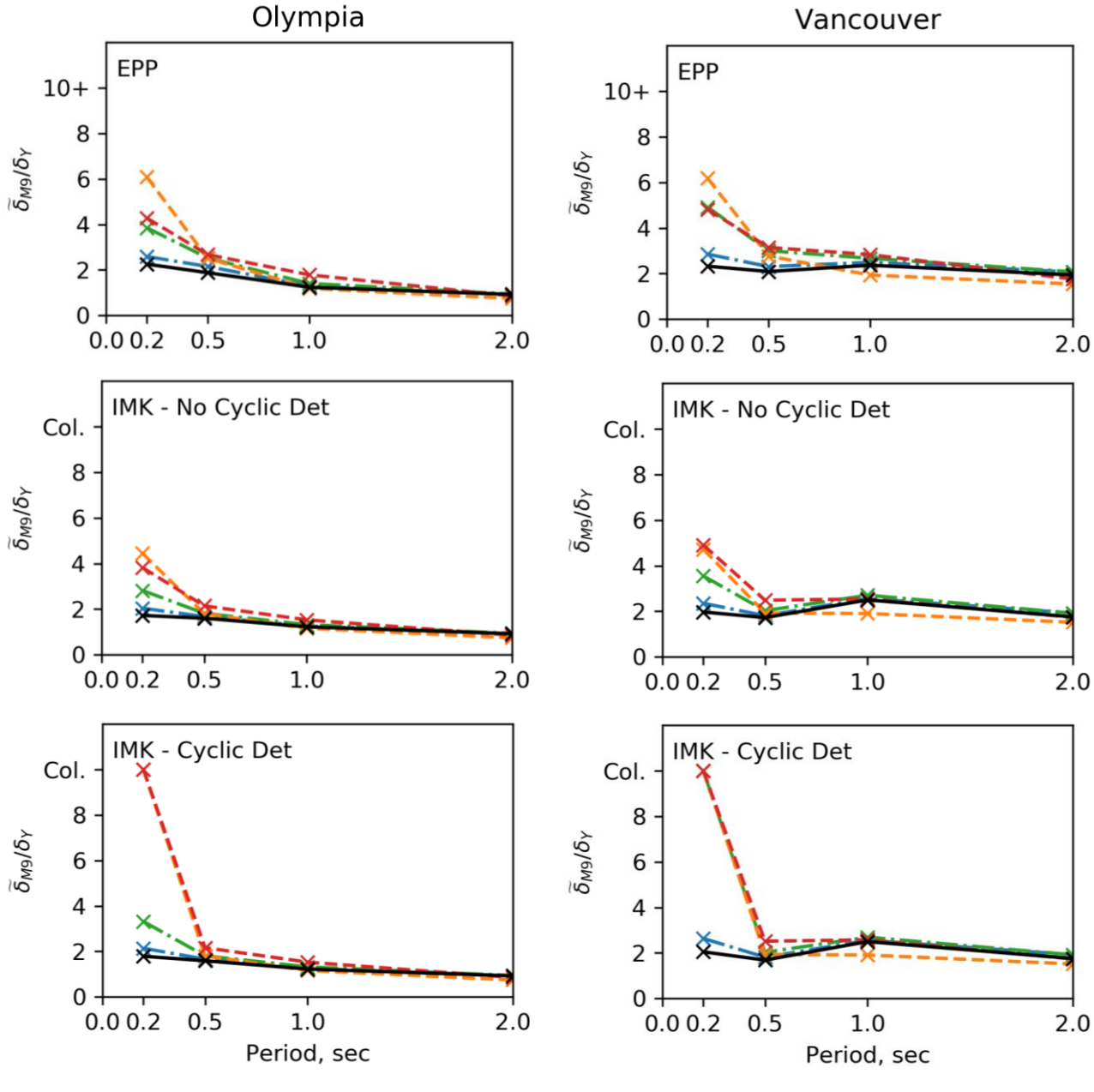

INLAND CITIES WITHOUT BASIN (CONTINUED)

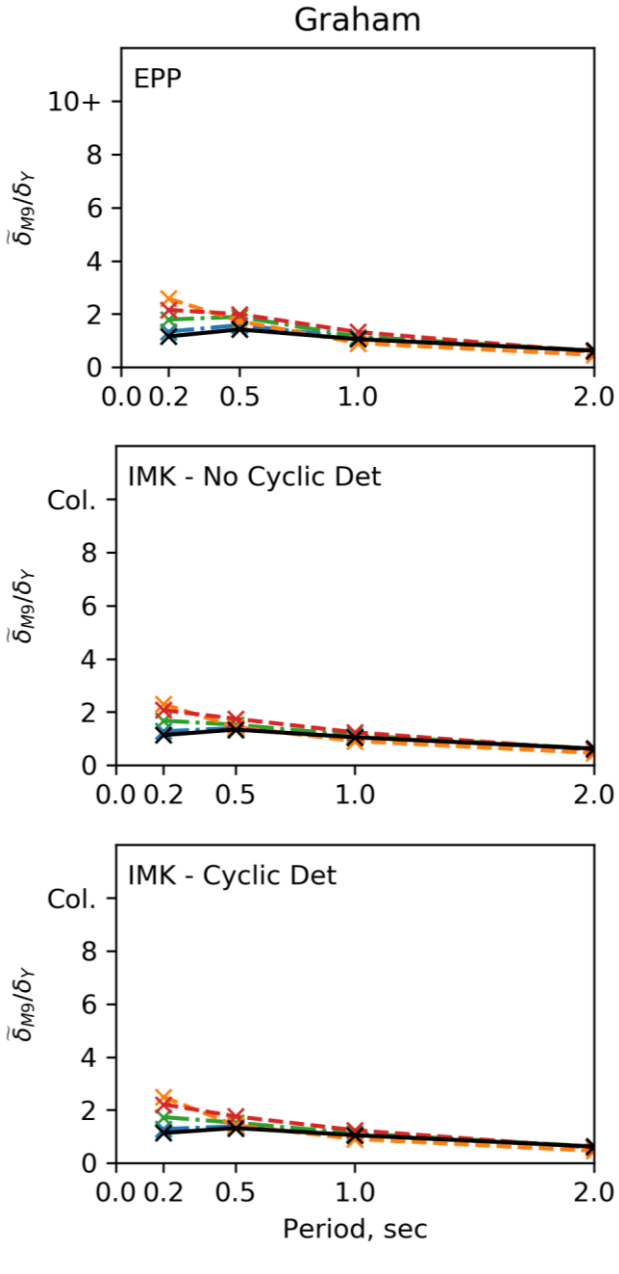

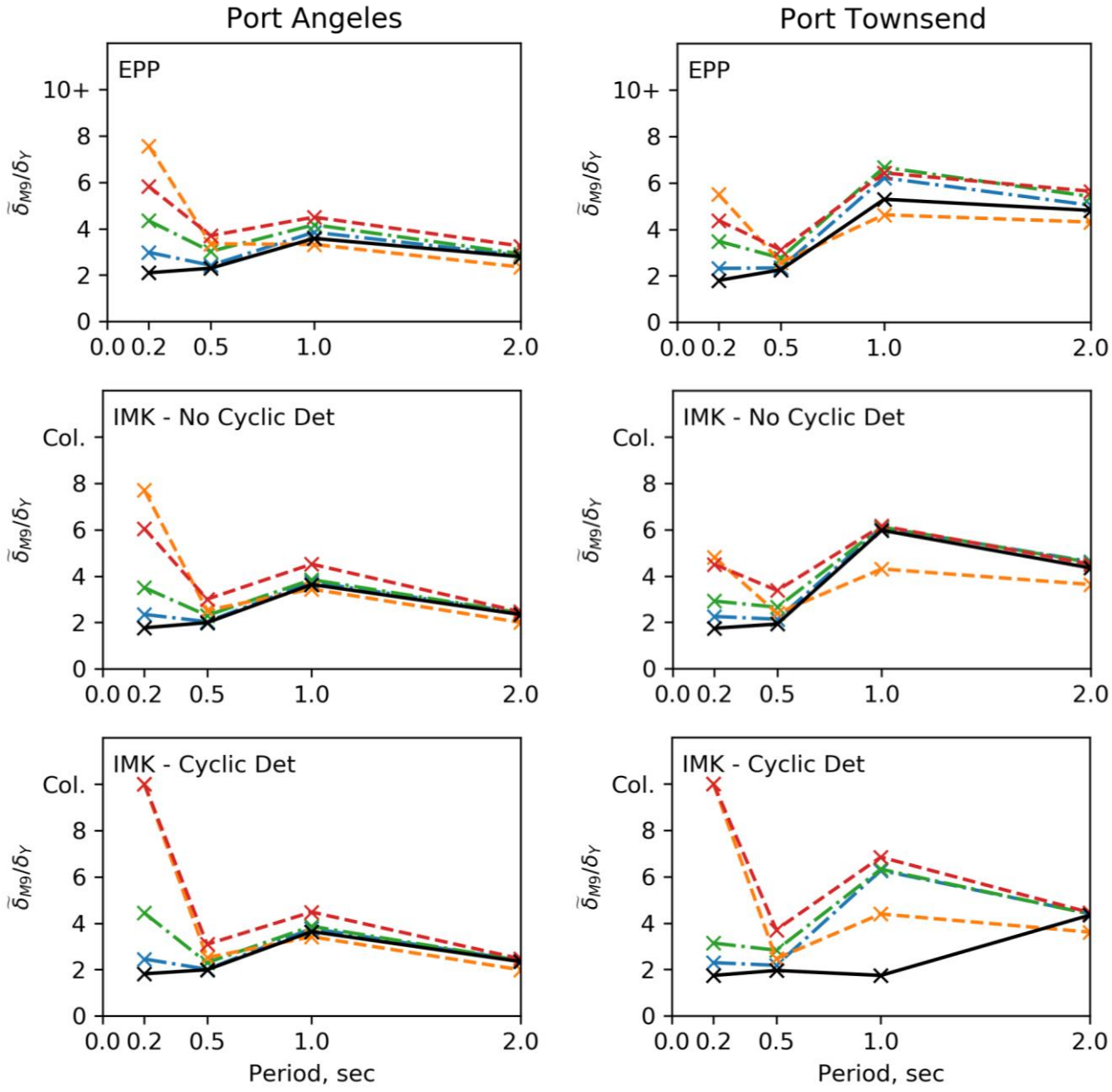
Port Angeles
Port Townsend
EPP
IMK - No Cyclic Det
IMK - Cyclic Det
Col.
10+
0.0 0.2 0.5 1.0 2.0
Period, sec

INLAND CITIES ON DEEP SEDIMENTARY BASINS (CONTINUED)

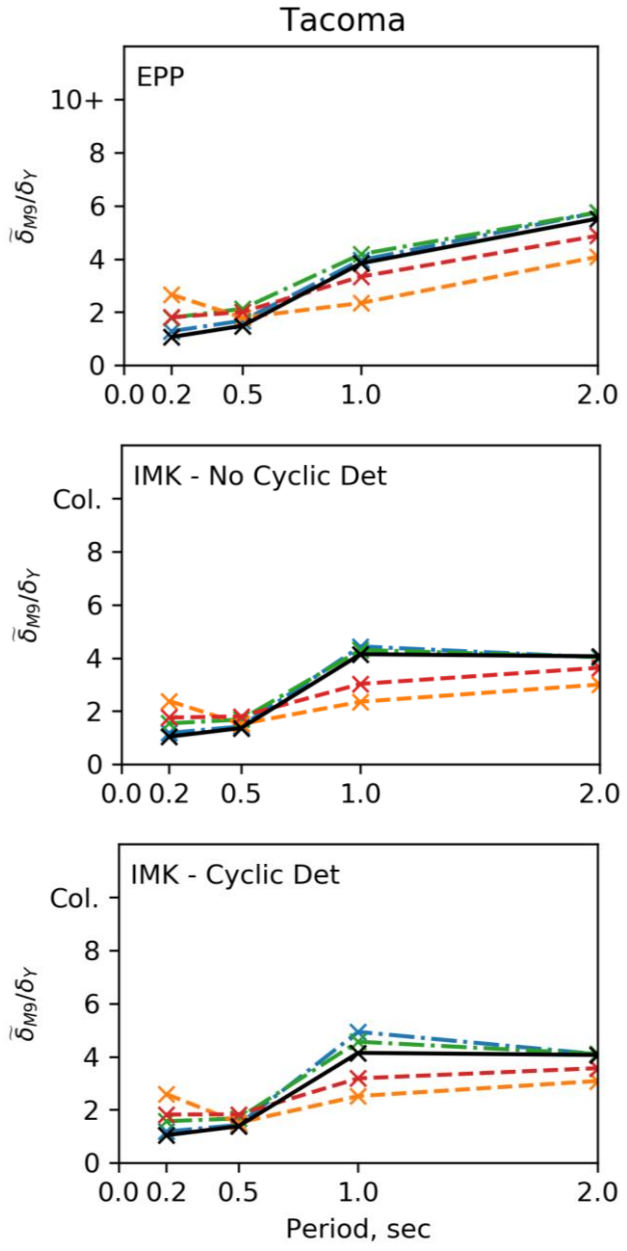

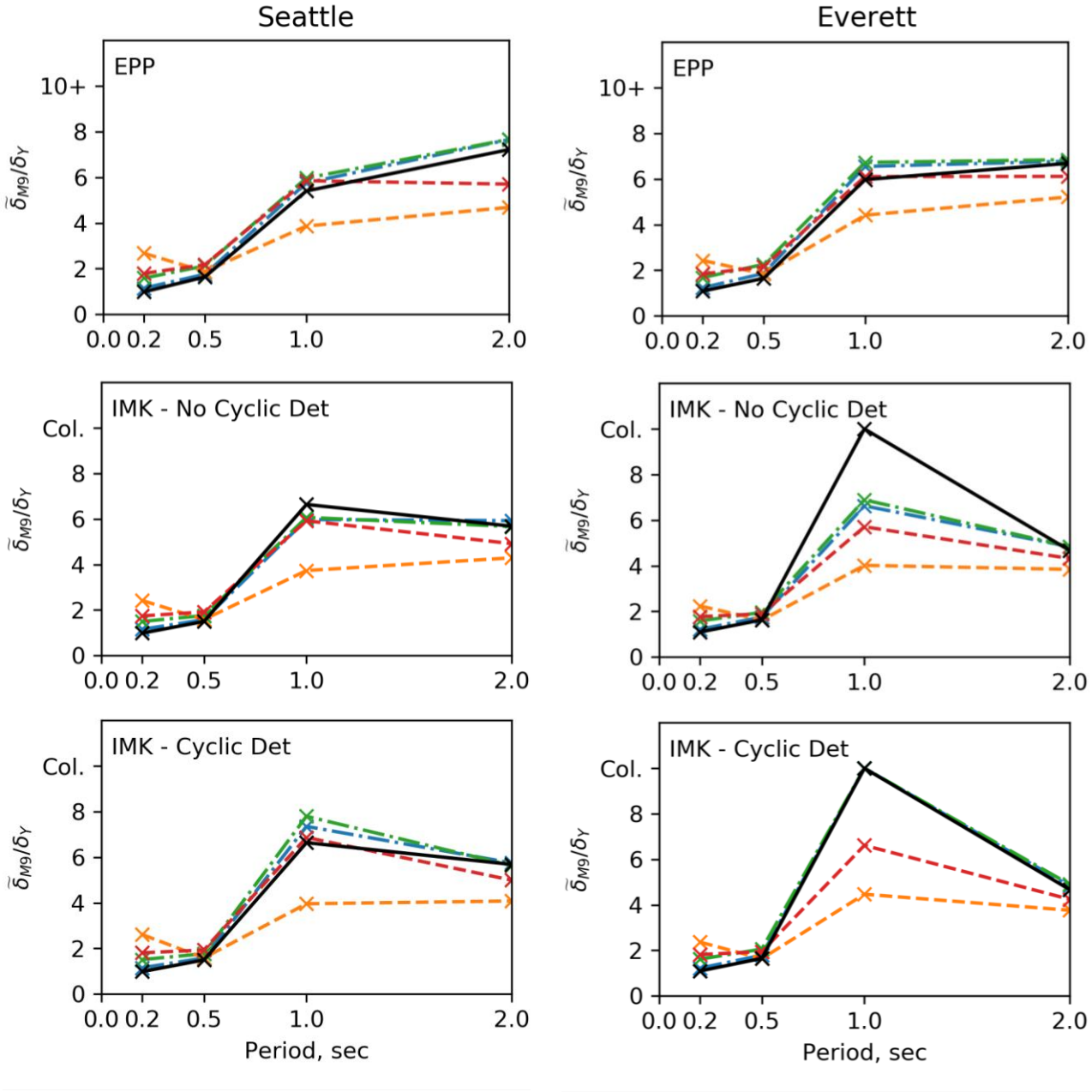
Seattle
Everett
EPP
IMK - No Cyclic Det
IMK - Cyclic Det
Col.
10+
0
2
4
6
8
0.0
0.2
0.5
1.0
2.0
Period, sec
$\widetilde{\delta}_{M9}/\delta_Y$